

ASPECTS OF MODIFIED GRAVITY

A THESIS SUBMITTED TO THE UNIVERSITY OF MANCHESTER
FOR THE DEGREE OF DOCTOR OF PHILOSOPHY
IN THE FACULTY OF ENGINEERING AND PHYSICAL SCIENCES

2013

By

EDWARD REEVES

School of Physics & Astronomy

Jodrell Bank Centre for Astrophysics

Contents

Abstract	9
Declaration	11
Copyright statement	13
The Author	15
Acknowledgements	17
Glossary	19
Useful Expressions	23
1 Introduction to Gravitational Theories and Cosmology	27
1.1 Introduction	27
1.2 General Relativity	28
1.2.1 General Relativity, covariant derivatives, energy-momentum tensor	28
1.2.2 The Riemann tensor and curvature and the Einstein tensor	29

1.2.3	Formulation of the Einstein equations	30
1.2.4	The FRW metric and the Ricci scalar	32
1.2.5	Density, pressure and equation of state	33
1.2.6	The Friedmann equations	34
1.2.7	Einstein equations derived from the action	34
1.3	A brief history of the Universe	36
1.3.1	The radiation era	37
1.3.2	The matter dominated era and the CMB	37
1.3.3	The vacuum era	38
1.4	Modifying gravity with $F(R)$ gravity models	38
1.4.1	A special case	40
1.4.2	A vacuum solution	42
1.4.3	A modified expression for the Hubble parameter and the effective equation of state	42
1.4.4	Dark energy	43
1.4.4.1	The cosmological constant	44
1.4.4.2	Quintessence	45
1.4.4.3	Effective dark energy	45
1.4.5	The modified gravity particle	45
1.4.6	The coincidence problem	46
1.4.7	The growth of matter and perturbations	47
1.4.8	Constraints on $F(R)$	47

<i>CONTENTS</i>	5
1.4.9 Conditions for an accelerating Universe	49
1.4.10 Probing the Growth of Large Scale Structure	49
2 Gravitation Models Which Mimic ΛCDM	53
2.1 Introduction	53
2.2 Finding all models which mimic Λ CDM	55
2.2.1 Algebraic solution for $R > 4\Lambda$	56
2.2.2 Algebraic solution which includes $R = 4\Lambda$	58
2.2.3 Matching conditions for the two expressions for $F(R)$	59
2.2.4 Application of constraints to the solutions	64
2.2.4.1 The condition that $F_R(R) > 0$	65
2.2.4.2 The condition that $F_{RR}(R) \geq 0$	65
2.2.4.3 The local gravity constraint	65
2.2.5 The matter growth index, γ	67
2.3 In the radiation era	68
2.4 Conclusion	71
3 Non-ΛCDM Gravitation Models	75
3.1 Introduction	75
3.2 Three models compared	78
3.2.1 The Erf model	79
3.2.1.1 The dark energy equation of state	80
3.2.1.2 Late-time behaviour	84

3.2.1.3	The matter growth index	87
3.2.2	The AB model	89
3.2.3	The HSS model	92
3.3	Conclusion	98
4	The $w_{\text{eff}} < -1$ Theorem for $F(R)$ Models	101
4.1	Introduction	101
4.2	The theorem	101
5	Evolution of Perturbations	105
5.1	Introduction	105
5.2	Matter perturbation equations in k -space for the Jordan Frame .	107
5.2.1	The Λ CDM model	109
5.3	Approximating algebraic solutions	110
5.3.1	Oscillatory solution	112
5.3.2	Non-oscillatory solution	116
5.3.3	The combined algebraic solution	117
5.3.4	Applying initial conditions to the algebraic approximation	119
5.4	Algebraic and numerical solutions compared	120
5.4.1	$k = 0.1h \text{ Mpc}^{-1}$	121
5.4.2	$k = 0.01h \text{ Mpc}^{-1}$	127
5.4.3	$k = 0$	130
5.4.4	Algebraic and numeric solutions for $x(N)$ compared for other models of chapter 3.	133

5.4.4.1	Model 2	133
5.4.4.2	Model 4	134
5.4.4.3	Model 5	135
5.4.5	Comment	135
5.5	Conclusion	136
5.5.1	Oscillations in δR	139
6	Conclusions	141
6.1	Summary	141
6.1.1	Models with standard Einstein Gravity expansion history .	142
6.1.2	Extreme values generated by $F(R)$ models	143
6.1.3	Theorem	144
6.1.4	Oscillations of the potentials of the perturbed FRW metric	144
6.2	Outlook	147
	Bibliography	149

Abstract

Algebraic expressions are determined for all $F(R)$ gravity models which mimic standard Einstein Gravity. We find that they are severely constrained by local gravity in the Solar System which makes them virtually indistinguishable from standard Einstein Gravity. In addition, we find that instead of $F(R) \rightarrow R$ as $R \rightarrow \infty$, there is the possibility that $F(R) \propto R^{4/3}$.

Aspects of two well-known $F(R)$ models are discussed together with a new model. For the three models, the evolution of the effective equation of state parameter, w_{eff} , is followed as well as the effective density parameter, Ω_{eff} , and the relationship between them. Also considered are the dependence of the potential on its defining field and the evolution of the matter growth index, which is also compared with that of standard Einstein Gravity. The problems that occur, the constraints that act in order to make these parameters extreme today, and the effect that a late-time de Sitter attractor has and how this can be evaded to give large deviations from $w_{\text{eff},0} = -1$ are discussed.

It is the case that in the radiation and matter eras, for $F(R)$ models that tend to standard Einstein Gravity as $R \rightarrow \infty$, $w_{\text{eff}} < -1$ and decreases with time. A proof of this is given as a theorem.

Matter oscillations of the perturbed, weak matter fields are considered and the equations solved algebraically to show how they evolve in time both in amplitude and frequency. They are compared with the numeric solutions of the equations and, under certain circumstances, they compare favourably.

Declaration

No portion of the work referred to in this thesis has been submitted in support of an application for another degree or qualification of this or any other university or other institution of learning.

Copyright statement

1. The author of this thesis (including any appendices and/or schedules to this thesis) owns certain copyright or related rights in it (the Copyright) and he has given The University of Manchester certain rights to use such Copyright, including for administrative purposes.
2. Copies of this thesis, either in full or in extracts and whether in hard or electronic copy, may be made only in accordance with the Copyright, Designs and Patents Act 1988 (as amended) and regulations issued under it or, where appropriate, in accordance with licensing agreements which the University has from time to time. This page must form part of any such copies made.
3. The ownership of certain Copyright, patents, designs, trade marks and other intellectual property (the Intellectual Property) and any reproductions of copyright works in the thesis, for example graphs and tables (Reproductions), which may be described in this thesis, may not be owned by the author and may be owned by third parties. Such Intellectual Property and Reproductions cannot and must not be made available for use without the prior written permission of the owner(s) of the relevant Intellectual Property and/or Reproductions.
4. Further information on the conditions under which disclosure, publication and commercialisation of this thesis, the Copyright and any Intellectual

Property and/or Reproductions described in it may take place is available in the University IP Policy¹, in any relevant Thesis restriction declarations deposited in the University Library, The University Library's regulations² and in The University's policy on presentation of theses.

¹<http://documents.manchester.ac.uk/display.aspx?DocID=487>

²<http://www.manchester.ac.uk/library/aboutus/regulations>

The Author

As a Senior Exhibitioner in Mathematics at Peterhouse, Cambridge, the author was awarded *Senior Optime* (Class II honours) in Part 2 of the Mathematical Tripos in 1968. On going down, he served in the Royal Navy as an Instructor Officer specialising in teaching Mathematics to skilled ratings and working on Programmed Learning techniques and also on computers and radar. He then taught Mathematics at Wycliffe College, Stonehouse, Glos, before going on to The King's School, Worcester where he was Head of the Mathematics Department for 24 years. He retired from teaching in 2006 when he joined the Particle Physics Group in the School of Physics and Astronomy at the University of Manchester as a part-time graduate student.

He is married to Ruth and has two married sons and four grandchildren.

Acknowledgements

I should like to thank all those in the Particle Physics Group and those at the Jodrell Bank Centre for Astrophysics for the help they have given me in their various ways. Especially to be mentioned must be Professor Fred Loebinger who initially made me very welcome and is instrumental, I believe, in making the Particle Physics Group very friendly. Even when he had not, he always had time to answer my mundane questions. Being part-time and remote in Worcester, for most of the time, means I have not mixed at all with other graduate students so he and others have been the butt of my questions when a full-time student would normally have asked a student colleague. I suppose it has helped that we are virtually the same age.

Also to be thanked are two very important people: Ann Morrow, Particle Physics Secretary, who has been helpful to me, and Sabah Salih, the Group's incredible computing man, who has helped on many occasions to sort out my computing woes. Both these people are treasures; thank you.

Then there are my two supervisors, Professors Jeff Forshaw and Richard Battye, two able and talented people who helped lift me from the abyss of not knowing anything about Cosmology to knowing a little more. While it has not been easy, I have learned much from them and I owe them a debt of gratitude.

I must also thank my Rotary club, the Rotary Club of Worcester South, for allowing me leave of absence for the last few months when I was writing this thesis. Especially, I must thank the two gentlemen of the club who took over my major responsibilities for the duration.

I could not bring this to a close if I did not thank my dear wife, Ruth. She has been unstinting in allowing me to work over the past seven years, uninterrupted, in my study.

Glossary

AU – Astronomical Unit = 1.5×10^8 km.

BCS – Blanco Cosmology Survey.

CDM – Cold dark matter.

COBE – Cosmic Background Explorer satellite. It was launched in November 1989 to measure infra-red and microwave radiation from the early Universe. It carried three instruments, a Diffuse Infrared Background Experiment (DIRBE) to search for the cosmic infrared background radiation, a Differential Microwave Radiometer (DMR) to map the cosmic radiation sensitively, and a Far Infrared Absolute Spectrophotometer (FIRAS) to compare the spectrum of the cosmic microwave background radiation with a precise blackbody [1, 2].

Expansion scale factor – the dimensionless parameter, a , which measures the expansion of the Universe. Today, a is defined as 1; the history of the Universe, to date, is described by $0 \leq a \leq 1$. Its natural logarithm is denoted by N .

Ghost – particle whose Hamiltonian contains negative energy terms.

GR – General Relativity represented in modified gravity by $F(R) = R$.

Hubble constant – today's value of the Hubble parameter. The Planck best fit value is $H_0 = 67.11 \text{ km s}^{-1} \text{ Mpc}^{-1}$.

Hubble parameter, H , – defined as \dot{a}/a , which measures the relative rate of expansion of the Universe. It has dimensions $[T^{-1}]$.

Λ CDM – cold dark matter with constant dark energy density represented in modified gravity by $F(R) = R - 2\Lambda$. Λ is termed the *cosmological constant* which could explain the accelerated expansion of the Universe. It is sometimes termed standard Einstein Gravity.

LSS– Large Scale Structure. On scales smaller than the scale of the Universe, galaxies and clusters of galaxies formed as a result of gravitational collapse in regions of higher average density which were, themselves, caused by perturbations early in the history of the Universe.

MACS – Massive Cluster Survey.

Newtonian gauge – a perturbation of the FRW metric. See equation (5.1).

The phantom divide – the line $w_{\text{eff}} = -1$.

Planck – a space observatory operated by the European Space Agency (ESA), and designed to observe anisotropies of the cosmic microwave background (CMB) at microwave and infra-red frequencies, with high sensitivity and small angular resolution. It began operation in 2009 and complemented and improved on WMAP measurements. Its results were published in February 2013 [3].

REFLEX – ROSAT-ESO Flux-Limited X-Ray galaxy cluster survey.

Ricci or curvature scalar, R , – a measure of the curvature of space-time due to energy sources in the Universe. It has dimensions $[T^{-2}]$.

R_{eq} – the value of the Ricci scalar at equality. This is when the radiation density equals the matter density. $R_{\text{eq}} \approx 3 \times 10^{10} H_0^2$.

R_Λ – the value of the Ricci scalar under Λ CDM.

R_s – the value of the Ricci scalar at the Solar System. In this thesis it is taken to have the value $10^6 H_0^2$.

ROSAT – the Röntgen Satellite, was an X-ray observatory developed through a cooperative program between Germany, the United States, and the United Kingdom.

Scalaron Mass – defined as M via $M^2 = \frac{F_R(R) - RF_{RR}(R)}{3F_{RR}(R)} \approx \frac{1}{3F_{RR}(R)}$. M has dimensions $[T^{-1}]$.

Solar System constraint – the constraint on the parameters of a model by the need for $R_s F_{RR}(R_s) \ll 10^{-23}$.

Today – in cosmological terms, the current time denoted by suffix 0 so that X_0 is the value of the variable X , today. The value of Ω_m , today, is denoted by $\Omega_{m,0}$. Today, $a = 1$ and $N = 0$.

WMAP – the NASA Wilkinson Microwave Anisotropy Probe launched in 2001 with the first results in February 2003 [4, 5] with a nine year update published in June 2013 [6, 7].

Useful Expressions

In a flat FRW Universe:

$$\begin{aligned}
 H &= \frac{\dot{a}}{a} \\
 N &= \log a \\
 ' &= \frac{d}{dN} \\
 \frac{d}{dt} &= H \frac{d}{dN} \\
 \rho_{\text{crit}} &= \frac{3H^2}{8\pi G} \\
 &= \rho_r + \rho_m + \rho_{\text{eff}} \\
 3H^2 &= 8\pi G\rho_r + 8\pi G\rho_m + 8\pi G\rho_{\text{eff}} \\
 \Omega_r &= \frac{\rho_r}{\rho_{\text{crit}}} = \frac{8\pi G\rho_r}{3H^2} \\
 \Omega_m &= \frac{\rho_m}{\rho_{\text{crit}}} = \frac{8\pi G\rho_m}{3H^2} \\
 \Omega_{\text{eff}} &= 1 - \Omega_m - \Omega_r \\
 &= \frac{8\pi G\rho_{\text{eff}}}{3H^2} \\
 w_{\text{eff}} &= -1 - \frac{\rho'_{\text{eff}}}{3\rho_{\text{eff}}} \\
 w_{\text{eff}}\Omega_{\text{eff}} &= -1 - \frac{2H'}{3H} - \frac{H_0^2 e^{-4N}\Omega_{r,0}}{3H^2} \\
 H^2 &= H_0^2 e^{-4N}\Omega_{r,0} + H_0^2 e^{-3N}\Omega_{m,0} + \frac{8\pi G\rho_{\text{eff}}}{3}
 \end{aligned}$$

$$\begin{aligned}
R &= 12H^2 + 6\dot{H} \\
&= 12H^2 + 6HH' \\
&= 3H_0^2 e^{-3N} \Omega_{m,0} + 8\pi G (4\rho_{\text{eff}} + \rho'_{\text{eff}}) \\
&= 3H_0^2 e^{-3N} \Omega_{m,0} + 8\pi G \rho_{\text{eff}} (1 - 3w_{\text{eff}}) \\
&= 3H^2 (1 - 3w_{\text{eff}} \Omega_{\text{eff}}) - 3H_0^2 e^{-4N} \Omega_{r,0} \\
\frac{\ddot{a}}{a} &= -\frac{4\pi G}{3} (2\rho_r + \rho_m + (1 + 3w_{\text{eff}}) \rho_{\text{eff}}) \\
\ddot{a} > 0 \Rightarrow w_{\text{eff}} &< -\frac{1 + \Omega_r}{3\Omega_{\text{eff}}}
\end{aligned}$$

*For Ruth and our grandchildren,
Charlotte, Hannah, Danny and Sophie*

Chapter 1

Introduction to Gravitational Theories and Cosmology

1.1 Introduction

This thesis is about some aspects of modifying the gravitational theory of General Relativity (GR) in the light of some well known problems. GR is not a particle theory but makes the suggestion that matter and other energy sources curve space-time which puts it at variance with traditional, Galilean and Newtonian mechanics. However, low energy, non-relativistic sources must and do, in their effects, tend to their Newtonian counterparts.

What we consider in this thesis are some aspects of what is termed $F(R)$ gravity but first, in this chapter, we review GR and consider a very brief history of the Universe. We then look at what is termed dark energy, consider a couple of perceived problems, consider matter perturbations and list the constraints which act on $F(R)$ models.

1.2 General Relativity

1.2.1 General Relativity, covariant derivatives, energy-momentum tensor

Our starting point [8–11] is to generalise Poisson’s equation $\nabla^2\Phi = 4\pi G\rho$ for mass density ρ ; Φ is the equivalent of the Newtonian potential such that, for a single mass m , it produces a gravitational potential a distance r away from it of $\Phi = -Gm/r$, G being Newton’s gravitational constant. We wish to find the General Relativity (GR) equivalent of Poisson’s equation. It is a second order differential equation which, in GR, should be a tensorial equation. It will become a second order differential equation involving the covariant derivative, ∇_μ . As is usual, let the metric for GR be $g_{\mu\nu}$ such that

$$ds^2 = g_{\mu\nu}dx^\mu dx^\nu, \quad (1.1)$$

with x^0 representing time and x^i being the space components. We use the convention $(-1, 1, 1, 1)$ for the signature of the metric and put $c = 1$.

The covariant derivative is defined on a vector V^μ via the Levi-Civita connection

$$\nabla_\mu V^\nu = \partial_\mu V^\nu + \Gamma^\nu_{\mu\lambda} V^\lambda, \quad (1.2)$$

where $\Gamma^\nu_{\mu\lambda}$ are termed the Christoffel symbols of the second kind. On a scalar, ϕ , this reduces to

$$\nabla_\mu \phi = \partial_\mu \phi. \quad (1.3)$$

Applied to tensor $T^{\mu\nu}$, it gives

$$\nabla_\mu T^{\nu\rho} = \partial_\mu T^{\nu\rho} + \Gamma^\nu_{\mu\lambda} T^{\lambda\rho} + \Gamma^\rho_{\mu\lambda} T^{\mu\lambda}. \quad (1.4)$$

A property we use is that the covariant derivative of the metric is zero, i.e., $\nabla_\rho g_{\mu\nu} = 0$. This means that $\nabla_\rho g^{\mu\nu} = 0$ and that the Levi-Civita connection can,

as a result, be defined by

$$\Gamma^\sigma_{\mu\nu} = \frac{1}{2}g^{\sigma\rho}(\partial_\mu g_{\nu\rho} + \partial_\nu g_{\rho\mu} - \partial_\rho g_{\mu\nu}). \quad (1.5)$$

In (1.4), we have used the torsion-free requirement that $\Gamma^\lambda_{\nu\mu} = \Gamma^\lambda_{\mu\nu}$. This being the case, we describe the connection as being torsion free. If this were not true we could form the ‘‘torsion tensor’’, $\Gamma^\lambda_{\mu\nu} - \Gamma^\lambda_{\nu\mu}$, which is anti-symmetric in its lower indices [11].

Now the tensor equivalent to the mass density ρ is the energy-momentum tensor, $T_{\mu\nu}$, mass and energy being synonymous in Special Relativity. It is defined by

$$T_{\mu\nu} = -\frac{2}{\sqrt{-g}} \frac{\delta(\sqrt{-g}) \mathcal{L}_M}{\delta g^{\mu\nu}}, \quad (1.6)$$

in which \mathcal{L}_M is the Lagrangian for all the physical fields contributing energy to the Universe and g is the determinant of $g_{\mu\nu}$.

In cosmology we assume the expansion of the Universe is controlled by the presence of perfect fluids. A perfect fluid is completely specified by its rest-frame density ρ and isotropic rest-frame pressure P . When the fluid has four-velocity U^μ the energy-momentum tensor can be expressed as

$$T_{\mu\nu} = (\rho + P)U_\mu U_\nu + P g_{\mu\nu}. \quad (1.7)$$

With respect to comoving coordinates, $U^\mu = (1, 0, 0, 0)$, $T^\mu_{\nu} = \text{diag}(-\rho, P, P, P)$. In Special Relativity, the energy-momentum conservation equation is $\partial_\mu T^{\mu\nu} = 0$. In GR, this becomes $\nabla_\mu T^{\mu\nu} = 0$ from which also follows $\nabla^\mu T_{\mu\nu} = 0$.

1.2.2 The Riemann tensor and curvature and the Einstein tensor

The Riemann tensor quantifies the curvature of space-time. It is $R_{\rho\sigma\mu\nu} = g_{\rho\lambda} R^\lambda_{\sigma\mu\nu}$ where

$$R^\rho_{\sigma\mu\nu} = \partial_\mu \Gamma^\rho_{\sigma\nu} - \partial_\nu \Gamma^\rho_{\sigma\mu} + \Gamma^\rho_{\lambda\mu} \Gamma^\lambda_{\sigma\nu} - \Gamma^\rho_{\lambda\nu} \Gamma^\lambda_{\sigma\mu}. \quad (1.8)$$

It has the following properties:

$$R_{\rho\sigma\mu\nu} = -R_{\sigma\rho\mu\nu}, \quad (1.9)$$

$$R_{\rho\sigma\mu\nu} = -R_{\rho\sigma\nu\mu}, \quad (1.10)$$

$$R_{\rho\sigma\mu\nu} = R_{\mu\nu\rho\sigma}, \quad (1.11)$$

$$R_{\rho\sigma\mu\nu} + R_{\rho\mu\nu\sigma} + R_{\rho\nu\sigma\mu} = 0. \quad (1.12)$$

The Bianchi identity holds:

$$\nabla_\lambda R_{\rho\sigma\mu\nu} + \nabla_\rho R_{\sigma\lambda\mu\nu} + \nabla_\sigma R_{\lambda\rho\mu\nu} = 0. \quad (1.13)$$

By contracting the Riemann tensor, the Ricci tensor is formed:

$$R_{\mu\nu} = R^\lambda{}_{\mu\lambda\nu}, \quad (1.14)$$

and the trace of this is the Ricci or curvature scalar:

$$R = g^{\mu\nu} R_{\mu\nu}. \quad (1.15)$$

Contracting the Bianchi identity twice:

$$g^{\mu\lambda} g^{\nu\sigma} (\nabla_\lambda R_{\rho\sigma\mu\nu} + \nabla_\rho R_{\sigma\lambda\mu\nu} + \nabla_\sigma R_{\lambda\rho\mu\nu}) = 0 \quad (1.16)$$

$$\Rightarrow \nabla^\mu R_{\rho\mu} - \nabla_\rho R + \nabla^\nu R_{\rho\nu} = 0 \quad (1.17)$$

$$\iff \nabla^\mu R_{\rho\mu} = \frac{1}{2} \nabla_\rho R. \quad (1.18)$$

From the Ricci tensor and the Ricci scalar is defined the Einstein tensor:

$$G_{\mu\nu} = R_{\mu\nu} - \frac{1}{2} g_{\mu\nu} R. \quad (1.19)$$

From (1.18), we see that $\nabla^\mu G_{\mu\nu} = 0$, just as $\nabla^\mu T_{\mu\nu} = 0$.

1.2.3 Formulation of the Einstein equations

In view of the property expressed in (1.19), and that we want a tensor indicating the curvature of space-time to relate to the energy-momentum tensor, we consider the equality

$$G_{\mu\nu} = \kappa T_{\mu\nu} \quad (1.20)$$

where $\kappa = 8\pi G$, and see if this is viable as a law of Physics. Let us consider our local, Minkowskian, frame of reference with metric $\eta_{\mu\nu}$ which the gravitational effects of static, local masses have altered to $g_{\mu\nu}$. It will be a small effect so we shall consider only first-order changes to $\eta_{\mu\nu}$. For matter, by which we mean baryons and dark matter, $P = 0$ and the energy-momentum tensor is given by $T^\mu{}_\nu = \text{diag}(-\rho, 0, 0, 0)$ and the trace of (1.20) gives $R = -\kappa T = \kappa\rho$.

The 00 component of (1.20) gives:

$$R_{00} + \frac{1}{2}R = \kappa\rho \quad (1.21)$$

$$\iff R_{00} = \frac{1}{2}\kappa\rho \quad (1.22)$$

Now, and since we can ignore time derivatives in a static field,

$$R_{00} = R^\lambda{}_{0\lambda 0} \quad (1.23)$$

$$= R^i{}_{0i0} \quad (1.24)$$

$$= \delta_i^i R^i{}_{0j0} \quad (1.25)$$

$$= \delta_{ij} \partial^j \Gamma^i{}_{00}, \text{ to first order,} \quad (1.26)$$

$$= -\frac{1}{2} \partial^i \partial_i g_{00}. \quad (1.27)$$

$g_{00} = -1 + h_{00}$, say, means that, to first order small quantities, $R_{00} = -\nabla^2 h_{00}/2$. This gives, as the 00 component of (1.20),

$$\nabla^2 h_{00} = -\kappa\rho. \quad (1.28)$$

Thus, identifying $-h_{00}/2$ with Φ gives Newtonian gravity, i.e., the Einstein equation reduces in the weak field limit to

$$\nabla^2 \Phi = \frac{\kappa}{2} \rho \quad (1.29)$$

$$= 4\pi G \rho. \quad (1.30)$$

We also have the possibility that, more generally,

$$G_{\mu\nu} = R_{\mu\nu} - \frac{1}{2}g_{\mu\nu}R = 8\pi G T_{\mu\nu}. \quad (1.31)$$

These are Einstein's equations. The trace of them gives

$$R = -8\pi GT \quad (1.32)$$

$$= 8\pi G(\rho - 3P). \quad (1.33)$$

1.2.4 The FRW metric and the Ricci scalar

Observation of the Universe suggests that a good, large-scale model is to be had by postulating it to be expanding and, on average, spatially homogeneous and isotropic, that is, that matter is spread out uniformly throughout the Universe in all directions no matter from which point of the manifold one is looking. Observations support the idea that space-time has no intrinsic curvature of its own which is thus described as being *flat*, which will be assumed throughout this thesis. In the past this has been perceived as being a problem and is discussed in [12]. The assumptions that the Universe is flat, homogeneous, isotropic and expanding is incorporated in the Friedmann-Lemaître-Robertson-Walker (FRW) metric defined by $g_{\mu\nu} = \text{diag}(-1, a^2, a^2, a^2)$. a is a parameter termed the *expansion scale factor* of the Universe. Initially, at the Big Bang, $a = 0$ and it increases with time to become, by definition, $a = 1$, today. For reviews see, for example, [13, 14].

The relative expansion rate of the Universe is the Hubble parameter, $H = \dot{a}/a$. If H is known, we can compute the age of the Universe. Today's value is H_0 determined in the recent Planck Collaboration as $H_0 = 100 h \text{ kms}^{-1}\text{Mpc}^{-1} = 67.4 \pm 1.4 \text{ kms}^{-1}\text{Mpc}^{-1}$ [15–17].

Denoting da/dt by \dot{a} , gives the following as the only non-zero Christoffel symbols:

$$\Gamma^0_{11} = \Gamma^0_{22} = \Gamma^0_{33} = a\dot{a}. \quad (1.34)$$

$$\Gamma^1_{10} = \Gamma^1_{01} = \Gamma^2_{20} = \Gamma^2_{02} = \Gamma^3_{30} = \Gamma^3_{03} = \frac{\dot{a}}{a}. \quad (1.35)$$

Replacing \dot{a} by aH , these Christoffel symbols lead to the Riemann tensor as

$$R_{\mu\nu} = \text{diag} \left(-\frac{3\ddot{a}}{a}, a\ddot{a} + 2\dot{a}^2, a\ddot{a} + 2\dot{a}^2, a\ddot{a} + 2\dot{a}^2 \right) \quad (1.36)$$

$$= \text{diag} \left(-3 \left(H^2 + \dot{H} \right), a^2 \left(3H^2 + \dot{H} \right), a^2 \left(3H^2 + \dot{H} \right), a^2 \left(3H^2 + \dot{H} \right) \right) \quad (1.37)$$

and the Ricci scalar as $R = 12H^2 + 6\dot{H}$.

1.2.5 Density, pressure and equation of state

In the expression for the energy-momentum tensor in subsection 1.2.1, mention is made of the energy density, ρ , and associated pressure, P , of the perfect fluids which are present in the Universe at any time. These fluids are radiation, in the form of photons, and other relativistic species, with density ρ_r , and matter, with density ρ_m . Some authors also admit to a vacuum or dark energy of density ρ_{vac} . Dark energy is discussed in subsection 1.4.4. Each fluid may exert a pressure and pressure is connected to fluid density by an equation of state, $P = w\rho$. w is termed the equation of state parameter and could vary with time, as we shall see. For radiation, $w = 1/3$ so that $P_r = \rho_r/3$, for matter $w = 0$ so $P_m = 0$, while for the vacuum, $w = -1$ so that $P_{\text{vac}} = -\rho_{\text{vac}}$.

Looking at the 0 component the conservation of energy equation, $\nabla^\mu T_{\mu\nu} = 0$, gives

$$\nabla^\mu T_{\mu 0} = 0, \quad (1.38)$$

$$\Rightarrow \partial_\mu T^\mu_0 + \Gamma^\mu_{\mu\lambda} T^\lambda_0 - \Gamma^\lambda_{\mu 0} T^\mu_\lambda = 0, \quad (1.39)$$

$$\iff -\partial_0 \rho - 3H(\rho + P) = 0. \quad (1.40)$$

using (1.34) and (1.35). (1.40) is true for each fluid in the energy-momentum tensor so that we have, for each,

$$\dot{\rho} = -3H(1 + w)\rho. \quad (1.41)$$

If w is constant for any fluid then we can integrate (1.41) to

$$\rho = \rho_0 a^{-3(1+w)}, \quad (1.42)$$

where ρ_0 is a constant of integration. Thus for radiation, $\rho_r \propto a^{-4}$, for matter, $\rho_m \propto a^{-3}$, and the density of the vacuum, ρ_{vac} , is constant.

1.2.6 The Friedmann equations

If we say that the densities and pressures in the energy-momentum tensor are given by ρ and by P , respectively, solving the Einstein equations gives, from the 00 component

$$3H^2 = 8\pi G\rho, \quad (1.43)$$

$$\iff \left(\frac{\dot{a}}{a}\right)^2 = \frac{8\pi G}{3}\rho, \quad (1.44)$$

which is referred to as the *Friedmann equation*. The ij components give

$$3H^2 + 2\dot{H} = -8\pi GP, \quad (1.45)$$

$$\Rightarrow \frac{\ddot{a}}{a} = -\frac{4\pi G}{3}(\rho + 3P). \quad (1.46)$$

This last equation is referred to as the *second Friedmann equation*.

1.2.7 Einstein equations derived from the action

There is an alternative way, proposed by Hilbert [10, 18], of deriving the Einstein equations and that is by considering the total action of the gravitational field and the action due to sources of energy, of whatever kind, which we call matter fields. Let the total action be $S = S_G + S_M$. The gravitational part of the action is defined to be

$$S_G = \frac{1}{2\kappa} \int d^4x \sqrt{-g} R, \quad (1.47)$$

where $\kappa = 8\pi G$, as in section 1.2.3, above. The action for the matter fields is

$$S_M = \frac{1}{2\kappa} \int d^4x \sqrt{-g} \mathcal{L}_M, \quad (1.48)$$

where \mathcal{L}_M is the Lagrangian for the matter fields and it is connected to the energy-momentum tensor by equation (1.6). Varying S_G with respect to the inverse metric, $g^{\mu\nu}$,

$$\delta S_G = \frac{1}{2\kappa} \int d^4x \delta(\sqrt{-g} R) \quad (1.49)$$

$$= \frac{1}{2\kappa} \int d^4x \delta(\sqrt{-g} g^{\mu\nu} R_{\mu\nu}) \quad (1.50)$$

$$= \frac{1}{2\kappa} \int d^4x [\delta(\sqrt{-g}) g^{\mu\nu} R_{\mu\nu} + \sqrt{-g} \delta(g^{\mu\nu}) R_{\mu\nu} + \sqrt{-g} g^{\mu\nu} \delta R_{\mu\nu}]. \quad (1.51)$$

Without going into too much detail,

$$\delta\sqrt{-g} = -\frac{1}{2\sqrt{-g}} \delta g \quad (1.52)$$

$$= -\frac{g}{2\sqrt{-g}} g^{\mu\nu} \delta g_{\mu\nu} \quad (1.53)$$

$$= -\frac{\sqrt{-g}}{2} g_{\mu\nu} \delta g^{\mu\nu}. \quad (1.54)$$

$$\delta R_{\mu\nu} = \delta R^{\lambda}_{\mu\lambda\nu} \quad (1.55)$$

$$= \nabla_{\lambda} \delta \Gamma^{\lambda}_{\nu\mu} - \nabla_{\nu} \delta \Gamma^{\lambda}_{\lambda\mu}, \quad (1.56)$$

$$\Rightarrow g^{\mu\nu} \delta R_{\mu\nu} = \nabla_{\lambda} (g^{\mu\nu} \delta \Gamma^{\lambda}_{\nu\mu}) - \nabla_{\nu} (g^{\mu\nu} \Gamma^{\lambda}_{\lambda\mu}) \quad (1.57)$$

$$= \nabla_{\sigma} [g^{\mu\nu} \delta \Gamma^{\sigma}_{\nu\mu} - g^{\mu\sigma} \delta \Gamma^{\lambda}_{\lambda\mu}]. \quad (1.58)$$

Thus the right hand term of (1.51) gives, by Stokes's Theorem, a boundary term.

We can set the boundary at infinity so this term vanishes. This leaves

$$\delta S_G = \frac{1}{2\kappa} \int d^4x [\delta(\sqrt{-g}) g^{\mu\nu} R_{\mu\nu} + \sqrt{-g} \delta(g^{\mu\nu}) R_{\mu\nu}] \quad (1.59)$$

$$= \frac{1}{2\kappa} \int d^4x \sqrt{-g} \left[-\frac{1}{2} R g_{\mu\nu} + R_{\mu\nu} \right] \delta g^{\mu\nu}. \quad (1.60)$$

For the matter fields,

$$\delta S_M = \int d^4x \frac{\delta(\sqrt{-g} \mathcal{L}_M)}{\delta g^{\mu\nu}} \delta g^{\mu\nu} \quad (1.61)$$

$$= -\frac{1}{2} \int d^4x \sqrt{-g} T_{\mu\nu} \delta g^{\mu\nu}. \quad (1.62)$$

so,

$$\frac{\delta S}{\delta g^{\mu\nu}} = 0, \quad (1.63)$$

$$\Rightarrow R_{\mu\nu} - \frac{1}{2} g_{\mu\nu} R - \kappa T_{\mu\nu} = 0, \quad (1.64)$$

$$\Leftrightarrow R_{\mu\nu} - \frac{1}{2} g_{\mu\nu} R = 8\pi G T_{\mu\nu}. \quad (1.65)$$

Varying the action in this way enables us to produce our own versions of Einstein's equations, which is what we do when we consider actions which modify gravity in section 1.4.

1.3 A brief history of the Universe

When considering the large scale structure of the Universe, as we do with modified gravity, we simply split up its history into the eras when the various energies represented in the energy-momentum tensor dominate. A detailed and scholarly account is given in Kolb and Turner [19]. Initially, there was the radiation era which was followed by the matter era. We include a third, the vacuum era, because the densities of radiation and matter eventually become negligible leaving just the vacuum. Conjectures on the past and future of the Universe are discussed in [20].

1.3.1 The radiation era

It is believed that immediately after the Universe came into being it underwent a brief period of very rapid expansion which smoothed out any original unevenness there might have been. This period is termed *inflation* and lasted until the Universe was about 10^{-32} s old. The radiation era stretched from just after inflation, to around 10^{11} s \approx 3000 years during which time the temperature fell from 10^{13} GeV to 10eV. It ended when the radiation density, which we have seen is proportional to a^{-4} , fell to such an extent that it equated to the matter density which was falling at a slower rate. The point at which this happened is termed *equality*. The following two epochs formed part of the radiation era.

1. Reheating occurred between 10^{-32} s to 1s as the temperature fell from 10^{13} GeV to 10MeV. It saw the creation of a dense soup of quarks, photons, gluons and leptons. Quarks and gluons formed hadrons which decayed to protons, electrons, photons and neutrinos. There was a slight imbalance of matter to antimatter of the order of $1 + 10^{-10} : 1$. This annihilated to leave a small residue of matter plus photons and neutrinos.
2. Big Bang Nucleosynthesis (BBN) then followed in which hydrogen and some of the lighter elements such as deuterium, helium and lithium formed. This epoch lasted until 200s when the temperature decreased to 0.1MeV.

1.3.2 The matter dominated era and the CMB

This era stretched from when the Universe was 3000 years old until it was 10^9 years old. During that time, the temperature fell from 10eV to 10meV. Initially, the Universe was opaque to light but, as cooling progressed, in the process known as *recombination*, when electrons and protons formed the light atoms, photons became decoupled to make the Universe transparent to light. We observe this today as the Cosmic Microwave Background (CMB) at $z \approx 10^3$ [21, 22]. The

CMB was studied in the recent Planck survey [3] following earlier measurements by COBE [23] and WMAP [6, 7]. From the Integrated Sachs-Wolfe (ISW) plateau of the CMB, [24], is determined the value of the dark energy density parameter and its equation of state parameter, [25]. With respect to the potentials, Φ and Ψ in the Newtonian gauge, of chapter 5, Amendola et al., in [26], state that $\Phi + \Psi$ could be measured using the ISW effect and from weak lensing while Ψ might be measured via measurements of the velocities of galaxies. The acoustic peaks of the CMB give us information about the various density parameters. From the first acoustic peak, it is found that the Universe is almost spatially flat, which we assume in this thesis. The second acoustic peak gives constraints on the baryon density and gives a value to the baryon density parameter while the third acoustic peak gives a value for the total matter density parameter.

1.3.3 The vacuum era

This is the era in which we now find ourselves. It commenced at around $z = 9$, 10^9 years after the Big Bang, when stars and galaxies were formed as were the heavier elements via supernovae. In this epoch the expansion of the Universe began to accelerate [27–29].

1.4 Modifying gravity with $F(R)$ gravity models

It is mainly because of the cosmological constant problem (see subsection 1.4.1) but also because observations do not confirm that the effective, or dark energy, equation of state parameter is necessarily equal to -1 , that $F(R)$ gravity models have been studied. It is shown that by exchanging R for $F(R)$ in the gravitational action then, without resorting to any vacuum energy whatsoever, the late, accelerated expansion of the Universe can be accounted for. $F(R)$ gravity models yield an effective energy which replaces the phenomenon known as dark energy.

For a review of $F(R)$ gravity, see [30–34].

In modified $F(R)$ gravity, we obtain the equivalent of the Einstein equations by replacing R in (1.47) with $F(R)$ in the gravitation action. Varying the total action with respect to $g^{\mu\nu}$ gives

$$g_{\mu\nu}\square F_R(R) - \nabla_\mu\nabla_\nu F_R(R) + R_{\mu\nu}F_R(R) - \frac{1}{2}g_{\mu\nu}F(R) = 8\pi GT_{\mu\nu}, \quad (1.66)$$

where $F_R(R)$ denotes $dF(R)/dR$ and $T_{\mu\nu}$ contains only contributions from radiation and matter. These are the field equations for $F(R)$ and are the modified gravity equivalent to the Einstein equations. It can be seen that putting $F(R) = R$ reduces (1.66) to the Einstein equations, (1.31).

Equation (1.66) can be derived as follows. Using the notation of subsection 1.2.7,

$$S_G = \frac{1}{2\kappa} \int d^4x \sqrt{-g} F(R), \quad (1.67)$$

$$\Rightarrow \delta S_G = \frac{1}{2\kappa} \int d^4x [F(R)\delta\sqrt{-g} + \sqrt{-g}\delta F(R)] \quad (1.68)$$

$$= \frac{1}{2\kappa} \int d^4x \sqrt{-g} \left[-\frac{1}{2}g_{\mu\nu}F(R)\delta g^{\mu\nu} + F_R(R)\delta(g^{\mu\nu}R_{\mu\nu}) \right] \quad (1.69)$$

$$= \frac{1}{2\kappa} \int d^4x \sqrt{-g} \left[-\frac{1}{2}g_{\mu\nu}F(R)\delta g^{\mu\nu} + F_R(R)R_{\mu\nu}\delta g^{\mu\nu} + F_R(R)g^{\mu\nu}\delta R_{\mu\nu} \right], \quad (1.70)$$

using (1.54) and (1.15). The right hand term of (1.70) is

$$\begin{aligned} \frac{1}{2\kappa} \int d^4x \sqrt{-g} F_R(R) g^{\mu\nu} \delta R_{\mu\nu} &= \frac{1}{2\kappa} \int d^4x \sqrt{-g} F_R(R) \nabla_\sigma [g^{\mu\nu} \delta \Gamma^\sigma_{\mu\nu} - g^{\mu\sigma} \delta \Gamma^\lambda_{\lambda\mu}] \\ &= \frac{1}{2\kappa} \int d^4x \sqrt{-g} F_R(R) [g_{\mu\nu} \square \delta g^{\mu\nu} - \nabla_\mu \nabla_\nu \delta g^{\mu\nu}] \\ &= \frac{1}{2\kappa} \int d^4x \sqrt{-g} [g_{\mu\nu} \square F_R(R) - \nabla_\mu \nabla_\nu F_R(R)] \delta g^{\mu\nu}, \end{aligned} \quad (1.71)$$

using (1.58) and after some manipulation involving integration by parts and employing Stoke's Theorem [35, 36]. Thus,

$$\delta S_G = \frac{1}{2\kappa} \int d^4x \sqrt{-g} \left[-\frac{1}{2} g_{\mu\nu} F(R) + R_{\mu\nu} F_R(R) + g_{\mu\nu} \square F_R(R) - \nabla_\mu \nabla_\nu F_R(R) \right] \delta g^{\mu\nu} \quad (1.72)$$

from which, using (1.63), (1.66) follows.

Taking the 00 component of (1.66) gives

$$-\square F_R(R) - \frac{d^2 F_R(R)}{dt^2} + R_{00} F_R(R) + \frac{1}{2} F(R) = 8\pi G T_{00}. \quad (1.73)$$

Now, for the FRW metric of subsection 1.2.4, $\square = -\partial_0^2 - 3H\partial_0$, as there is no spatial dependence. Thus,

$$3H \frac{d}{dt} F_R(R) - 3 \left(H^2 + \dot{H} \right) F_R(R) + \frac{1}{2} F(R) = 8\pi G (\rho_r + \rho_m), \quad (1.74)$$

$$\iff -3H\dot{R}F_{RR}(R) + 3 \left(H^2 + \dot{H} \right) F_R(R) - \frac{1}{2} F(R) = -8\pi G (\rho_r + \rho_m), \quad (1.75)$$

where $F_{RR}(R) = d^2 F(R)/dR^2$. Taking the trace of (1.66), gives

$$\begin{aligned} 3\square F_R(R) + R F_R(R) - 2F(R) &= 8\pi G T \\ &= 8\pi G (-\rho + 3P), \end{aligned} \quad (1.76)$$

in which, of course, the only pressure term on the right hand side is due to radiation. Observe that (1.75) is a second order differential equation in $F(R)$ while (1.76) is third order. When we come to solving such equations we shall generally solve (1.75) which will be loosely referred to as the *field equation*.

1.4.1 A special case

If we put $F(R) = R - 2\Lambda$, where Λ is some constant, into (1.66) we have

$$R_{\mu\nu} - \frac{1}{2} g_{\mu\nu} R + \Lambda g_{\mu\nu} = 8\pi G T_{\mu\nu}. \quad (1.77)$$

It is noticed that Einstein could have had these as his original equations in place of (1.19) because the covariant derivative of the left hand side is zero just as it is for the left hand side of (1.19).

If we subtract $\Lambda g_{\mu\nu}$ from both sides and absorb the term into the energy-momentum tensor, comparing the new equation with (1.19) would suggest that Λ could be thought of as contributing to the density of the vacuum, i.e., $\Lambda = 8\pi G\rho_{\text{vac}}$. That being the case, substituting $F(R) = R - 2\Lambda$ into the field equation, (1.75) gives $3H^2 = 8\pi G(\rho_r + \rho_m + \rho_{\text{vac}})$, the Friedmann equation. But there is a problem with this.

At late time when the effects of radiation and matter may be considered to be negligible, $H = \dot{a}/a \simeq \sqrt{8\pi G\rho_{\text{vac}}/3}$, which is constant. Solution of this yields a solution for a as an exponential function of time with, $\ddot{a} = aH^2$; i.e., an accelerating, expanding Universe. If we equate $8\pi G\rho_{\text{vac}}$ with $3H_0^2\Omega_{\text{vac}} \approx 2.1H_0^2$, we find that $\rho_{\text{vac}} = 5 \times 10^{-47} \text{ GeV}^4$. The problem is that, if we consider all the energy available in the vacuum, it is of the order of 10^{120} times this [37–39] so why is only a small fraction of the available energy being used to accelerate the expansion? See [40–42] for the history of this. This is a reason why do not accept any vacuum energy in the energy-momentum tensor when we modify gravity. This is not to decry attempts to come to terms with this cosmological problem [43].

Historically, Λ , originally denoted λ , was introduced into the Einstein equations [44] to solve a problem perceived by Lemaître that without it the Universe would expand while, at the time (1916-1919), Einstein thought that the Universe was static. It was abandoned, however, when Hubble discovered, in 1929, that the Universe was expanding. Today, we still make use of Λ and, when we do, we term it the *cosmological constant*. The problem referred to in the previous paragraph is termed *the cosmological constant problem*. We term $F(R) = R - 2\Lambda$ Λ CDM, which is based on GR, with $\Lambda \neq 0$.

1.4.2 A vacuum solution

It is noticed that when all the energy content of the energy-momentum tensor has run out, at the end of the vacuum era, (1.33) gives $R = 0$. This, of course, assumes that there is no residual vacuum energy, then. It is desired that this, too, should be a solution of (1.76). If there is a time independent solution, then we have $R F_R(R) - 2F(R) = 0$ and so $F(0) = 0$. It is also possible that $R F_R(R) - 2F(R) = 0$ has an attractor solution $R > 0$. This is termed the de Sitter solution [45, 46]. There could, instead, be a time-dependent solution which would yield oscillations [47]. See subsection 3.2.1.2 for an example of this.

1.4.3 A modified expression for the Hubble parameter and the effective equation of state

It is clear by comparing (1.75) with (1.77) that modifying gravity will produce a term in the expression for H^2 which might be taken to be a form of energy missing from the energy-momentum tensor. So, rather than using the term, ρ_{vac} , which suggests it represents the vacuum, let us term it an effective energy density, ρ_{eff} . We can assume it to have the properties of a perfect fluid with pressure, P_{eff} , and equation of state parameter, w_{eff} , such that $P_{\text{eff}} = w_{\text{eff}}\rho_{\text{eff}}$ and $\dot{\rho}_{\text{eff}} = -3H(1 + w_{\text{eff}})\rho_{\text{eff}}$. In allusion to the earlier expression we had for H^2 , namely, $3H^2 = 8\pi G(\rho_r + \rho_m + \rho_{\text{vac}})$ let

$$H^2 = \frac{8\pi G}{3}(\rho_r + \rho_m + \rho_{\text{eff}}), \quad (1.78)$$

$$\iff \rho_{\text{crit}} = \rho_r + \rho_m + \rho_{\text{eff}}. \quad (1.79)$$

where $8\pi G\rho_{\text{crit}} = 3H^2$. Define also the density parameters for radiation and matter by $\Omega_r = \rho_r/\rho_{\text{crit}}$ and $\Omega_m = \rho_m/\rho_{\text{crit}}$, respectively, and replace $\rho_{\text{eff}}/\rho_{\text{crit}}$ by Ω_{eff} , and we have

$$1 = \Omega_r + \Omega_m + \Omega_{\text{eff}}. \quad (1.80)$$

We define Ω_{eff} from (1.80) and it equals $8\pi G\rho_{\text{eff}}/(3H^2)$. We know from subsection 1.2.5 that $\rho_r = \rho_{r,0}a^{-4}$ and $\rho_m = \rho_{m,0}a^{-3}$, where $\rho_{r,0}$ and $\rho_{m,0}$ are today's values of ρ_r and ρ_m , respectively, because we define today by putting $a = 1$. This leads us to

$$H^2 = \frac{8\pi G}{3} (\rho_{r,0}a^{-4} + \rho_{m,0}a^{-3} + \rho_{\text{eff}}) \quad (1.81)$$

$$= H_0^2 (\Omega_{r,0}a^{-4} + \Omega_{m,0}a^{-3}) + \frac{8\pi G}{3} \rho_{\text{eff}}, \quad (1.82)$$

where H_0 is today's value of the Hubble parameter, termed the Hubble constant.

In this thesis, rather than taking time to be our universal parameter, we use $N = \log a$, which is dimensionless. If we denote differentiation with respect to N by $'$, then $d/dt = Hd/dN$ so that $\dot{g} = Hg'$, for generic function $g(t)$. Then

$$\dot{\rho}_{\text{eff}} = -3H(1 + w_{\text{eff}})\rho_{\text{eff}} \quad (1.83)$$

$$\Rightarrow w_{\text{eff}} = -1 - \frac{\rho'_{\text{eff}}}{3\rho_{\text{eff}}} \quad (1.84)$$

from which follows

$$w_{\text{eff}}\Omega_{\text{eff}} = -1 - \frac{2H'}{3H} - \frac{H_0^2 e^{-4N}\Omega_{r,0}}{3H^2} \quad (1.85)$$

$$\approx -1 - \frac{2H'}{3H}, \text{ in the matter and vacuum eras.} \quad (1.86)$$

In $F(R)$ models, it is a fact that w_{eff} decreases very slowly from being -1 at the start of the radiation era and continues to become more negative into the matter era. This is proved in Chapter 4. We say that, at early times, w_{eff} lies below the *phantom divide* so that $w_{\text{eff}} < -1$ for much of its history and until recent times [48–50].

1.4.4 Dark energy

Dark energy [37, 51–53] is the name given to what might be vacuum energy or the effective energy derived from the geometrical nature of modifying gravity.

It was mooted, in 1998, after the discovery that the Universe's expansion was accelerating [40, 54, 55]. Without dark energy [56], the expansion would slow down and eventually come to a halt as matter runs out. Dark energy is defined to be the fluid which causes the expansion of the Universe to accelerate. Theories suggest that it was dark energy which was responsible for the initial inflation of the Universe [12] but we are concerned with what happened after inflation and since the beginning of the radiation era. It has been known for a long time that the equation of state parameter for dark energy, which we dub, w_{eff} , is close to -1 suggesting that ρ_{eff} , if it varies, varies slowly and eventually becomes the dominant energy in the Universe as the matter density, being proportional to a^{-3} , continues to decrease [57].

Possible ways of accounting for dark energy are contained in [37, 52, 58–63]. In this thesis the $F(R)$ gravity option has been studied but there are two other main contenders.

1.4.4.1 The cosmological constant

This is a strong contender to explain the accelerated expansion of the Universe as even the latest measurements [3, 17] do not rule it out. The measurements are not definitive in making the equation of state parameter tightly constrained around -1 but have $w_{\text{vac},0} = -1.04_{-0.69}^{+0.72}$ at the 95% significance level and $dw_{\text{vac},0}/da < 1.32$, at the same level when pure ΛCDM would give $dw_{\text{vac},0}/da = 0$.

There is, however, the cosmological constant problem to worry about as mentioned in subsection 1.4.1.

1.4.4.2 Quintessence

Briefly, in this theory, dark energy is modelled by a slow-rolling scalar field ϕ coupled to potential $V(\phi)$ [64–67]. The equation of state parameter is given by

$$1 + w_{\text{vac}} = \frac{\dot{\phi}^2}{\dot{\phi}^2/2 + V(\phi)}. \quad (1.87)$$

Initially, at high z , $\dot{\phi} \sim 0$, because we have Λ CDM. As time progresses, $\dot{\phi}^2$ increases and, providing $V(\phi) > 0$, so does $1 + w_{\text{vac}}$, that is $1 + w_{\text{vac}} > 0$, for all time. Some quintessence models have a phantom potential, $V(\phi) < 0$, which must decrease such that $V(\phi) < -\dot{\phi}^2/2$. In this case, $1 + w_{\text{vac}} < 0$ for all time. So one feature of quintessence models is that w_{vac} remains firmly on one side of the phantom divide. This is unlike the case for $F(R)$ models for which the effective equivalent to w_{vac} is less than -1 before the present day [68].

1.4.4.3 Effective dark energy

If we let $F(R) = R + f(R)$, substitute it into equation (1.66) and rearrange it so that it resembles the form of (1.65), where the left hand sides of both equations agree, we could say that $F(R)$ gravity creates a fluid; effective dark energy with density ρ_{eff} . It also has equation of state parameter, w_{eff} , and density parameter, Ω_{eff} as have been mentioned at the beginning of this subsection. One aspect of effective dark energy is that, for models which tend to Λ CDM as $R \rightarrow \infty$, w_{eff} starts from being -1 , decreases into the phantom zone and continues to do so until a local minimum is reached when it returns to be closer to -1 today, [48, 69].

1.4.5 The modified gravity particle

Associated with $F(R)$ gravity is a massive particle dubbed the *scalaron* [70] which has mass M defined by

$$M^2 = \frac{F_R(R) - RF_{RR}(R)}{3F_{RR}(R)}. \quad (1.88)$$

Owing to the various constraints on $F(R)$, this is often approximated to $M^2 = 1/[3F_{RR}(R)]$. Generally, $F(R)$ does not deviate greatly from Λ CDM, for which $F(R) = R - 2\Lambda$, so the mass of the scalaron is generally large. For models where the deviation from Λ CDM increases with time, then the mass of the scalaron decreases with time.

Where there are oscillations of the weak field potentials (Chapter 5), the frequency of oscillation is shown to be proportional to $1/M$ at high z , in the early stages of the matter era, which increases as z increases backwards in time.

1.4.6 The coincidence problem

This is simply the question as to why is $\Omega_{\text{eff},0} \approx 0.7$ of the same order of magnitude as Ω_m . If we look at a graph of Ω'_{eff} against N , Figure 1.1, we see that Ω'_{eff} is close to zero for much of the history and future, so why does “now”, i.e., $a = 1$, $N = 0$, occur when Ω'_{eff} is close to its maximum?

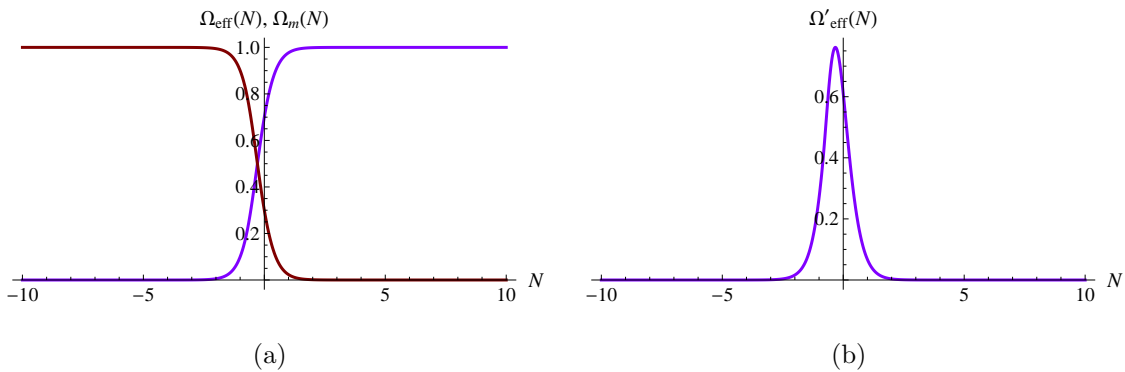


Figure 1.1: The coincidence problem. (a) Evolution of the matter and effective density parameters. (b) Ω'_{eff} against N . The local maximum in Ω'_{eff} occurs at around $z = 0.3$.

1.4.7 The growth of matter and perturbations

In Chapter 3, subsection 3.2.1.3, the standard matter perturbation equation is solved numerically for the various models used in that chapter. It yields the time-dependent parameter, γ , [56, 71–75] which indicates the expansion growth history of matter. γ is termed the *matter growth index* and is very sensitive to models in that different models representing the same expansion history will yield different values of γ at any given stage in the history of the Universe. This is illustrated especially in Figure 2.6 in which the models illustrated share the same Λ CDM history. The matter growth indices for $F(R)$ models show features which are not seen in the matter growth index for Λ CDM. How the Λ CDM matter growth index evolves can be seen in Figure 3.9(b). Ascertaining the value of γ_0 would be evidence in helping decide whether or not Λ CDM is or is not, realistically, the current theory of gravity.

In Chapter 5, we consider how non-relativistic matter sources perturb the FRW metric in the Jordan frame, the frame with FRW metric $g_{\mu\nu}$, to produce matter perturbation potentials. Algebraic approximations, appropriate for all time up to the present, to the defining equations for these potentials are found and compared with numerical solutions to the same equations. Providing the co-moving wavenumber, k , is large enough in the sub-horizon regime, we shall see that there is good agreement.

1.4.8 Constraints on $F(R)$

Constraints on the parameters of $F(R)$ models are explained in [76–79] as follows:

1. $F_R(R) > 0$, otherwise there would be *ghosts*, that is, particles with negative kinetic energy, [80–83].
2. $F_{RR}(R) > 0$, otherwise there would be generic instabilities, and the scalaron

mass would be negative or zero, [84–86].

If it is desired to have $F(R) \rightarrow R - 2\Lambda$, as $R \rightarrow \infty$ then we must have [76]:

3. $F_R(R) < 1$.

4. $F_R(R) \rightarrow 1$ as $R \rightarrow \infty$.

Then there are local gravity constraints, discussed in [33], of which the severest is the Solar System constraint. Local gravity constraints are derived from the effective Newtonian gravitation constant which is derived under a weak field approximation by considering a spherical mass of constant density, ρ , surrounded by matter of very small average density, effectively zero. As shown in [33, 49], using linear perturbation theory in a Minkowskian background with a perturbation $h_{\mu\nu}$ such that F perturbs to $F + \delta F$, F_R perturbs to $F_R + \delta F_R$, etc, this gives for the effective Newtonian gravitation constant

$$G_{\text{eff}} = \frac{G}{F_R(R)} \left(1 + \frac{e^{-Ml}}{3} \right) \quad (1.89)$$

where l is the scale of the experiment and M is the scalaron mass as defined in (1.88), which can be approximated by $M^2 \approx 1/(3F_{RR}(R))$ when $F_R(R) \approx 1$ and $RF_{RR}(R) \ll 1$, which will be true in the high curvature regimes. $Ml \gg 1$ (see [49]) which translates in [87] to

$$m \ll \frac{\rho}{\rho_0} \left(\frac{l}{H_0^{-1}} \right)^2 \quad (1.90)$$

where $m = RF_{RR}(R)/F_R(R) \approx RF_{RR}(R)$.

For the Solar System, the scale of the experiment is $1\text{AU} = 1.5 \times 10^{13}$ cm, $\rho \sim 10^{-23}$ g/cm³ and (1.90) gives $m \ll 10^{-23}$. Using $R = 8\pi G\rho$, this density corresponds to $R \sim 10^6 H_0^2$. Weaker constraints come from the Shapiro time-delay effect and laboratory, Cavendish-type experiments to establish the value of G . In the Shapiro case, $l \sim 7 \times 10^{10}$ cm and $\rho \sim 10^{-15}$ g/cm³ which give $m \ll 10^{-20}$ and $R \sim 10^{14} H_0^2$. In Cavendish-type experiments, $l \sim 10^{-2}$ cm and $\rho \sim 10^{-12}$ g/cm³ to give $m \ll 10^{-43}$ and $R \sim 10^{17} H_0^2$.

To see which is of these constraints is the strongest, we model $f(R)$ as

$$f(R) = -2\Lambda + \mu H_0^2 \left(\frac{R}{H_0^2} \right)^{-n} \quad (1.91)$$

where n is very large and positive because, at these values of R , $F(R)$ very closely approximates to Λ CDM. Keeping n constant, in each of the three cases, let us see what constraint the condition on m places on μ .

The Solar System constraint, for which $m \ll 10^{-23}$, gives $n(n+1)\mu \ll 10^{6n-17}$. The Shapiro case gives $n(n+1)\mu \ll 10^{14n-6}$ while the Cavendish case gives $n(n+1)\mu \ll 10^{17n-26}$. Thus, providing, $n > 9/11$, the tightest constraint put upon μ is from the Solar System constraint.

All viable $F(R)$ models that tend to standard Einstein Gravity should automatically, by their construction, satisfy constraints 1. to 4. Some $F(R)$ models need only satisfy constraints 1. and 2. but all must suffer the application of the local gravity constraint which will constrain the model's parameters.

1.4.9 Conditions for an accelerating Universe

From (1.46), the expansion of the Universe continues to accelerate provided $\rho + 3P < 0$. Ignoring radiation, this gives us in $F(R)$ gravity, $3w_{\text{eff}}\Omega_{\text{eff}} < -1$. This means, from *Useful Expressions* on page 24, that $R > 6H^2$. Thus any solution which has $R < 6H^2$ or R oscillating and going below $6H^2$, as with the example of Figure 3.8, represents a more complicated Universe than one in which the rate of expansion is monotonic.

1.4.10 Probing the Growth of Large Scale Structure

Despite the Universe being isotropic on very large scales, perturbations, which owe their origin to times before recombination (section 1.3.2), caused matter, after recombination, to clump into galaxies and clusters of galaxies. Thereby

also formed voids, to give the structure we see today from surveys such as the Two Degree Field Galaxy Redshift Survey (2dfGRS) [88] and the Sloan Digital Sky Survey (SDSS) [89]. Measurements from these surveys provide tests for the existence of effective dark energy. These and other surveys probe at redshifts lower, often considerably lower, than that at which the CMB was formed. This is useful because effective dark energy makes its effects known during the vacuum and later matter eras.

Large scale structures (LSS) consist mainly of dark matter and observational probes consist of weak lensing surveys, cluster counts and measurements of baryon acoustic oscillations (BAO). The results are compared with numerical simulations for various models of effective dark energy. Ongoing surveys include SDSS-III [90] and BOSS (Baryon-Oscillation Spectroscopic Survey) [91]. BOSS will supply stand-alone constraints on the properties of effective dark energy, Quasi-Stellar Objects (QSO), $H(z)$ and provide insights into the matter content of the Universe. BOSS operates at two ranges of redshift. First, $0.2 < z < 0.8$ on 1.5 million luminous red galaxies and, secondly, $2.3 < z < 2.8$ on 160,000 QSOs at precisions in excess of 1.5%.

For any large scale structure being probed, using the acoustic peak as a standard ruler, two ratios are measured which give the *angular diameter distance*, $d_A(z)$ [52], and $H(z)$, independently of each other. Also can be found, by observing the power spectrum of the structure, is the wavenumber at equality, k_{eq} , given by

$$k_{\text{eq}} = H_0 \sqrt{\frac{2\Omega_{\text{m},0}}{a_{\text{eq}}}} \quad (1.92)$$

where a_{eq} is the scale factor at equality. In these cases, simple scenarios can be tested for dark energy, e.g., the CDM model, in which $\Omega_{\text{m},0} \sim 1.0$, or the Λ CDM model, for which, $\Omega_{\text{m},0} \sim 0.3$, with the result that dark energy models are favoured above CDM models.

Ongoing is also the Dark Energy Survey (DES)¹ which will combine probes of Type 1a supernovae, BAO, Galaxy Clusters and Weak Lensing. For the future are planned the EUCLID satellite², which will, from 2020, look at the distance – redshift relationship and the evolution of cosmic structures up to $z \sim 2$, and the wide aperture Large Synoptic Survey Telescope (LSST)³ in Chile which, from 2022, will map over a period of ten years the sky and the Galaxy and detect transient events.

¹<http://www.darkenergysurvey.org>

²<http://sci.esa.int/euclid>

³<http://www.lsst.org/lsst>

Chapter 2

Gravitation Models Which Mimic Λ CDM

2.1 Introduction

The standard flat Λ CDM model has $F(R) = R - 2\Lambda$, as discussed in Chapter 1. All $F(R)$ models must solve the underlying field equation, (1.74). If $3\dot{H}$ is replaced by $R/2 - 6H^2$ and the dependence of ρ_r and ρ_m on the expansion scale factor, a , introduced, using (1.78) and (1.82), equation (1.74) becomes

$$-3H \frac{d}{dt} F_R(R) + \left(\frac{R}{2} - 3H^2 \right) F_R(R) - \frac{1}{2} F(R) = -3H_0^2 \left(\frac{\Omega_{r,0}}{a^4} + \frac{\Omega_{m,0}}{a^3} \right). \quad (2.1)$$

Generally, when solving this equation for a specific model, $F(R)$, we re-write it as a relationship between $H(N)$ and $N = \log a$, eliminating R via $R = 12H^2 + 6HH'$. When solving for those $F(R)$ with a given Λ CDM history, we can simplify it to give a relationship between $F(R)$ and R , as in (2.6).

If $F(R) = R - 2\Lambda$ were inserted into (2.1), the following expression for H^2

would be obtained:

$$H^2 = \frac{H_0^2 \Omega_{r,0}}{a^4} + \frac{H_0^2 \Omega_{m,0}}{a^3} + \frac{\Lambda}{3}, \quad (2.2)$$

for which, using $R = 12H^2 + 6H H'$,

$$R = \frac{3H_0^2 \Omega_{m,0}}{a^3} + 4\Lambda. \quad (2.3)$$

Today, we have $\Omega_{r,0} + \Omega_{m,0} + \Omega_{\text{eff},0} = 1$ from which, using (2.2), we find $H_0^2 \Omega_{\text{eff},0} = \Lambda/3$.

Models which do not have a Λ CDM history have a Hubble parameter given by

$$H^2 = \frac{H_0^2 \Omega_{r,0}}{a^4} + \frac{H_0^2 \Omega_{m,0}}{a^3} + H_0^2 \Omega_{\text{eff},0} \chi_{\text{eff}}(a), \quad (2.4)$$

where $\chi_{\text{eff}}(a)$ characterises how $\rho_{\text{eff}}(a)$ scales with a such that $\chi_{\text{eff}}(1) = 1$.

In this chapter, we aim to find algebraic forms for $F(R)$ for all models with a Λ CDM history such that (2.2) holds. Clearly, $F(R) = R - 2\Lambda$ is one solution but we show it is not unique. Solving the field equation, algebraically, through all eras, viz, radiation, matter and vacuum, would seem to be impossible but, if we restrict ourselves to the later two eras, then an algebraic solution is attainable, as is shown below.

There has been some discussion, for example in [92], as to whether or not solutions other than $F(R) = R - 2\Lambda$ exist in all eras, with the result that there are. Fay et al., in [92], used the concept of *critical points* to suggest simple, approximating expressions for $F(R)$. It has even been suggested, for example in [93], that there is no real algebraic solution other than $F(R) = R - 2\Lambda$ but this is not true. The mistake that Dunsby et al. make in [93] is to choose the wrong variable with which to express the series solution for $F(R)$. The expression they find is divergent in terms of this variable. Further, they say that at values of $R \geq 4\Lambda$, the series makes $F(R)$ complex so the only option is to choose the constants of integration to be zero leaving the particular integral, $F(R) = R - 2\Lambda$, as the only possibility.

Other than the standard $F(R) = R - 2\Lambda$ solution, the solutions we find are infinite power series which fall into two categories. First, we solve the field equation when $R > 4\Lambda$. This solution is highly convergent at large R but the convergence is very slow as $R = 4\Lambda$ is approached. Secondly, we find a power series solution for which convergence does include $R = 4\Lambda$ but the convergence only extends as far as $R = 5\Lambda$. That there is some overlap between these two solutions means that we must reconcile them with regard to the constants of integration and this is done next.

Finally, we investigate algebraic solutions to the field equation in the radiation era, that is large R . Here, we find that, as R increases, $F(R)$ may be approximated by R or by $R^{4/3}$, depending on the parameter choice.

In this chapter, $\Omega_{m,0}$, will be taken to be 0.3. If we ignore radiation, this means that $\Omega_{\text{eff},0} = 0.7$ and $R_0 = 9.3H_0^2$.

2.2 Finding all models which mimic Λ CDM

Our goal is to establish all functions, $F(R)$, which lead to the same expansion history as $F(R) = R - 2\Lambda$. We demand that the Universe evolves according to $H^2 = \Omega_{r,0}H_0^2e^{-4N} + \Omega_{m,0}H_0^2e^{-3N} + \Lambda/3$, i.e., exactly as for Λ CDM. For any $F(R)$, $R = 12H^2 + 6HH'$ and $R' = -3(R - 4\Lambda)$ are determined uniquely once the scale factor is fixed. This means that equation (2.1) can be written as:

$$9H^2(R - 4\Lambda)F_{RR}(R) - \left(3H^2 - \frac{R}{2}\right)F_R(R) - \frac{1}{2}F(R) = -3H^2 + \Lambda. \quad (2.5)$$

In the matter and vacuum eras, we can make the approximation that $R \approx 3H^2 + 3\Lambda$, which allows us to write (2.5) as a differential equation in R , i.e.

$$3(R - 3\Lambda)(R - 4\Lambda)F_{RR}(R) - \left(\frac{R}{2} - 3\Lambda\right)F_R(R) - \frac{1}{2}F(R) = -R + 4\Lambda. \quad (2.6)$$

This has an obvious particular integral, $F(R) = R - 2\Lambda$, which will be utilised in the series solutions, below.

2.2.1 Algebraic solution for $R > 4\Lambda$

Define the dimensionless parameter $p = \Lambda / (R - 3\Lambda) = \Lambda / (3H^2) = H_0^2 \Omega_{\text{eff},0} / H^2$. Given in terms of $N = \log a$, it is $p = \Omega_{\text{eff},0} / (\Omega_{\text{m},0} e^{-3N} + \Omega_{\text{eff},0})$. It obviously takes finite positive values in the range $0 < p < 1$. To start with we work in the matter era, i.e., we take $z < 1000$ which means, when we take $\Omega_{\text{m},0} = 0.3$, that $R < 4 \times 10^8 \Lambda \approx 10^9 H_0^2$, $N > -6.9$ and $p > 2 \times 10^{-9}$. Figure 2.1(a) shows how p varies with N . We shall return to earlier times in section 2.3.

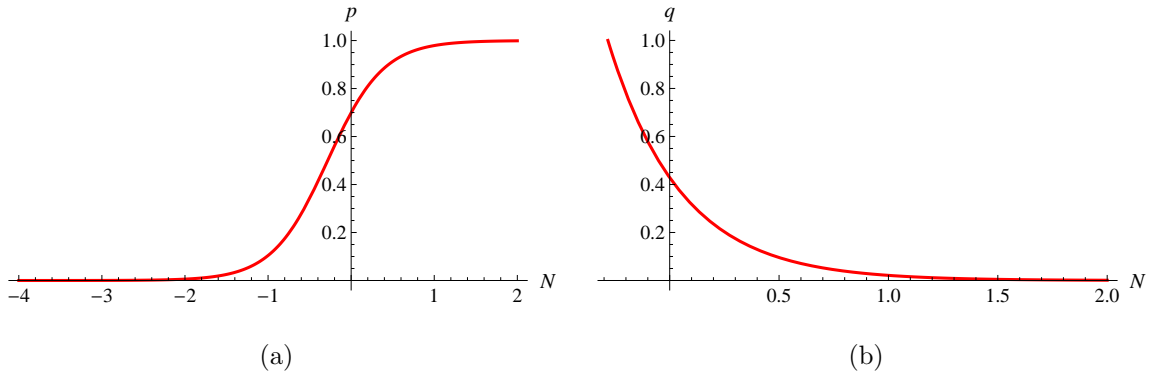


Figure 2.1: (a) p against $N = \log a$ and (b) q against N . q is defined in subsection 2.2.2. Axes cross at the current time when $p = \Omega_{\text{eff},0} = 0.7$ and when $q \approx 0.43$.

This substitution for R in terms of p converts the homogeneous part of equation (2.6) into

$$-6p^2 (1 - p) F_{pp} + p(15p - 13) F_p + F = 0. \quad (2.7)$$

Looking for solutions of the form

$$F = p^n \sum_{i=0}^{\infty} a_i p^i, \quad (2.8)$$

where the coefficients a_i are constant, and putting this into (2.7) gives the solutions

$$F = C p^{n_1} [\alpha_0 + \alpha_1 p + \alpha_2 p^2 + \dots] + D p^{-n_2} [\beta_0 + \beta_1 p + \beta_2 p^2 + \dots] \quad (2.9)$$

in which C, D are constants of integration, and $n_1 = (-7 + \sqrt{73})/12 \approx 0.129$ and $n_2 = (7 + \sqrt{73})/12 \approx 1.295$. n_1 and n_2 are found, using the Frobenius Method, by forming the indicial equation, $6n^2 + 7n - 1 = 0$. This has roots n_1 and $-n_2$.

The coefficients α_i and β_i satisfy

$$(\alpha_0, \beta_0) = (1, 1), \quad (2.10)$$

$$(\alpha_i, \beta_i) = \left[\frac{3[n+i-1][2(n+i)+1]}{6(n+i)^2 + 7(n+i) - 1} \right] (\alpha_{i-1}, \beta_{i-1}), \quad (2.11)$$

$$= \left[1 - \frac{2[5(n+i)+1]}{6(n+i)^2 + 7(n+i) - 1} \right] (\alpha_{i-1}, \beta_{i-1}), \quad (2.12)$$

for $i \geq 1$ and where $n = n_1$ for the α_i and $n = -n_2$ for the β_i . Table 2.1 gives the first six values of α_i and β_i .

i	α_i	β_i
0	1	1
1	0.0865	0.625
2	0.0375	-0.193
3	0.0218	-0.0635
4	0.0146	-0.0336
5	0.0105	-0.0214

Table 2.1: Values of α_i and β_i for solution (2.9), to 3 significant figures.

The complete solution of equation (2.6) is thus

$$F(R) = R - 2\Lambda + C\Lambda f(R) + D\Lambda g(R) \quad (2.13)$$

$$\text{where } f(R) = \left(\frac{R - 3\Lambda}{\Lambda} \right)^{-n_1} \sum_{i=0}^{\infty} \alpha_i \left(\frac{R - 3\Lambda}{\Lambda} \right)^{-i} \quad (2.14)$$

$$\text{and } g(R) = \left(\frac{R - 3\Lambda}{\Lambda} \right)^{n_2} \sum_{i=0}^{\infty} \beta_i \left(\frac{R - 3\Lambda}{\Lambda} \right)^{-i} \quad (2.15)$$

It can be seen from (2.12) that, as $i \rightarrow \infty$, $|\alpha_{n+1}/\alpha_i| \rightarrow 1$ and $|\beta_{n+1}/\beta_i| \rightarrow 1$ so that convergence of the series is only guaranteed when $|p| < 1$, that is, $R > 4\Lambda$. Only when R is close to 4Λ is a large number of terms in (2.14) and (2.15) required but, for $R \gg 4\Lambda$, a very good approximation is

$$F(R) = R - 2\Lambda + C\Lambda \left(\frac{R - 3\Lambda}{\Lambda}\right)^{-n_1} + D\Lambda \left(\frac{R - 3\Lambda}{\Lambda}\right)^{n_2} \quad (2.16)$$

$$\simeq R \left[1 + D \left(\frac{R}{\Lambda}\right)^{n_2-1}\right], \quad (2.17)$$

for sufficiently large R .

Solutions (2.13) for typical values of C and D are shown in Figure 2.2. It is clear that only when $D = 0$ does the solution tend to $R - 2\Lambda$, the standard Einstein Gravity solution, as R increases.

2.2.2 Algebraic solution which includes $R = 4\Lambda$

This is achieved by setting $q = (R - 4\Lambda)/\Lambda$. How q varies with N is shown in Figure 2.1(b), above. Equation (2.6), in terms of q , is

$$-6q(1+q)F_{qq} - (2-q)F_q + F = 2q. \quad (2.18)$$

The homogeneous form of (2.6) has indicial equation with roots $n = 2/3$ and $n = 0$ so that (2.6) has series solution

$$F(R) = \Lambda \left[q + 2 + C' \sum_{i=0} \gamma_i q^{i+2/3} + D' \sum_{i=0} \delta_i q^i \right]. \quad (2.19)$$

The first six values of γ_i and δ_i are listed in Table 2.2 and are such that their sums to infinity are convergent. They satisfy

$$(\gamma_0, \delta_0) = (1, 1) \quad (2.20)$$

$$(\gamma_i, \delta_i) = \left(-\frac{6i^2 - 11i + 2}{2i(3i+2)} \gamma_{i-1}, -\frac{6i^2 - 19i + 12}{2i(3i-2)} \delta_{i-1} \right), \quad (2.21)$$

for $i \geq 1$. In the form of (2.11) they are

$$(\gamma_i, \delta_i) = - \left[\frac{6(n+i)^2 - 19(n+i) + 12}{2(n+i)(3(n+i)-2)} \right] (\gamma_{i-1}, \delta_{i-1}), \quad (2.22)$$

for $i \geq 1$ where $n = 2/3$ for the γ_i and $n = 0$ for the δ_i .

i	γ_i	δ_i
0	1	1
1	3/10	1/2
2	-0.0375	0.0625
3	0.01307	-0.01339
4	-0.00630	0.00536
5	0.00360	-0.00276

Table 2.2: Values of γ_i and δ_i for solution (2.19), to 3 significant figures.

In terms of R , (2.19) is

$$F(R) = R - 2\Lambda + \Lambda \left[C' \sum_{i=0} \gamma_i \left(\frac{R - 4\Lambda}{\Lambda} \right)^{i+2/3} + D' \sum_{i=0} \delta_i \left(\frac{R - 4\Lambda}{\Lambda} \right)^i \right]. \quad (2.23)$$

Convergence of (2.19) is valid for $|q| \leq 1$, that is $4\Lambda \leq R \leq 5\Lambda$ and $F(4\Lambda) = (2 + D')\Lambda$. Note that if $D' = 0$, $F(4\Lambda) = 2\Lambda$, the same as the late time de Sitter limit for standard Λ CDM. If $C' \neq 0$ then $F_R(4\Lambda)$ is unbounded and, as $R \rightarrow 4\Lambda$, $F_R(R)$ takes the sign of C' . However, if $C' = 0$, $F_R(R) \rightarrow 1$ as $R \rightarrow 4\Lambda$, just as it does in standard cosmology. Two curves for which $C' = 0$ are shown in Figure 2.4.

2.2.3 Matching conditions for the two expressions for $F(R)$

The expression for $F(R)$ of section 2.2.1 must be the same as the expression for $F(R)$ from subsection 2.2.2 where they have common values of R , i.e., $4\Lambda < R \leq 5\Lambda$. In terms of $q \neq 0$, where $p = 1/(1 + q)$, they are

$$F(R) = \Lambda \left[q + 2 + C \sum_{i=0} \alpha_i (1+q)^{-(i+n_1)} + D \sum_{i=0} \beta_i (1+q)^{-(i-n_2)} \right], \quad (2.24)$$

$$= \Lambda \left[q + 2 + C' \sum_{i=0} \gamma_i q^{i+2/3} + D' \sum_{i=0} \delta_i q^i \right], \quad (2.25)$$

which are the same when $0 < q \leq 1$. Note that (2.24) does not have a Maclaurin expansion in terms of q .

Numerically, C' and D' are linearly dependent on C and D according to the approximate relations,

$$C' = -0.774 C + 0.970 D, \quad (2.26)$$

$$D' = 1.256 C + 1.187 D. \quad (2.27)$$

This correspondence between coefficients C and D and coefficients C' and D' was obtained by equating (2.24) with (2.25), and their derivatives with respect to q , at some value of q between 0 and 1. In fact, the parameter choice we made was $q = 1$, as convergence of the series is fastest the further one is away from $R = 4\Lambda$.

Figure 2.2 shows graphs of $F(R)/(R - 2\Lambda)$ against p for various values of C and D and with the corresponding values of C' and D' as defined by (2.26) and (2.27) listed in Table 2.3.

To demonstrate the overlap between the solutions of (2.13) and (2.23), curves **2** and **3** of Figure 2.2 and their counterparts as defined from (2.23), using the relations, (2.26) and (2.27), are shown in Figure 2.3. Also shown is how quickly each curve diverges from its counterpart.

Figure 2.4 shows two examples with $C' = 0$, as has already been mentioned. From (2.26) we see that, in this case, $D \neq 0$, for any given non-zero C , so that the $F(R)$ is bound to diverge from $R - 2\Lambda$ at large values of R , as p approaches zero. From (2.23), the limit of $F(R)$ as $R \rightarrow 4\Lambda$ is $(2 + D')\Lambda$ where $D' = 2.23C$.

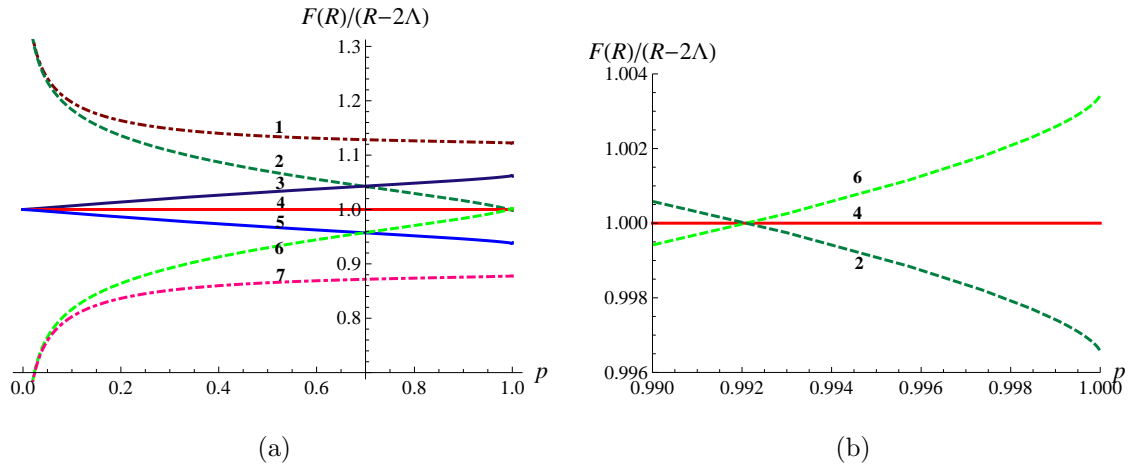


Figure 2.2: $F(R)/(R-2\Lambda)$ against $p = \Lambda/(R-3\Lambda)$. (a) shows seven numbered curves for values of C and D . In (a), axes cross at the current time, “today”, when $p = 0.7$. In (b), axes cross at some time in the future. (b) shows detail very close to $p = 1$ for curves **2**, **4** and **6** to indicate their gradients as $p \rightarrow 1$. Values of the pairs (C, D) for each of the seven curves are: **1** (dot-dashed, maroon), $(0.1, 0.1)$; **2** (dashed, dark green), $(-0.1, 0.1)$; **3** (continuous, dark blue), $(0.1, 0)$; **4** (continuous, red), $(0, 0)$, standard Einstein Gravity; **5** (continuous, royal blue), $(-0.1, 0)$; **6** (dashed, green), $(0.1, -0.1)$; **7** (dot-dashed, pink), $(-0.1, -0.1)$.

Curve No.	C	D	C'	D'	$F_R(R)$ as $p \rightarrow 1$
1	0.1	0.1	0.0196	0.244	$+\infty$
2	-0.1	0.1	0.174	-0.00691	$+\infty$
3	0.1	0	-0.0773	0.126	$-\infty$
4	0	0	0	0	1
5	-0.1	0	0.0773	-0.126	$+\infty$
6	0.1	-0.1	-0.174	0.00691	$-\infty$
7	-0.1	-0.1	-0.0196	-0.244	$-\infty$

Table 2.3: Values of C , D , C' and D' for each of the solution curves in the left hand pane of Figure 2.2 and the behaviour of $F_R(R)$ as $R \rightarrow 4\Lambda$ ($p \rightarrow 1$). Curve No. **4** is standard Einstein Gravity. The values of C , D , C' and D' chosen are for representative purposes only.

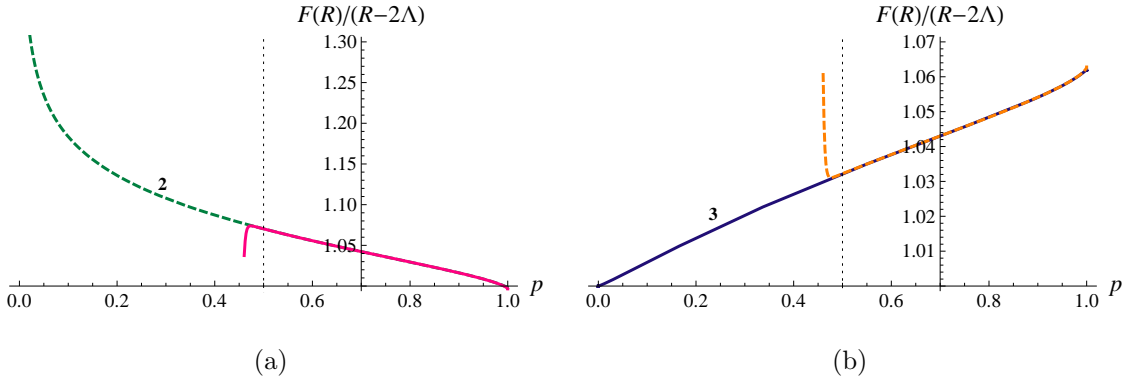


Figure 2.3: Two example curves from Figure 2.2 and subsets of their counterparts as defined from (2.23). (a) shows curve **2** (dashed, dark green) and its counterpart (continuous, pink) while (b) shows curve **3** (continuous, dark blue) and its counterpart (dashed, orange). The dotted, black line is at $p = 0.5$. Each pair of curves has common points when $4\Lambda < R \leq 5\Lambda$ which is $0.5 \leq p < 1$. Axes cross at the current time, $p = 0.7$.

Thus, the limits, as $p \rightarrow 1$ of $F(R)/(R - 2\Lambda)$ of the two examples of Figure 2.4, are 1.11 when $C' = 0$ and $C = 10^{-1}$, and 1.01 when $C' = 0$ and $C = 10^{-2}$.

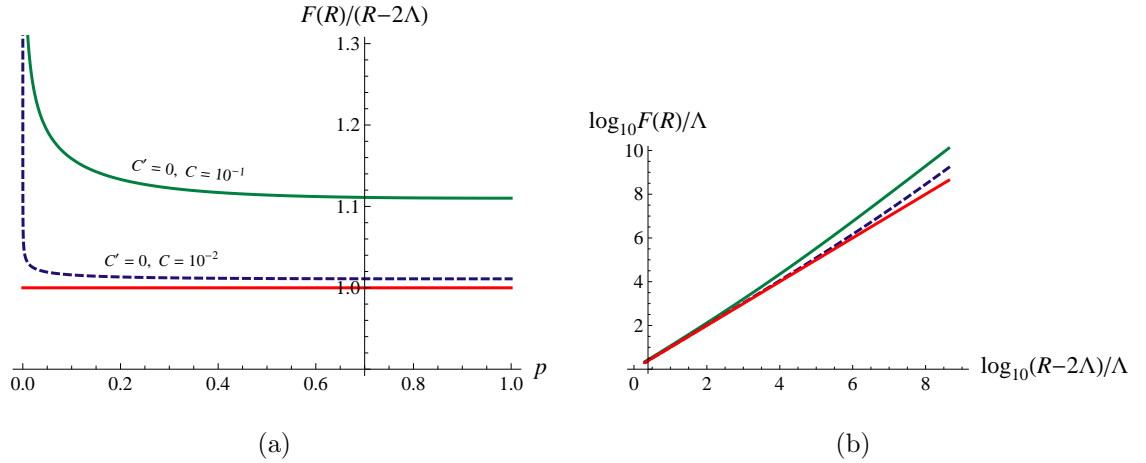


Figure 2.4: $F(R)/(R - 2\Lambda)$ against p , and $\log_{10}[F(R)/\Lambda]$ against $\log_{10} [(R - 2\Lambda) / \Lambda]$ for two solutions for which $C' = 0$. The straight lines (in red) are the standard Einstein Gravity curves for comparison. Notice how, the smaller C is, the more the solution curve “hugs” the standard Λ CDM curve for a longer time before finally veering away at large R . For both curves, $D > 0$. Time goes from left to right in (a) and from right to left in (b). Axes cross at the current time.

From (2.2), the matter density equals the “effective” vacuum density when $H_0^2 \Omega_{m,0}/a^3 = \Lambda/3$ to give, using (2.3), $R = 5\Lambda$. 5Λ thus represents the value of R at what one might describe as equality between matter and “effective” vacuum densities, in analogy to equality between radiation and matter densities.

We note that, providing $D \neq 0$, $F(R)$ deviates significantly from $R - 2\Lambda$ at early times in the matter era. At late times, in the vacuum era, the behaviour of $F(R)$ is governed by the values of both C' and D' and only when $D' = 0$ will the limit of $F(R)$ coincide with the limit of $R - 2\Lambda$ as $R \rightarrow 4\Lambda$.

2.2.4 Application of constraints to the solutions

Apart from local tests of gravity, which we shall reconsider later, the general requirements of $F(R)$ are taken to be $F_R(R) > 0$ and $F_{RR}(R) \geq 0$ [76, 77]. They have been discussed in subsection 1.4.8. The two quantities are connected via the mass, M , of the scalaron, viz

$$M^2 = \frac{F_R(R) - RF_{RR}(R)}{3F_{RR}(R)}, \quad (2.28)$$

$$\iff F_R(R) = (3M^2 + R) F_{RR}(R). \quad (2.29)$$

Thus, except when $M \rightarrow \infty$, $F_R(R) > 0 \iff F_{RR}(R) > 0$, and $F_R(R) < 0 \iff F_{RR}(R) < 0$. In standard Einstein Gravity, $F_{RR}(R) = 0$ and $M^2 \rightarrow \infty$. If $M \rightarrow \infty$, $F_{RR}(R) = 0$ and $F(R)$ is a linear function of R which could be thought of as rescaled standard Einstein Gravity.

Defining the two variables m and r , as is standard in texts on modified gravity [49, 52, 77, 87, 92], by $m = RF_{RR}(R)/F_R(R)$ and $r = -RF_R(R)/F(R)$, it is noted in [49] that “viable cosmological trajectories are restricted to be in the range $m > 0$ and $r < 0$.”

We shall define R_1 to be the smallest value of R at which we shall apply $F_R(R) > 0$ and $F_{RR}(R) \geq 0$ to the solution (2.13). Today’s value of $R = R_0 = 4.4\Lambda$ so we choose $R_1 \geq 4.4\Lambda$. R_2 is the largest value of R at which we can apply these criteria. $R_2 \sim R_{\text{eq}}$, the curvature at the time of equal matter and radiation. Generally, we take $R_2 = 10^{10}\Lambda$.

2.2.4.1 The condition that $F_R(R) > 0$

$F_R(R) > 0$ gives $1 + C\Lambda f_R(R) + D\Lambda g_R(R) > 0$ which rearranges at $R = R_2$ and $R = R_1 = 4.4\Lambda$ as

$$C < -\frac{1}{\Lambda f'(R_2)} - \frac{g_R(R_2)}{f_R(R_2)} D, \quad (2.30)$$

$$= \frac{1}{n_1} \left(\frac{R_2}{\Lambda}\right)^{n_1+1} + \frac{n_2}{n_1} \left(\frac{R_2}{\Lambda}\right)^{n_1+n_2} D, \quad (2.31)$$

$$\approx 1.5 \times 10^{12} + 1.8 \times 10^{15} D, \quad (2.32)$$

$$\text{and } C < -\frac{1}{\Lambda f'(R_1)} - \frac{g_R(R_1)}{f_R(R_1)} D, \quad (2.33)$$

$$\approx 3.2 + 4.9 D. \quad (2.34)$$

Boundaries for the regions defined in (2.30) and in (2.33) meet at $C = 3.2$ and at $D = -8.6 \times 10^{-4}$. The boundaries are shown in Figure 2.5 as $F_R(R_2) = 0$ and $F_R(R_1) = 0$, respectively.

2.2.4.2 The condition that $F_{RR}(R) \geq 0$

$F_{RR}(R) \geq 0$ is $C\Lambda f_{RR}(R) + D\Lambda g_{RR}(R) \geq 0$ which rearranges to

$$C \geq -\frac{n_2(n_2-1)}{n_1(n_1+1)} \left(\frac{R_2}{\Lambda}\right)^{n_1+n_2} D, \quad (2.35)$$

$$\approx -4.6 \times 10^{14} D, \quad (2.36)$$

$$\text{and } C \geq -\frac{g_{RR}(R_1)}{f_{RR}(R_1)} D, \quad (2.37)$$

$$\approx 0.58 D, \quad (2.38)$$

since $-g_{RR}(R_1)/f_{RR}(R_1)$ has a maximum value of approximately 0.58 at $R_1 = R_0$. The two boundaries of this region are shown in Figure 2.5 as $F_{RR}(R_1) = 0$ and $F_{RR}(R_2) = 0$.

2.2.4.3 The local gravity constraint

As discussed in subsection 1.4.8, the local gravity constraint implies $m \ll 10^{-23}$ [33, 49, 94] at $R = R_s \approx 10^6\Lambda$, which is well inside the matter era. In terms of the

scalaron mass, via (2.29), this translates to $3M_s^2/R_s \gg 10^{23}F_R(R_s)$, where M_s is the value of M at $R = R_s$. The smallness of $F_{RR}(R)$ and the closeness of $F_R(R)$ to unity mean that the scalaron mass, defined from (2.28), is approximated by $3M_s^2 = 1/F_{RR}(R_s)$. Thus, on rearrangement, we have

$$C = \frac{R_2}{3M_s^2 n_1 (n_1 + 1)} \left(\frac{R_s}{\Lambda}\right)^{n_1+1} - \frac{n_2 (n_2 - 1)}{n_1 (n_1 + 1)} \left(\frac{R_s}{\Lambda}\right)^{n_1+n_2} D, \quad (2.39)$$

$$\approx \frac{1.36 \times 10^{13} \Lambda}{M_s^2} - 9.2 \times 10^8 D, \quad (2.40)$$

$$\ll 4.1 \times 10^{-16} - 9.2 \times 10^8 D. \quad (2.41)$$

The boundary of the region represented by (2.41) meets the boundary of the region defined by (2.35) at (D_2, C_2) , where

$$C_2 = \frac{R_s}{3M_s^2 n_1 (n_1 + 1)} \left(\frac{R_s}{\Lambda}\right)^{n_1+1} \left[1 - \left(\frac{R_s}{R_2}\right)^{n_2+n_1}\right]^{-1}, \quad (2.42)$$

$$\approx 4.1 \times 10^{-16}, \quad (2.43)$$

$$D_2 = -\frac{R_s}{3M_s^2 n_2 (n_2 - 1)} \left(\frac{R_s}{\Lambda}\right)^{-n_2+1} \left[\left(\frac{R_2}{R_s}\right)^{n_2+k_1} - 1\right]^{-1}, \quad (2.44)$$

$$\approx -8.9 \times 10^{-31}. \quad (2.45)$$

The boundary of the region represented by (2.41) meets the boundary of the region defined by (2.37) at $(D_0, C_0) = (4.4 \times 10^{-25}, 4.0 \times 10^{-26})$. It is noted that $C_2 \gg \{-D_2, C_0, D_0\}$. The boundaries (2.32), (2.34), (2.36) and (2.38) and the line (2.39) are shown schematically in Fig. 2.5.

If we require $F_{RR}(R)$ not to be singular as $R \rightarrow 4\Lambda$ then we must set $C' = 0$ in equation (2.26). This adds the further constraint $C = 1.25D$, which is shown as the short green line in Figure 2.5. This meets the Solar System constraint boundary (2.39) at $(D_3, C_3) = (4.4 \times 10^{-25}, 5.5 \times 10^{-25})$.

To see which terms of (2.16) for the expression for $F(R)$ are relevant, with the above constraints imposed, near equality $D \sim 10^{-25}$, $R \sim 10^{10} \Lambda$ give

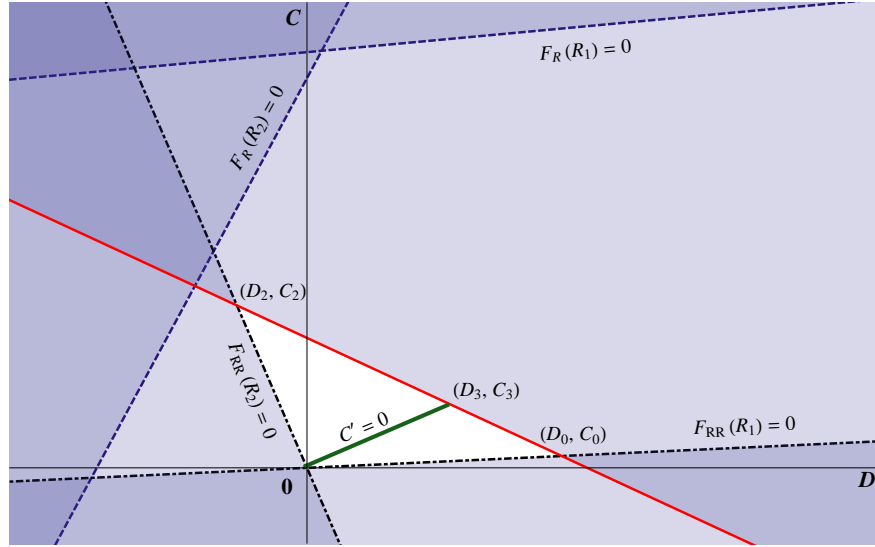


Figure 2.5: Schematic diagram showing the constraints from $F(R) > 0$ and $F_{RR}(R) \geq 0$ and from local gravity. The axes are labelled $0D$ and $0C$ with 0 being the origin. The solid, diagonal, red line on which lie the points (D_0, C_0) , (D_2, C_2) and (D_3, C_3) , is the line represented by (2.39) when M_s takes its smallest value. The allowed region is thus the unshaded triangular region with the origin as one vertex.

$D\Lambda (R/\Lambda)^{n_2} \sim 10^{-12} \Lambda$. From this we conclude that the range of values of (C, D) which are compatible with $F_R(R) > 0$, $F_{RR}(R) > 0$ and the local gravity constraint is very restricted to being close to $(0, 0)$. Therefore, it appears that the only models meeting these criteria are effectively standard Einstein Gravity.

2.2.5 The matter growth index, γ

We investigate what bearing various solutions have on the matter growth index, γ , as introduced in Chapter 1 and expanded upon in Chapter 3. We define the matter growth index, γ , by [74]

$$(\Omega_m)^\gamma = \frac{d \log \delta_m}{d \log a} \quad (2.46)$$

$$= \frac{\delta'_m}{\delta_m}. \quad (2.47)$$

where δ_m , known as the matter density contrast, is defined in terms of perturbations in the matter density as $\delta_m = \delta\rho_m/\rho_m$.

We shall ignore the severe parameter constraints of subsection 2.2.4, for illustrative reasons, because to include them we should not be able to differentiate between them and standard Einstein Gravity. We show it for completeness and to illustrate how the same $a(t)$ can give very different γ .

We shall use the expression of equation (2.13). Clearly if $F(R)$ is to tend to standard Einstein Gravity at high R we must let $D = 0$. Thus, we are dealing with a one-parameter set of solutions. We choose $C = 0, 10^{-5}, 10^{-4}$ and 10^{-3} . The first of these is, of course standard Einstein Gravity. We cannot allow C to be negative when $D = 0$ as this would result in $F_{RR}(R)$ being negative for all values of R greater than some minimum value. The results acquired by numerical integration are shown against redshift z in Figure 2.6 and the trend as C varies is seen clearly. At high z , there is Λ CDM, $\gamma \approx 6/11 = 0.545$ while, as $z \rightarrow -1$, γ tends to $2/3$ for all models, again, as for Λ CDM. This is discussed further in Chapter 3. With C as small as in the allowed triangle of Figure 2.5, the result is indistinguishable from Λ CDM and if, further, we must have $C' = 0$, then the only solution is $C = D = 0$, i.e., Λ CDM.

2.3 In the radiation era

It can be seen in Figure 2.2 that curves **1**, **2**, **6** and **7**, curves for which $D \neq 0$, are not tending to standard Einstein Gravity at high curvature, that is as $p \rightarrow 0$. It is thus worth investigating what happens to solutions like these in the radiation era, which we have ignored so far.

In the radiation era, we may take $R \approx 3H_0^2\Omega_{m,0}e^{-3N}$ and $H^2 \approx H_0^2\Omega_{r,0}e^{-4N}$, i.e., $H^2 = \kappa R^{4/3}$, where $\kappa = \Omega_{r,0}/(81H_0^2\Omega_{m,0}^4)^{1/3}$. Since $H^2 \gg \Lambda$, we may rewrite

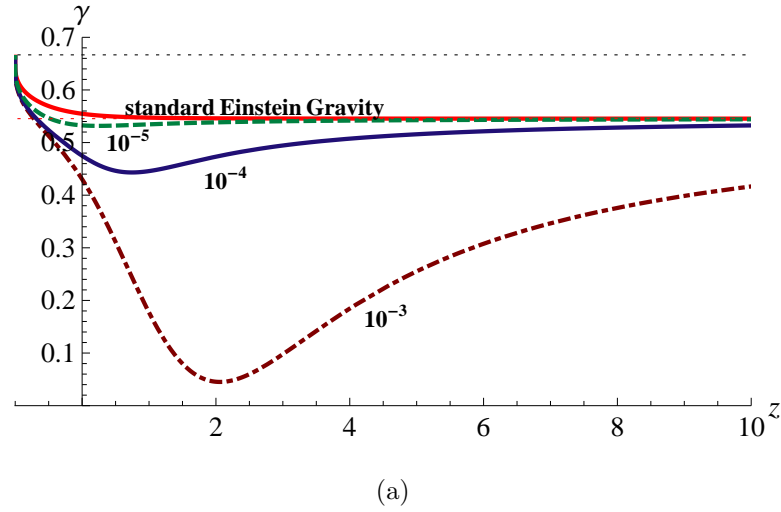


Figure 2.6: Curves of the matter growth index, γ , against z for four examples of the solution to equation (2.13). The values of C are indicated except when $C = 0$ when the curve is labelled standard Einstein Gravity. Today's values of γ for each curve are as follows: $C = 0, \gamma_0 = 0.555$; $C = 10^{-5}, \gamma_0 = 0.533$; $C = 10^{-4}, \gamma_0 = 0.475$; $C = 10^{-3}, \gamma_0 = 0.430$. In all cases, $D = 0$.

the field equation, (2.5), as

$$3RF_{RR} - \left(1 - \frac{R^{-1/3}}{6\kappa}\right)F_R - \frac{R^{-4/3}}{6\kappa}F + 1 = 0. \quad (2.48)$$

This has solution $F(R) = R$ and asymptotic solution $F(R) = \alpha R^{4/3}$, where α is constant. We see that as R increases without limit, either $F(R)/R \rightarrow 1$ or $F(R)/R^{4/3} \rightarrow \text{constant}$. Notice that the matter era solution, (2.16), has $n_2 = 1.295$ which is close to $4/3$, so the two solutions match quite nicely.

If we want a power series solution to (2.48), it is helpful to rewrite it in terms of the scale factor a as

$$aF_{aa} + 5F_a - \frac{3}{2} \frac{\Omega_{m,0}}{\Omega_{r,0}} F = -\frac{9H_0^2 \Omega_{m,0}}{a^4}, \quad (2.49)$$

where $0 < a \ll 1$.

Equation (2.48) has particular integral $F(R) = R$ while we look for solutions to the homogeneous form of (2.49) of the form $F(R) = a^n \sum_{i=0} \eta_i a^i$. The indicial

equation is $n(n - 1) + 5n = 0$ giving $n = 0$ or -4 which leads to the general solution

$$F(R) = R + A\Lambda \left(\frac{R}{\Lambda}\right)^{4/3} \sum_{i=0} \rho_i \left(\frac{R}{\Lambda}\right)^{-i/3} + (A \log a + B) \Lambda \sum_{i=0} \sigma_i \left(\frac{R}{\Lambda}\right)^{-i/3}, \quad (2.50)$$

where $a = (\Omega_{m,0}/\Omega_{\text{eff},0})^{1/3} (R/\Lambda)^{-1/3}$ and ρ_i, σ_i are constants, the first six of which are given in Table 2.4, and A and B are constants of integration. The introduction of the log term has been necessitated by the roots of the indicial equation differing by an integer. See, for example, [95].

i	ρ_i	σ_i
0	-1.09×10^{-12}	1
1	1.23×10^{-9}	6.79×10^2
2	-1.04×10^{-6}	1.91×10^5
3	1.18×10^{-3}	3.10×10^7
4	1	3.29×10^9
5	-1.36×10^2	2.48×10^{11}

Table 2.4: The first six coefficients of equation (2.50). The fact that these coefficients are becoming numerically larger with increasing i does not matter as each is also multiplied by $(R/\Lambda)^{-i/3}$ where R/Λ is large.

For R/Λ sufficiently large, $F(R) = R + A\Lambda\rho_0 (R/\Lambda)^{4/3}$ is a good approximation. By sufficiently large, in this context, we mean that $R \gtrsim 10^{16} \Lambda$ which is before equality, well into the radiation era. The point at which $A\Lambda\rho_0 (R/\Lambda)^{4/3}$ overtakes R depends on the value of $A\Lambda\rho_0$.

Only if $A = 0$ is the large R solution equal to that of standard Einstein Gravity, otherwise it is given by $F(R) \sim R^{4/3}$. Of course, as we have seen,

the Solar System constraint must make $A\rho_0$ very small; we have seen its counterpart, D , in the matter era has to be of order 10^{-25} or smaller. We expect $A\Lambda\rho_0(R/\Lambda)^{4/3} \sim D\Lambda(R/\Lambda)^{n_2}$ at equality which means that the $R^{4/3}$ term will only become dominant when $R \gtrsim 10^{76} \Lambda$, when $z \gtrsim 10^{25}$.

2.4 Conclusion

In this chapter we have shown that there are functions, $F(R)$, which satisfy the field equation

$$-3H^2 R' F_{RR}(R) + \left(\frac{R}{2} - 3H^2 \right) F_R(R) - \frac{1}{2} F(R) = -3H^2 + \Lambda, \quad (2.51)$$

other than the standard Λ CDM model, $F(R) = R - 2\Lambda$. These solutions share the same history as defined by the Hubble parameter, H , where $H^2 = \Omega_{r,0} H_0^2 e^{-4N} + \Omega_{m,0} H_0^2 e^{-3N} + \Lambda/3$ and $N = \log a$. In the matter and vacuum eras, when the effects of radiation may be neglected, algebraic expressions have been found which fall into two groups:

- I. There is an infinite series solution, expressed as a power series in $\Lambda/(R - 3\Lambda)$, which is convergent for $R > 4\Lambda$. The significance of 4Λ is that it is the limiting, de Sitter, value of R at the end of the vacuum era, when $3H^2 = \Lambda$.
- II. There is also an infinite series solution, this time expressed as a power series in $(R - 4\Lambda)/\Lambda$, but which is only convergent in the range $4\Lambda \leq R \leq 5\Lambda$.

Where the convergence ranges of these two groups overlap, i.e., when $4\Lambda < R \leq 5\Lambda$, the solutions have been matched in terms of their particular constants of integration showing one set to be a linear combination of the other set. The relationship between the two sets is given in equations (2.26) and (2.27) with graphical correspondence between two pairs of examples being shown in Figure 2.3.

The late time value of the standard Einstein Gravity model is $F(4\Lambda) = 2\Lambda$. A feature of these more general solutions is that at late times it is possible for $F(4\Lambda)$ to equal 2Λ by choosing D' to be zero. Recall that C' and D' are defined in (2.19). In no other sense does the general $F(R)$ tend to $R - 2\Lambda$ because for $F_R(R)$ to tend to a common value of unity, C' must be zero, as well, and if both are zero we have $F(R) = R - 2\Lambda$, for all R .

At early times in the matter era, the general $F(R)$ can tend to $R - 2\Lambda$ which requires D of (2.13) to be equal to zero. With D not being zero $F(R)$ diverges away from $R - 2\Lambda$ as R increases. When $R \gg 4\Lambda$, we find $F(R) \propto R^{n_2}$ where $n_2 \approx 1.3$.

Then we considered what could happen in the radiation era by solving a simplified field equation applicable when $R \gg R_{\text{eq}}$. Here, we were only concerned with the leading terms of any series solution but found that either $F(R) \rightarrow R$, as R increases, or $F(R)/R^{4/3} \rightarrow \text{constant}$.

For none of the solutions illustrated in Figures 2.2, 2.3 and 2.4 were local gravity constraints applied. When they were applied it was seen that the solutions are extremely close to standard Einstein Gravity; the coefficients C , D , C' and D' were in the range $\mathcal{O}(10^{-16})$ to $\mathcal{O}(10^{-25})$, or smaller. Further, if there is to be no singularity in $F_R(R)$ as $R \rightarrow 4\Lambda$, then either the solution is standard Einstein Gravity or solutions must run backwards through time very close to $F(R) = R - 2\Lambda$ until well past R_s when they diverge such that $F(R) \propto R^{4/3}$ as R increases further. In this case, C , D , C' and D' are of order 10^{-25} , or smaller.

As an extension of this work, we could specify the history of H in some other way or specify the history of w_{eff} , of Ω_{eff} or of R . Generally these would all be equivalent to specifying the history of H by use of the following relationships,

again ignoring the radiation era although this could be included if necessary:

$$\Omega_{\text{eff}} = 1 - \frac{H_0^2 e^{-3N} \Omega_{\text{m},0}}{H^2} \quad (2.52)$$

$$w_{\text{eff}} = -\frac{3H^2 + 2HH'}{3H^2 - 3H_0^2 e^{-3N} \Omega_{\text{m},0}} \quad (2.53)$$

$$R = 12H^2 + 6HH' \quad (2.54)$$

We would then be left with a differential equation for $F(N)$ in terms of N . Whether or not this is soluble, algebraically, would depend upon circumstances.

Chapter 3

Non- Λ CDM Gravitation Models

3.1 Introduction

Currently, there is some doubt as to today's value of what we term the “effective” equation of state, $w_{\text{eff},0}$. While the latest results from the Planck Collaboration [17] do not rule out Λ CDM as a valid model describing the history of the Universe, they do not confirm $w_{\text{eff},0}$ to be -1 . Instead Planck gives a broad range of values at the 95% level of significance, namely, $w_{\text{eff},0} = -1.04^{+0.72}_{-0.69}$. It should be noted that quintessence models [96] have $w_{\text{eff}} \geq -1$ while $F(R)$ models have w_{eff} close to -1 but always below it, at high redshift, which becomes more negative until a local minimum is reached when w_{eff} increases to cross the phantom boundary, $w_{\text{eff}} = -1$, some time later [49, 68]. With a particular $F(R)$ model it is possible that $1 + w_{\text{eff},0}$ is positive, zero or negative [97–100].

In this chapter we look at three models which, while they cleave to Λ CDM at high curvature in the matter era, veer away from it in the late matter or the early vacuum eras to give values of $w_{\text{eff},0}$ different from -1 . The three models chosen will be:

- I. the HSS (Hu-Sawicki-Starobinsky) model, [101]. It is a modified version of

the Hu-Sawicki model described in [97],

- II. the AB (Appleby-Battye) model, also described in [101] but first introduced in [76],
- III. a new model, defined in subsection 3.2.1 of this thesis, which we call the Erf model because it is based on the error function, $\text{erf}(x)$.

The AB model is a two-parameter model while the Erf and HSS models, have three parameters. For all of them, we see how $w_{\text{eff},0}$ and $\Omega_{\text{eff},0}$ vary as their parameters are varied. Similarly, we see the relation between $w_{\text{eff},0}$ and $\Omega_{\text{eff},0}$ and between $w'_{\text{eff},0}$ and $w_{\text{eff},0}$

For each of the Erf, AB and HSS models, two examples are chosen and, for each, it is seen how $f(R)$, $f_R(R)$, w_{eff} and Ω_{eff} vary with time. For these six examples it is arranged that $\Omega_{\text{eff},0} = 0.7$. This is just a round figure as it is noted that Planck [17, 102] gives its value as 0.686 ± 0.020 at the 68% significance level. This result, which is numerically smaller than previously measured [5], was found using the Doran and Roberts model for dark energy [103] in the context of Λ CDM. The Λ CDM model is used as a background model because it has proved to be so successful. If some other model were substituted then the results of Planck and previous attempts such as WMAP might change. A quote from the introductory paper to the Planck results [3]: *... the Planck data are in remarkable accord with a flat Λ CDM model; however, there are tantalizing hints of tensions both internal to the Planck data and with other data sets. While such tensions are model-dependent, none of the extensions of the Λ CDM cosmology we explored resolve them. It is to be hoped that more data and further analysis will shed light on these areas of tension. Along these lines, we expect significant improvement in data quality and the level of systematic error control, plus the addition of polarization data, from Planck in the near future.*

One of the demands of General Relativity is that $F(0) = 0$, that is, letting

$F(R) = R + f(R)$, $f(R) \rightarrow 0$ as $R \rightarrow 0$. Just because $f(0) = 0$ does not necessarily mean that R can become zero, however. This is because there could be a de Sitter attractor [46, 104], R_{dS} , which prevents this so that $R \rightarrow R_{\text{dS}}$ as $N = \log a \rightarrow \infty$. How this happens, whether R gradually decreases to R_{dS} or whether it oscillates around it with ever-decreasing size, is discussed. The parameter space of the contour plots that we present in this chapter is generically divided into two regions; one region where there would be a de Sitter attractor, $R_{\text{dS}} \geq 0$, and another where there is a Minkowski solution $R = 0$, as $N \rightarrow \infty$ [105]. In fact, the de Sitter region is split up into two; a region in which R oscillates on its way to the attractor, we call this the de Sitter oscillating region, and another region in which there is a gradual movement towards the de Sitter attractor with no oscillation, we call this the de Sitter non-oscillating region. What happens in the Minkowski region can be more complicated especially when R oscillates as, when R is close to zero, at some point, it will go negative. See subsection 3.2.1.2.

We use the phrase *would be* in the previous paragraph because the purpose of this exercise is to see how large we can make $|1 + w_{\text{eff},0}|$ without any regard to the future. If we were restricted to the de Sitter region, we would not see the greater possibilities of straying into the Minkowski region. We find that for examples in the Minkowski region, if left unaltered, give future values of w_{eff} and Ω_{eff} which are unacceptable. See, for example, subsection 3.2.1.2.

Note, there are some graphs in this chapter with an axis marked as $f'(R)$. This means $f_R(R) = df(R)/dR$ and not $df(R)/dN$. Where some graphs are plotted against $N = \log a$, today is always represented by $N = 0$ so that redshift $z = e^{-N} - 1$.

3.2 Three models compared

Three models are compared; The AB and HSS models and also a new function which we dub the Erf function. The first two have been extensively studied and are represented in [78, 97, 101].

As has been explained elsewhere in this thesis, all successful models approximate to Λ CDM at high curvature. This requirement might not be strictly necessary but it tends to be assumed because of the severe constraint imposed by the Solar system [49] at $R = R_s = 10^6 H_0^2$. Also, using data from measurements of supernovae type Ia and from the CMB, $m = R F_{RR}(R)/F_R(R)$ [49, 77, 106] must be less than $\mathcal{O}(0.1)$ [49, 87]. In effect, this means that $0 < F_{RR}(R) < 0.1/R$ which means that when R is very large, as in the early matter era just past equality, deviations for $F(R) = R + f(R)$ from Λ CDM, that is $F(R) = R - 2\Lambda$, must be very small indeed. Thus it is assumed that $F(R) \rightarrow R - 2\Lambda$ as $R \rightarrow \infty$, as a practical convenience.

We also demand that at the end of time if $R \rightarrow 0$ so should $F(R)$. This is to be compatible with GR, i.e., $F(0) = 0$.

As always in this thesis, $F(R) = R + f(R)$ so that $f(R)$ denotes deviations of $F(R)$ from GR. As $R \rightarrow \infty$, $f(R) \rightarrow -2\Lambda_\infty$; Λ_∞ being an effective cosmological constant.

An intrinsic feature of all models is that R_0 , $w_{\text{eff},0}$ and $\Omega_{\text{eff},0}$ are connected via $R_0 = 3H_0^2(1 - 3w_{\text{eff},0}\Omega_{\text{eff},0})$, if we neglect the tiny effect of radiation; see *Useful Expressions* on page 24. This poses a problem if we wish to have $\Omega_{\text{eff},0}$ equal to a fixed value like 0.7, say, because R_0 is constrained to be within a certain range. Thus, large differences in $w_{\text{eff},0}$ between models are bound to be impossible. Applying data from Planck, which assumed GR, gives an idea that R_0 lies in the approximate range $7 H_0^2 < R_0 < 12 H_0^2$.

3.2.1 The Erf model

This model was derived in an attempt to see if the values of $w_{\text{eff},0}$ it produced could deviate more from -1 than the values delivered by other models. It is based on the error function $\text{erf}(x)$ which is defined as

$$\text{erf}(x) = \frac{2}{\sqrt{\pi}} \int_0^x e^{-t^2} dt. \quad (3.1)$$

It is an odd function in that $\text{erf}(-x) = -\text{erf}(x)$ and continuously takes all values between -1 , when $x \rightarrow -\infty$, and 1 , when $x \rightarrow \infty$.

For general positive parameter b , the Erf model is

$$f(R) = -2\Lambda_\infty \left(\frac{\text{erf}[c + bR/H_0^2] - \text{erf}[c]}{1 - \text{erf}[c]} \right); \quad (3.2)$$

$$f_R(R) = -\frac{4\Lambda_\infty b}{\sqrt{\pi} H_0^2 (1 - \text{erf}[c])} \exp \left[-\left(c + b \frac{R}{H_0^2} \right)^2 \right]. \quad (3.3)$$

It is a three-parameter model; b , c and Λ_∞ being the parameters.

For given values of b and c the model approaches Λ CDM as R increases so it is able to pass the Solar System test (3.5) for suitable values of b and c . Typically, $R_0 \simeq 10H_0^2$; Λ CDM gives $R_0 = 9.3H_0^2$. For R_0 of this order (R_0 changes slightly as the parameters change), decreasing the value of b from a large positive value to a smaller, positive one effects a swing away from Λ CDM. $f_R(R)$ changes from being numerically very small to being numerically larger, as can be seen from (3.3). The negative, squared exponent in (3.3) ensures that $F(R)$ adheres very closely to Λ CDM until it swings away when it does so rapidly, just as e^{-x^2} clings to zero until x becomes sufficiently close to zero. Some other models may not have the facility to do this because local gravity tests constrain model parameters to such an extent that they are not able to deviate sufficiently from Λ CDM, today.

For numerically extremely small b , $f(R)$ approximates to

$$f(R) \sim -\frac{4\Lambda_\infty b e^{-c^2}}{\sqrt{\pi} (1 - \text{erf}[c])} \frac{R}{H_0^2} \quad (3.4)$$

which can be considered to give re-scaled GR, but we do not get this far as we are limited as to how small R can go. As can be seen from (3.2), increasing the value of $c + b R/H_0^2$, takes the Erf model closer to Λ CDM, so increasing the value of c does the same thing as can be seen in the contour plots of Figure 3.4.

The behaviours of $f(R)$ and its derivative with respect to R , when plotted against N , are illustrated in Figure 3.1. We choose two representative points in parameter space, both of which satisfy the Solar System constraint [49], namely,

$$R_s f_{RR}(R_s) \ll 10^{-23}, \quad (3.5)$$

where $R_s \approx 10^6 H_0^2$. For the general Erf model this is

$$\frac{8\Lambda_\infty R_s b^2 (c + b R_s/H_0^2)}{H_0^4 \sqrt{\pi} (1 - \text{erf}[c])} \exp \left[- \left(c + b \frac{R_s}{H_0^2} \right)^2 \right] \ll 10^{-23}. \quad (3.6)$$

Because of the negative squared exponent, this does not place practical constraints on the parameters. It is sufficient that $b \gtrsim 10^{-5}$. When $c = 1$, $b \gg 10^{-5.2}$ which falls, when $c = 6$, to $b \gg 10^{-6.3}$.

The model for which $c = 1.5$, $\log_{10} b = -1.517$ and $\Lambda_\infty = 2 H_0^2$, which will be represented by continuous, pink curves, below, we shall term Model 1 while that for which $c = 1.5$, $\log_{10} b = -0.914$ and $\Lambda_\infty = 2 H_0^2$, represented by dashed, mauve curves, we shall term Model 2.

3.2.1.1 The dark energy equation of state

For the parameter values of Figure 3.1, the corresponding values of w_{eff} and Ω_{eff} over the history of the Universe are shown in Figure 3.3. They were derived by solving the field equation (1.75) for $H(N)$, for given $F(R)$, on the assumption that at the initial value of N , N_i , the theory is Λ CDM, that is, $H^2(N_i) = H_0^2 \Omega_{m,0} e^{-3N_i} + \Lambda_\infty/3$. $w_{\text{eff}} \Omega_{\text{eff}}$ is then found from (1.86) while Ω_{eff} is defined as $8\pi G \rho_{\text{eff}} / (3H^2)$

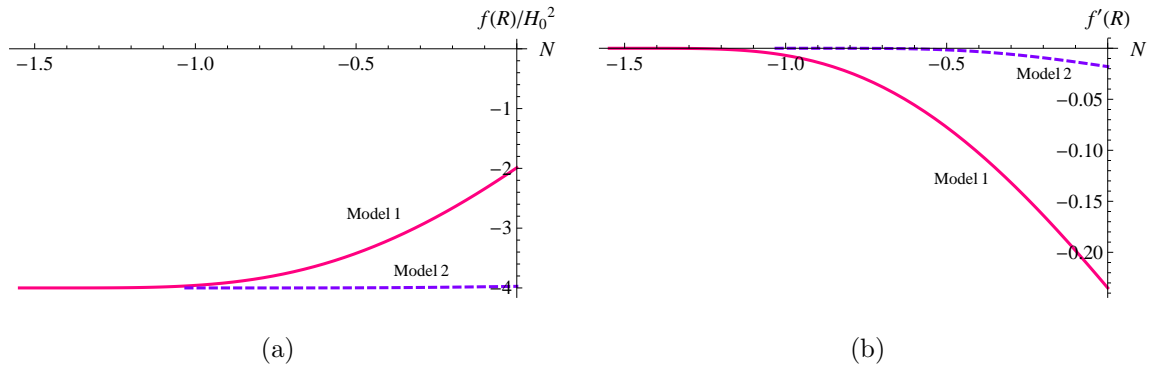


Figure 3.1: $f(R)/H_0^2$ and $f'(R)$ against $N = \log a$.

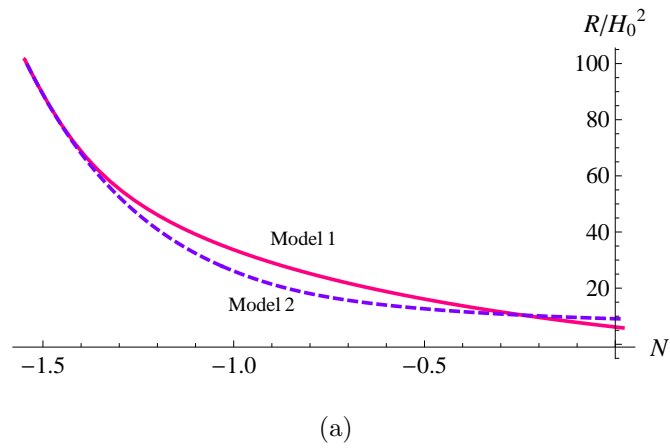


Figure 3.2: R/H_0^2 against N . For Model 1, $R_0 = 6.2 H_0^2$ while for Model 2, $R_0 = 9.1 H_0^2$.

using (1.82), assuming the effects of radiation are negligible. This gives

$$\Omega_{\text{eff}}(N) = 1 - \frac{H_0^2 e^{-3N} \Omega_{\text{m},0}}{3H(N)^2}, \quad (3.7)$$

$$w_{\text{eff}}(N) = -\frac{3H(N)^2 + 2H(N)H'(N)}{3H(N)^2 - 3H_0^2 e^{-3N} \Omega_{\text{m},0}}. \quad (3.8)$$

$\Omega_{\text{m},0}$ is taken to be 0.3 to give $\Omega_{\text{eff},0} = 0.7$. The slight mismatch at $N = N_i$ between what $H(N)$ should be and the Λ CDM value we use manifests itself in graphs of w_{eff} as small but rapid oscillations which die out as N increases. This can be seen in the Erf Model 1 graph of Figure 3.3(a). These oscillations can be reduced by starting the numerical integration to find $H(N)$ at a slightly smaller value of N_i , as can be seen in the Erf Model 2 graph.

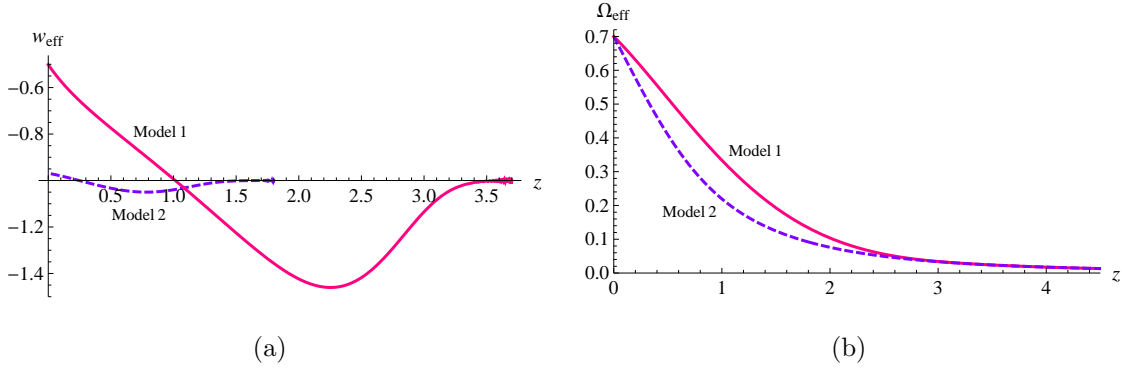


Figure 3.3: w_{eff} and Ω_{eff} against z for the curves of Figure 3.1.

Figure 3.4 shows how today's values of w_{eff} and Ω_{eff} vary with the parameters c and $\log_{10} b$, for the case when $\Lambda_{\infty} = 2H_0^2$. The points in parameter space representing Models 1 and 2 are indicated by spots, pink for Model 1 and mauve for Model 2. The large c region corresponds to GR while $c = 0$, and large b coincides with Λ CDM, with $\Omega_{\text{eff},0}$ tending to $\Lambda_{\infty}/3$. In the limit $b \rightarrow 0$, $f(R) \rightarrow 0$ which would give GR if it were not for the fact that before that could happen R_0 becomes zero.

In Figure 3.5, we plot w_{eff} against $\Omega_{\text{eff},0}$ and $w'_{\text{eff},0}$ against $w_{\text{eff},0}$ for various values of Λ_{∞} as indicated when $c = 1.5$. We see that along each curve, b increases towards the fixed point at which $\Omega_{\text{eff},0} = \Lambda_{\infty}/(3H_0^2)$.

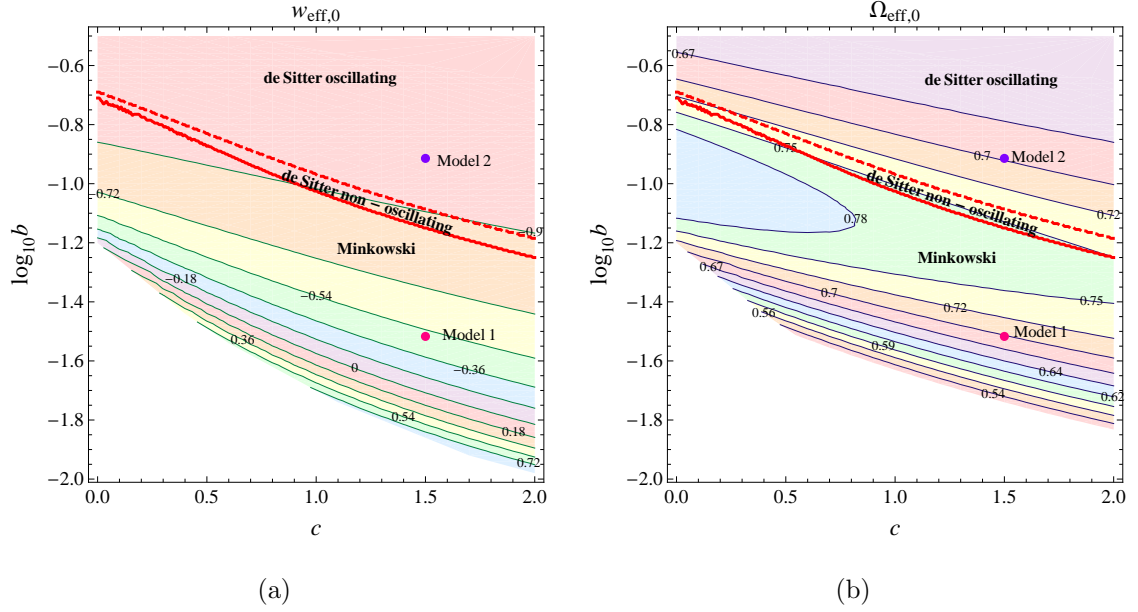


Figure 3.4: For $\Lambda_\infty = 2H_0^2$, contour plots of $w_{\text{eff},0}$ and $\Omega_{\text{eff},0}$ as functions of c and $\log_{10} b$. The lower boundary is where R_0 comes close to being zero.

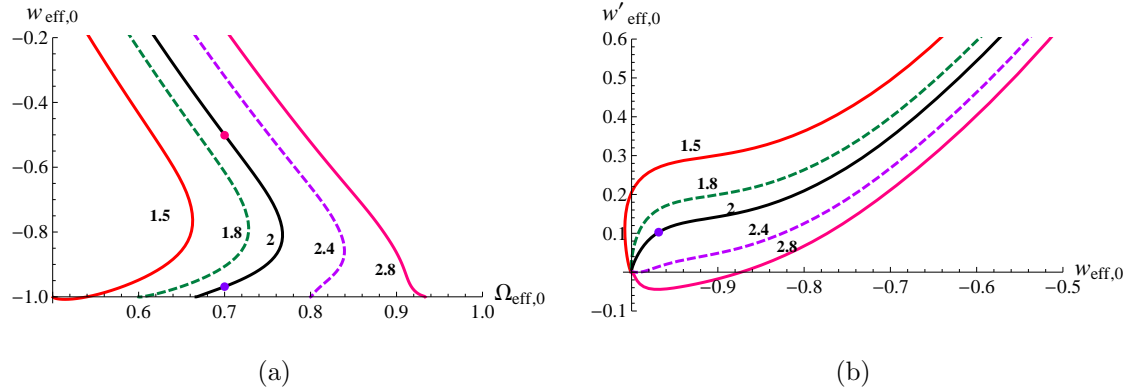


Figure 3.5: For $c = 1.5$, $w_{\text{eff},0}$ as a function of $\Omega_{\text{eff},0}$ and $w'_{\text{eff},0}$ as a function of $w_{\text{eff},0}$. The fixed points are in (a) $(\Lambda_\infty/(3H_0^2), -1)$ and in (b) $(-1, 0)$. Each curve is represented by a value of Λ_∞/H_0^2 which is indicated. The spots represent Model 1 which is at $(0.7, -0.50)$ in (a) and at $(-1, 0)$ (not shown owing to the scale of the diagram) in (b), and also by Model 2 at $(0.7, -0.97)$ in (a) and at $(-0.97, 0.10)$ in (b).

3.2.1.2 Late-time behaviour

This thesis is concerned with the the history of the Universe up to the present time. How do parameters such as $H(N)$, $R(N)$, $w_{\text{eff}}(N)$, $\Omega_{\text{eff}}(N)$ etc develop? The thesis is not concerned with the future, as has been discussed in the introduction to this chapter. As has been said, if our models give unacceptable problems after today, such as can be seen in Figure 3.8, that can be remedied simply by altering the model so that an appropriate change can be put into effect, then, to keep the model well behaved. However it is instructive to gain an insight into what would happen if the models were not altered.

It will be noticed in Figure 3.4 that three regions, viz, de Sitter oscillating, de Sitter non-oscillating and Minkowski, covering the whole parameter plane, have been marked separated by boundaries coloured red. These regions represent the late-time, vacuum state behaviour of the model. Following Frolov in [107], we identify the scalar field, $\phi(R) = F_R(R) - 1 = f_R(R)$ with associated potential $V(\phi(R))$ given by

$$V(\phi(R)) = \int_{\infty}^R \frac{1}{3} (r + 2f(r) - r f_R(r)) f_{RR}(r) dr. \quad (3.9)$$

As has already been said, the late-time value of R is not necessarily equal to zero but is defined where $V(\phi)$ is a local minimum. The resulting equation to be satisfied is

$$R + 2f(R) - Rf_R(R) = 0. \quad (3.10)$$

If such a stable solution exists, $R = R_{\text{dS}}$ is termed the late-time de Sitter attractor solution. Putting all the time derivatives (equivalently, derivatives with respect to $N = \log a$) and densities in the field equation (q.v.) equal to zero gives equation (3.10). There is always a solution for which $R = 0$ when space is completely flat and this solution is thus termed the GR or Minkowski solution [108]. If this solution is not a de Sitter solution, it may be unacceptable because

R will tend to oscillate around zero as it decays to zero. However, as can be seen from Figure 3.4, the Minkowski region has the potential to give larger values of $|1 + w_{\text{eff},0}|$ than would otherwise be the case for the de Sitter region. The de Sitter solutions fall into two groups; oscillating, for which w_{eff} , R and H exhibit late-time oscillations, and non-oscillating, for which these variables increase or decrease to their final values. An example of the latter is Λ CDM where $w_{\text{eff}} = -1$, $\Omega_{\text{eff}} \rightarrow 1$, $R \rightarrow 4\Lambda$ and $H^2 \rightarrow \Lambda/3$ with no oscillations.

Two examples when $\Lambda_\infty = 2H_0^2$ for the Erf model are shown in Figures 3.6 and 3.7. One is in the oscillating de Sitter region of Figure 3.4 and one is in the non-oscillating de Sitter region. The differing ways in which R/H_0^2 and w_{eff} vary with time in the future are clearly shown.

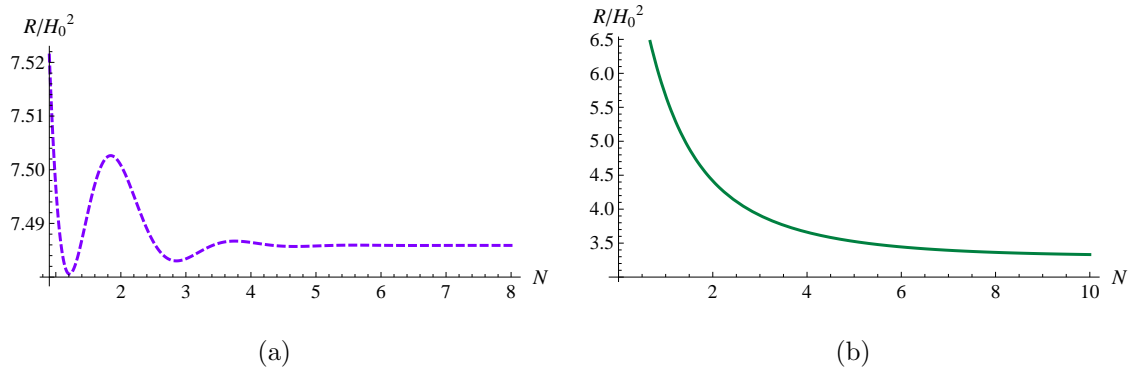


Figure 3.6: R/H_0^2 against $N = \log a$ for two examples of the Erf model at times well after today. (a) shows Model 2 with $\Lambda_\infty = 2H_0^2$, $c = 1.5$ and $\log_{10} b = -0.914$, which is in the de Sitter oscillating region, and (b) shows an example with $\Lambda_\infty = 2H_0^2$, $c = 1.5$ and $\log_{10} b = -1.12$, which is in the de Sitter non-oscillating region. Solving (3.10) for R , gives the de Sitter values of R as (a) $7.486 H_0^2$ and (b) $3.309 H_0^2$, respectively.

It is also instructive to see what happens in the Minkowski region and here we shall consider Model 1. Just like Model 2 there are oscillations but there are also oscillations in $\Omega_{\text{eff}}(N)$. For example, in the de Sitter region, $\Omega_{\text{eff}}(N)$ simply keeps growing until it tends to unity as $N \rightarrow \infty$. We can see that from the expressions for w_{eff} and $w_{\text{eff}}\Omega_{\text{eff}}$ in the glossary entitled *Useful Expressions*,

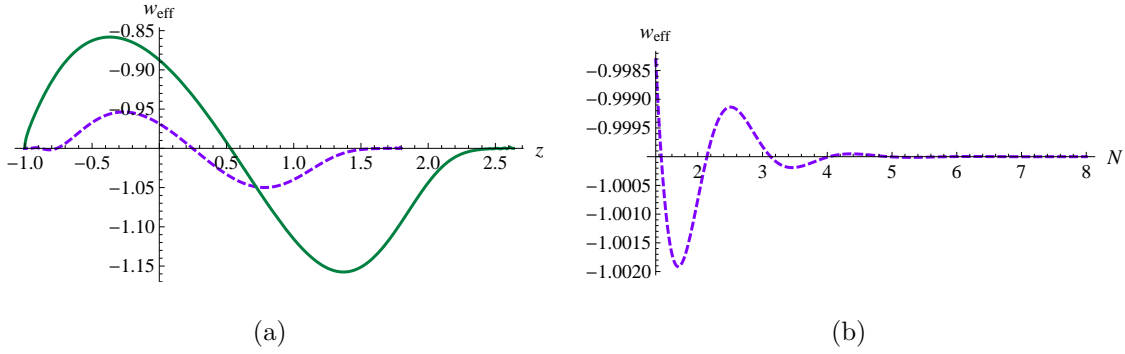


Figure 3.7: w_{eff} for the two examples of the Erf model in Figure 3.6. (a) shows both examples plotted against z . (b) shows the late-time oscillations of Model 2 when w_{eff} is plotted against N . Note the severe gradient in (a) of w_{eff} for the non-oscillating curve (continuous, green) as $z \rightarrow -1$. While $dw_{\text{eff}}/dN \rightarrow 0_+$, $dz/dN \rightarrow 0_-$.

putting the derivative with respect to N equal to zero gives final de Sitter values of $w_{\text{eff}, \text{dS}} = -1$ and $\Omega_{\text{eff}, \text{dS}} = 1$.

For Model 1, however, R/H_0^2 oscillates between positive and negative values of ever-decreasing amplitude while $\Omega_{\text{eff}}(N)$ oscillates between fixed negative and positive values as shown in Figure 3.8. This means, that w_{eff} would tend to infinity at some point in the future. This is because $w_{\text{eff}}\Omega_{\text{eff}} = -1 - 2H'/(3H)$ (1.86) with H'/H , though it oscillates, remaining finite.

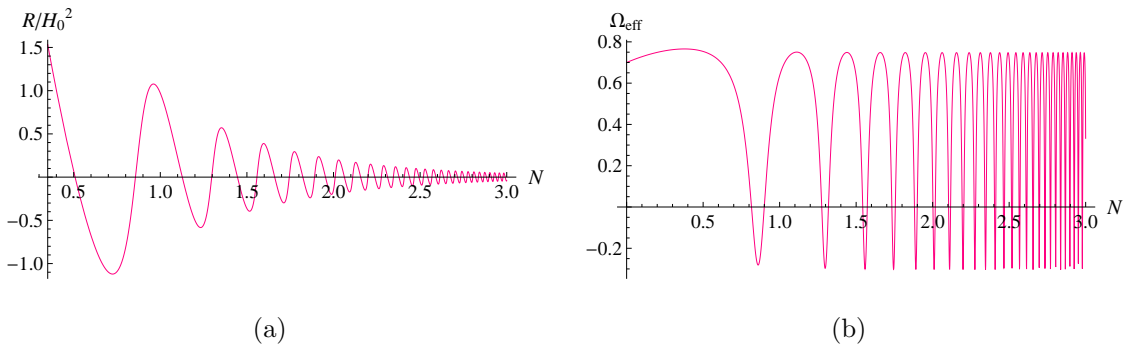


Figure 3.8: Showing the late-time oscillations in R/H_0^2 and Ω_{eff} for Model 1 in the Minkowski region.

3.2.1.3 The matter growth index

Starting from the standard, linearised, matter perturbation equation in the sub-horizon regime [74, 109–113], which is derived in [112],

$$\ddot{\delta}_m + 2H\dot{\delta}_m - 4\pi\frac{G}{F_R(R)}\left(\frac{3 + 4k^2/(aM(a))^2}{3 + 3k^2/(aM(a))^2}\right)\rho_m\delta_m = 0, \quad (3.11)$$

where k is the comoving wavenumber and M is the scalaron mass defined by equation (1.88) with approximation given by

$$M^2 \approx \frac{1}{3F_{RR}(R)}, \quad (3.12)$$

we can define the matter growth index, γ , as a function of the matter density contrast, as already stated in section 2.2.5, by

$$(\Omega_m)^\gamma = \frac{d \log \delta_m}{d \log a} \quad (3.13)$$

$$= \frac{\delta'_m}{\delta_m}. \quad (3.14)$$

Equation (3.11) can be re-cast as

$$\gamma' \log \Omega_m + \gamma \frac{\Omega'_m}{\Omega_m} + (\Omega_m)^\gamma + 2 + \frac{H'}{H} = \frac{3}{2}\eta(a)(\Omega_m)^{1-\gamma}, \quad (3.15)$$

in which

$$\eta(a) = \frac{1}{F_R(R)} \left[\frac{1 + 4\frac{k^2}{a^2}\frac{F_{RR}(R)}{F_R(R)}}{1 + 3\frac{k^2}{a^2}\frac{F_{RR}(R)}{F_R(R)}} \right]. \quad (3.16)$$

The factor in square brackets on the right hand side of equation (3.16) increases from being 1 at early times to being 4/3 at late times. Equation (3.15) can be solved numerically, with the initial condition at large R being that $\gamma = 6/11$ (as appropriate for Λ CDM, [111, 113]). The Λ CDM value of γ at high R can be deduced from (3.15) by varying Ω_m with respect to Λ/H^2 .

The solution for γ , again corresponding to the parameters used in Figure 3.1 are shown in Figure 3.9(a) for $k = 0.14 h \text{ Mpc}^{-1}$. This value of k is also used

in the examples, where relevant, of sections 3.2.2 and 3.2.3. For comparison, in Figure 3.9(b) we show how γ varies in Λ CDM. Clearly the range of values for γ_0 can, under certain circumstances, be larger than has been previously supposed [74, 114].

Ignoring those cases when $\gamma(N)$ has been taken to be constant or linear, authors have commented on the value of γ_0 only in respect of particular models. In [114], in which five models are considered, it is found that all of these models have $0.40 \lesssim \gamma_0 \lesssim 0.55$. We find that both the AB and the Erf models can give values of γ_0 lower than 0.40. Measurements of galaxy clusters by Rapetti et al. [73], using data from ROSAT, BCS, REFLEX and Bright MACS, with a background Λ CDM model, give $\gamma_0 = 0.55^{+0.13}_{-0.10}$. Using XLF data, they find a γ_0 with a mean value of 0.38. See also see [110].

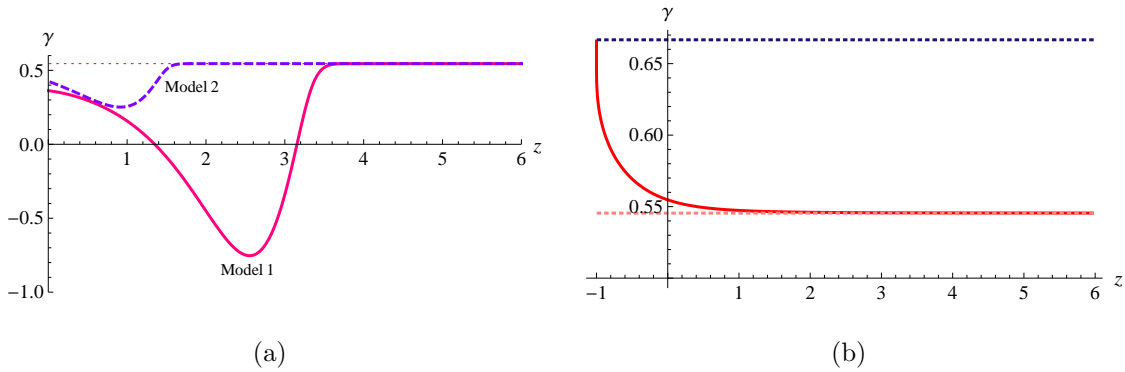


Figure 3.9: Erf model: γ against z for the examples of Figure 3.1. The dotted, red line represents the asymptotic Λ CDM value $6/11$. The general behaviour of γ , as z decreases, is to increase initially away from $6/11$, as it would in Λ CDM, to a local maximum before decreasing to a local minimum from which it rises to today's value. The value of γ_0 for curve for Model 1 is 0.362 while for Model 2 it is 0.426. (b) shows γ for the Λ CDM model which has $\Omega_{m,0} = 0.3$. At early times γ is asymptotic to $6/11$. As z decreases, γ increases to approach the value $2/3$ as $\gamma' \rightarrow 0$ and $z' \rightarrow 0$ making $d\gamma/dz$ undefined. Solution of the Λ CDM equivalent to (3.15) shows that, for $\Omega_{m,0} = 0.3$, then $\gamma_0 = 0.55472 \pm 8 \times 10^{-6}$ and $\gamma'_0 = 0.01688 \pm 4 \times 10^{-6}$.

3.2.2 The AB model

The AB model [101] is

$$f(R) = -\frac{R}{2} + \frac{\epsilon_{\text{AB}}}{2} \log \left[\frac{\cosh(R/\epsilon_{\text{AB}} - b)}{\cosh b} \right], \quad (3.17)$$

$$\epsilon_{\text{AB}} = \frac{R_{\text{vac}}}{b + \log(2 \cosh b)}, \quad (3.18)$$

$$R_{\text{vac}} = 4\Lambda_{\infty}. \quad (3.19)$$

It is a two-parameter model and it, like the Erf model, similarly adheres closely to Λ CDM until comparatively late in the history of the Universe. The Solar System constraint means that $b \gg -4$, although very large values of Λ_{∞} reduce this limit slightly, e.g., $\Lambda_{\infty} = 10$ means $b \gg -3$. Positive values of b means the Solar System test is passed with ease. For example, $\Lambda_{\infty} = 2H_0^2$, $b = 0$ gives $R_s f_{RR}(R_s) = 5 \times 10^{-75,253}$. In the paper where it was introduced [76], Appleby and Battye take the parameter $b \gtrsim 1.2$. This was done because current data suggests that we are approaching a late time de Sitter vacuum state (not Minkowski space). Since Λ CDM tends to a late-time de Sitter vacuum state, Appleby and Battye wanted to find models that behaved like Λ CDM (because the data are consistent with Λ CDM), but which had no true cosmological constant. This, however, restricts the value of $|1 + w_{\text{eff},0}|$ to be less than 0.04 [101].

Figure 3.11 shows how the fixed points are approached, as b increases, for a range of Λ_{∞} .

For Figures 3.12, 3.13 and 3.14, two examples have been chosen, one with $b = 0.2$ and $\Lambda_{\infty} = 1.65H_0^2$, which we term Model 3, and one with $b = 1.2$ and $\Lambda_{\infty} = 1.92H_0^2$, which we term Model 4. Both give $\Omega_{\text{eff},0} = 0.7$ and are indicated by spots in Figures 3.10 and 3.11.

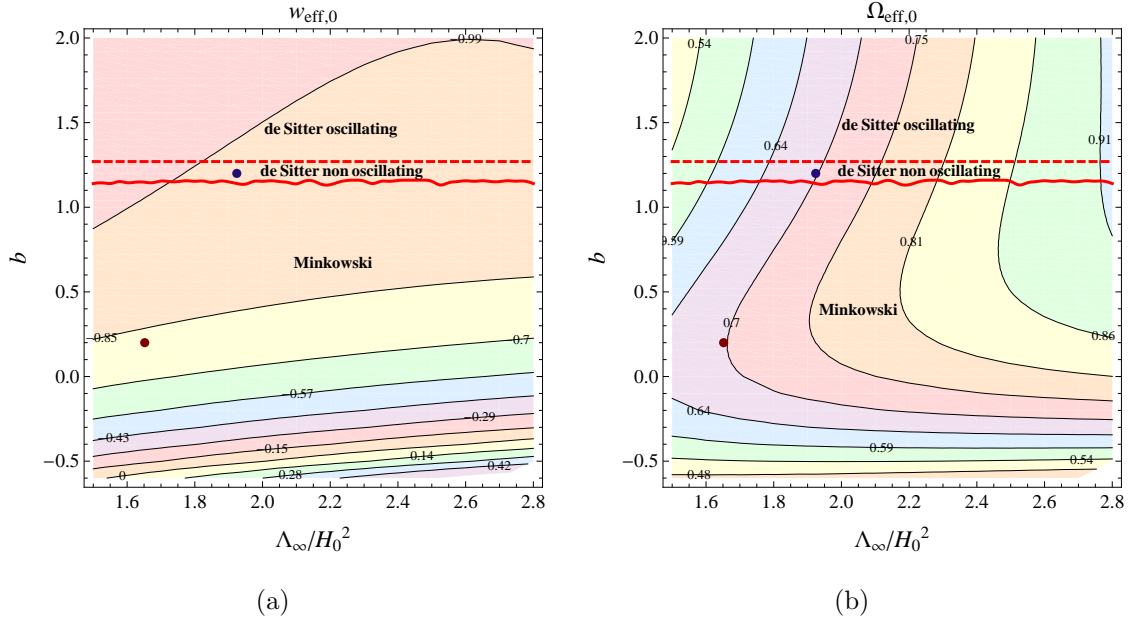


Figure 3.10: Contour plots for the AB model. Though they do not show up at all well, in (a) all values $w_{\text{eff},0}$ are negative. The two spots represent Models 3 and 4, see below. Note the inclusion of the late-time de Sitter and Minkowski regions.

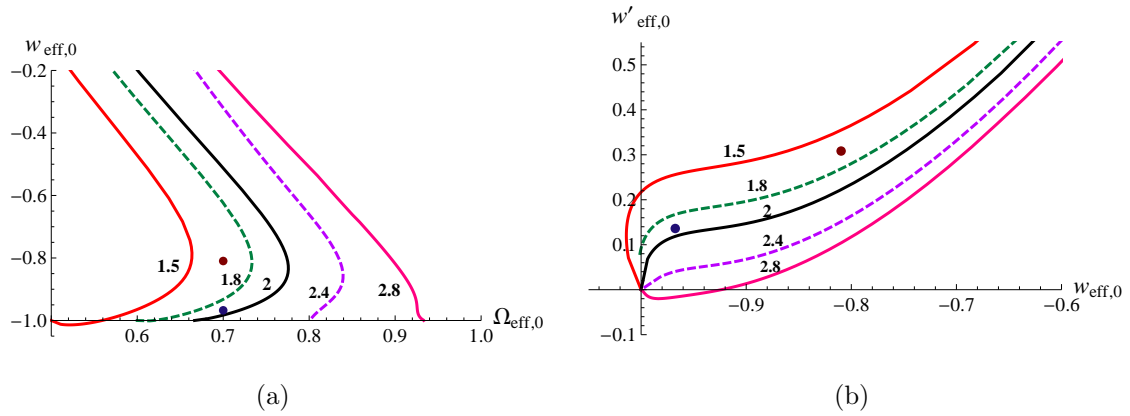


Figure 3.11: AB model: $w_{\text{eff},0}$ as a function of $\Omega_{\text{eff},0}$ and $w'_{\text{eff},0}$ as a function of $w_{\text{eff},0}$ for the values of Λ_∞/H_0^2 indicated. The fixed points are in (a) $(\Lambda_\infty/(3H_0^2), -1)$ and in (b) $(-1, 0)$. Parameter b starts at the top of each curve and increases towards the fixed points.

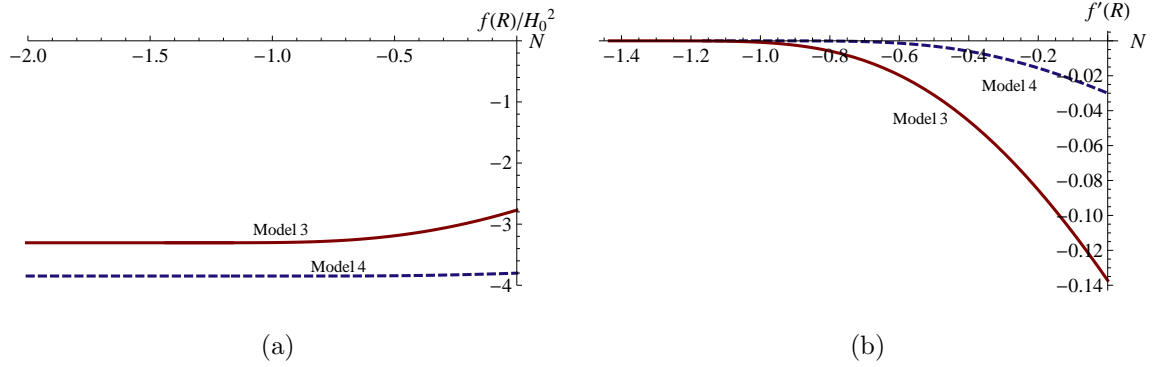


Figure 3.12: AB model: $f(R)/H_0^2$ and $f'_R(R)$ against N .

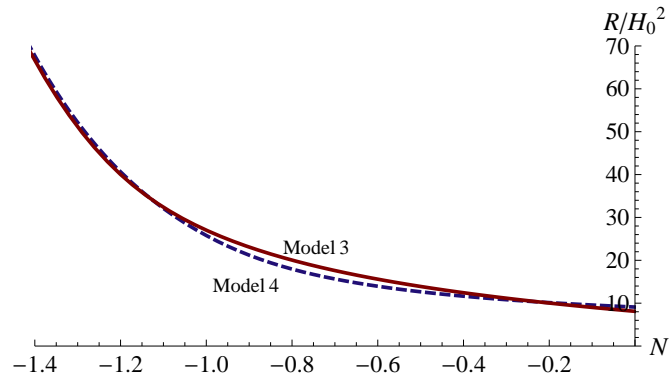


Figure 3.13: AB model: R/H_0^2 against N for the curves of Figure 3.12. For Model 3, $R_0 = 8.1 H_0^2$ and, for Model 4, $R_0 = 9.1 H_0^2$.

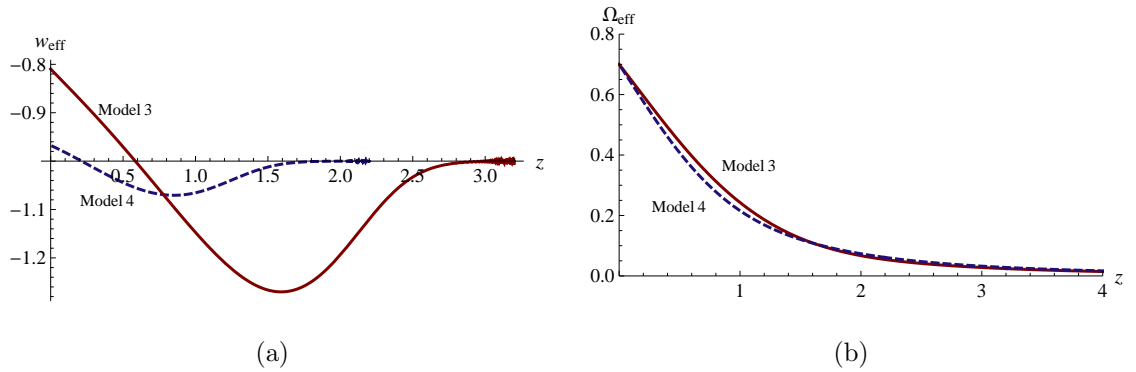


Figure 3.14: AB model: w_{eff} and Ω_{eff} against z for the curves of Figure 3.12.

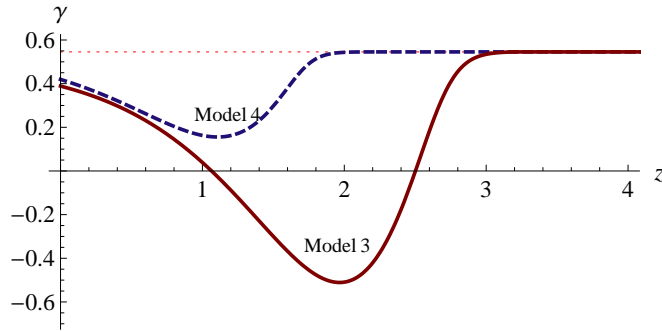


Figure 3.15: AB model: Evolution of γ against z for the examples of Figure 3.12. The values of γ_0 are 0.39 for Model 3 and 0.42 for Model 4.

3.2.3 The HSS model

Like the Erf model, the HSS model is a three parameter model:

$$f(R) = -\frac{R_{\text{vac}}}{2} \frac{c (R/R_{\text{vac}})^{2n}}{1 + c (R/R_{\text{vac}})^{2n}}, \quad (3.20)$$

$$R_{\text{vac}} = 4\Lambda_{\infty}, \quad (3.21)$$

with $n > 0$. In fact, for this model to pass the Solar System test, we must have $n > 1$. For $n < 2$, when $\Lambda_{\infty} = 2H_0^2$, for instance, it passes this test only for some values of R_{vac} , as c varies, so it is safest to have $n \geq 2$. For very large but unrealistic values of Λ_{∞} the lower limit on n may have to be increased to 3. The limit as $R \rightarrow \infty$ is $f(\infty) = -R_{\text{vac}}/2$ which is Λ CDM with cosmological constant equal to $R_{\text{vac}}/4$, as for the AB model. It should be noted that up to the present time $R > R_0$. If $R_0/R_{\text{vac}} > 1$ this model tends to Λ CDM if either of c or n should tend to infinity.

Graphical examples below are for $n = 2$ and $n = 6$. The blank ‘triangular’ region at the bottom right hand corner of the contour plots is owing to the fact that, for small enough c , $f_{RR}(R_0)$ will become zero (see, for example, Figure 3.22(b)). The value of c for which this happens is given by

$$c = \frac{2n - 1}{2n + 1} \left(\frac{R_0}{R_{\text{vac}}} \right)^{-2n}. \quad (3.22)$$

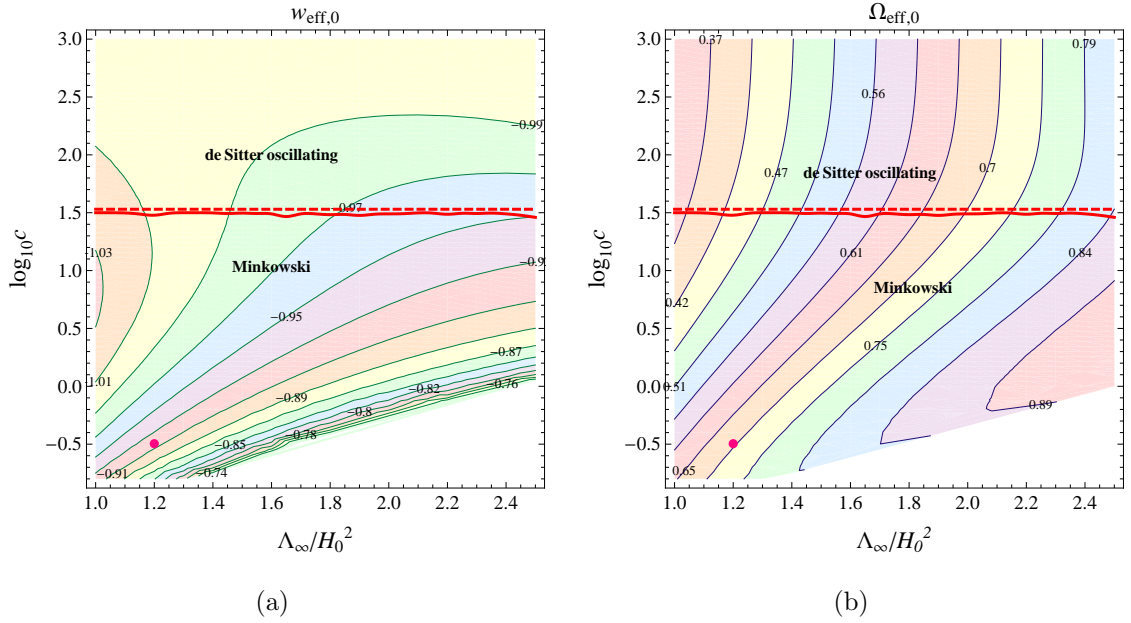


Figure 3.16: Contour plots for the HSS model of $w_{\text{eff},0}$ and $\Omega_{\text{eff},0}$ against Λ_∞/H_0^2 and $\log_{10} c$ when $n = 2$. The pink spot represents Model 6, see below. The narrow late-time de Sitter non-oscillating region has not been labelled.

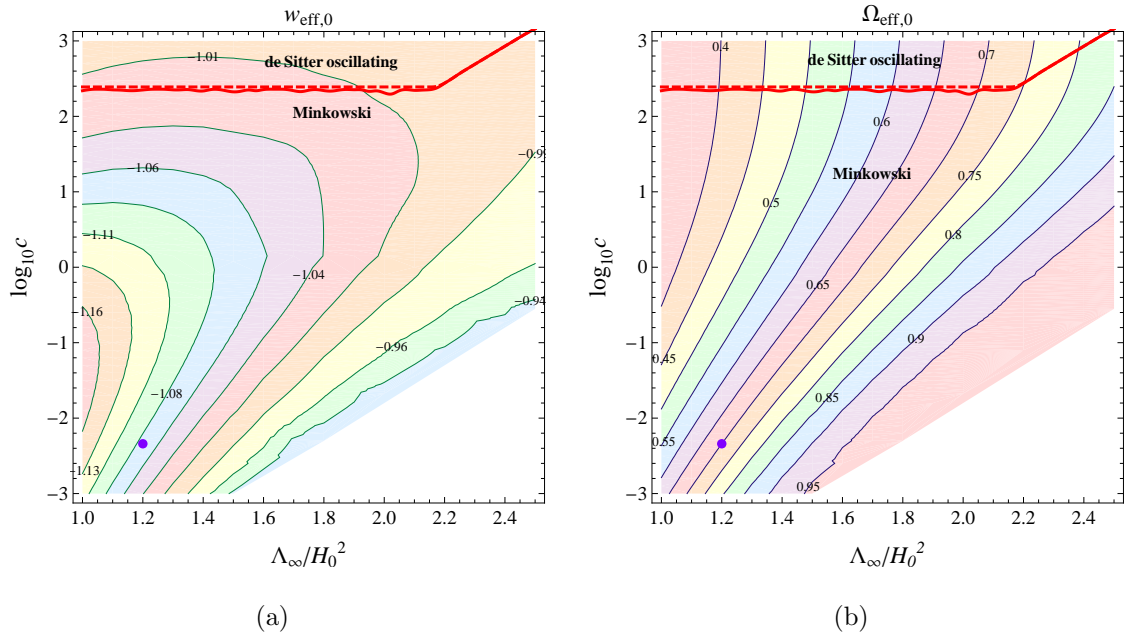


Figure 3.17: Contour plots for the HSS model of $w_{\text{eff},0}$ and $\Omega_{\text{eff},0}$ against Λ_∞/H_0^2 and $\log_{10} c$ when $n = 6$. The mauve spot locates Model 5, see below.

Notice, from Figures 3.16 and 3.17, how restricting solutions to the de Sitter regions gives values of $|1 + w_{\text{eff},0}| \lesssim 0.04$. How the fixed points are approached, for a given value of Λ_∞/H_0^2 , is shown in Figures 3.18 and 3.19.

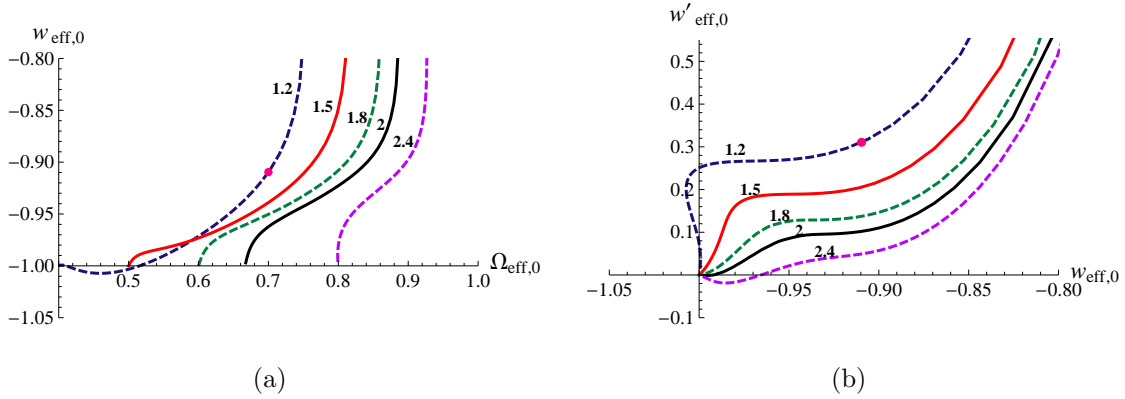


Figure 3.18: HSS model: $w_{\text{eff},0}$ as a function of $\Omega_{\text{eff},0}$ and $w'_{\text{eff},0}$ as a function of $w_{\text{eff},0}$ when $n = 2$. The fixed points are in (a) $(\Lambda_\infty/(3H_0^2), -1)$ and in (b) $(-1, 0)$. Each curve is labelled with its value of Λ_∞/H_0^2 ; parameter c increases towards the fixed point. The pink spot locates the example we term Model 6.

Of the plethora of possibilities, we choose just two to illustrate the nature and properties of the HSS $f(R)$. The chosen examples, both with $\Lambda_\infty = 1.2 H_0^2$ have $n = 6$, which we call Model 5, or $n = 2$, which is Model 6, and appropriate values of c to give $\Omega_{\text{eff},0} = 0.7$.

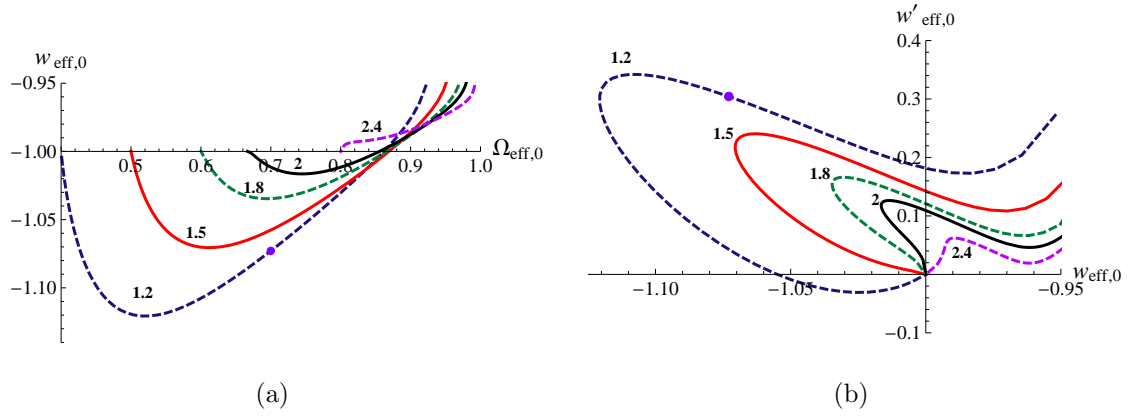


Figure 3.19: HSS model: $w_{\text{eff},0}$ as a function of $\Omega_{\text{eff},0}$ and $w'_{\text{eff},0}$ as a function of $w_{\text{eff},0}$ when $n = 6$. The fixed points are in (a) $(\Lambda_\infty / (3H_0^2), -1)$ and in (b) $(-1, 0)$. Each curve is labelled with its value of Λ_∞ / H_0^2 ; parameter c increases towards the fixed point. The mauve spot locates the example we term Model 5.

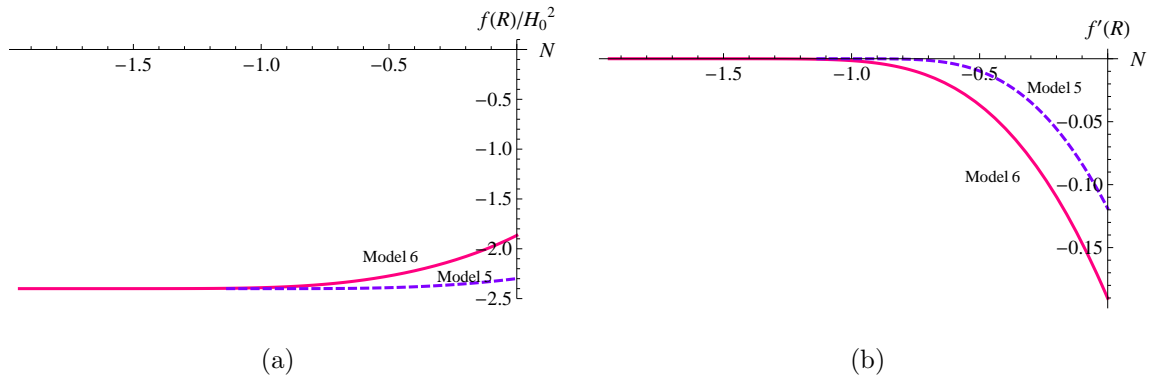


Figure 3.20: HSS model: $f(R)/H_0^2$ and $f'_R(R)$ against N when $\Lambda_\infty = 1.2 H_0^2$ and for two values of n . Model 5 has $n = 6$ and $\log_{10} c = -2.34$ while Model 6 has $n = 2$ and $\log_{10} c = -0.496$.

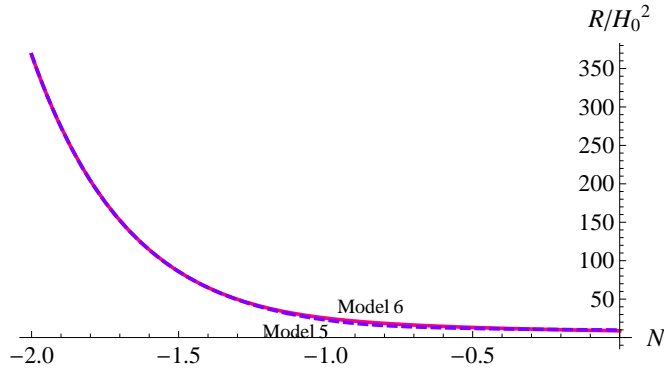


Figure 3.21: HSS model: R/H_0^2 against N for the curves of Figure 3.20. Model 5 has $R_0 = 9.8 H_0^2$ while Model 6 has $R_0 = 8.7 H_0^2$.

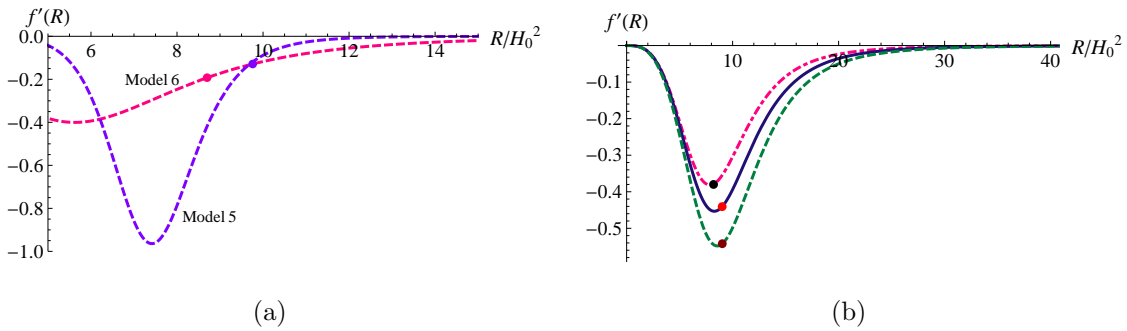


Figure 3.22: HSS model: $f'_R(R)$ against R for Models 5 and 6, and three examples when $n = 2$ with parameters close to the lower boundary of Figure 3.16. (a) shows how far the values of R_0 , denoted by spots, are from the turning points. In (b) the curves have parameters $(\Lambda_\infty/H_0^2, \log_{10} c)$, as follows: dot-dashed, pink curve, $(1.6, -0.58)$; blue, $(2, -0.28)$; dashed, green $(2.5, 0.05)$. The spots indicate the respective values of R_0 and indicate how close they are to the problematic values of R for which $f_{RR}(R) = 0$.

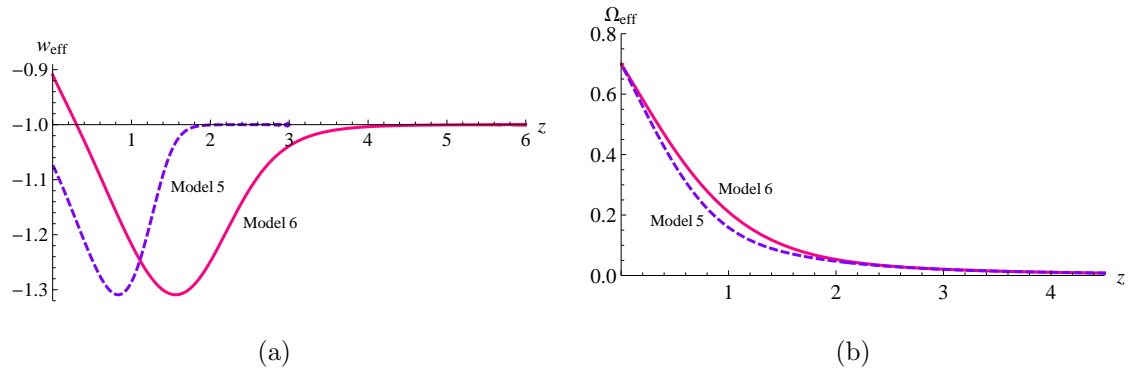


Figure 3.23: HSS model: w_{eff} and Ω_{eff} against z for the curves of Figure 3.20.

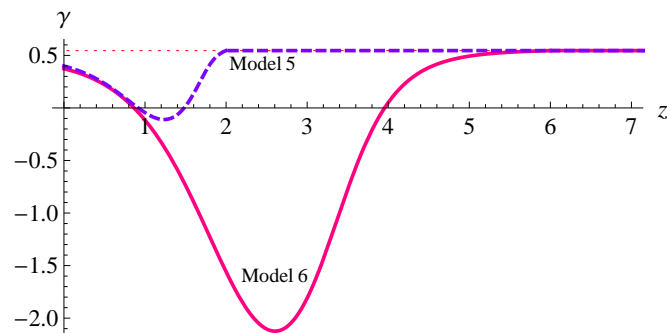


Figure 3.24: HSS model: Evolution of γ against z for the examples of Figure 3.20.

Model 5 gives $\gamma_0 = 0.40$ while Model 6 gives $\gamma_0 = 0.37$.

3.3 Conclusion

The results of Planck do not conclusively show that we are living in a Λ CDM Universe, though they do not rule that out. Essentially, there is still some doubt as to today's value of the effective dark energy equation of state parameter, which we have called w_{eff} . It was decided to review the properties of some $F(R)$ models and to produce one of our own in order to see how large a deviation from -1 we could obtain for $w_{\text{eff},0}$. Constraining $w_{\text{eff},0}$, constrains R_0 for, using $R = 3H^2(1 - 3w_{\text{eff}}\Omega_{\text{eff}})$ (from *Useful Expressions* on page 24), $|1 + w_{\text{eff},0}| < \delta$ means that $|R_0 - R_{\Lambda,0}| < 9H_0^2\Omega_{\text{eff},0}\delta$. In this regard we went beyond the bounds set by Planck and its predecessor, WMAP, to see what would happen but ensuring that $\Omega_{\text{eff},0}$ was always the same.

All $F(R) = R + f(R)$ models are constrained quite severely by the Solar System which has the effect of ensuring that $f(R)$ lies close to $-2\Lambda_\infty$ until comparatively recently. Until then, w_{eff} always lies close to -1 . When $f(R)$ then swings away from $-2\Lambda_\infty$ then $f_R(R)$ swings away from being close to zero, though still negative, and w_{eff} swings away from -1 , first in a negative sense, then reaching a local minimum in the recent past before returning to give a value for $w_{\text{eff},0}$.

For each generic model, we have seen how varying the parameters of those models varies the values of $w_{\text{eff},0}$ and $\Omega_{\text{eff},0}$, how $w_{\text{eff},0}$ and $\Omega_{\text{eff},0}$ and how $w'_{\text{eff},0}$ and $w_{\text{eff},0}$ are connected when one specific parameter changes. We have also seen how, if left unmodified, what the future of each model might be. In some instances, the potential of the scalar field, $\phi = f_R(R)$, reaches a stable minimum, at R_{dS} , as a de Sitter attractor which can be reached by R oscillating with decaying amplitude about R_{dS} or by simply decreasing to it without any oscillations. It could be that $R_{\text{dS}} = 0$. Alternatively, R tends to zero by wild oscillations with Ω_{eff} oscillating between positive and negative values thereby driving w_{eff} to infinity and back again, repeatedly, with ever-increasing frequency.

The matter growth index was studied for all six examples which showed that, while those models which kept close to Λ CDM at the present time gave values of γ , the matter growth index, of 0.4 or slightly higher, those which swung away markedly from Λ CDM gave values of γ_0 less than 0.4. The perceived wisdom to date is that $F(R)$ models give γ_0 in the approximate range 0.4 to 0.55. The γ for Λ CDM, itself, increases from the value $6/11 = 0.545$ at high curvature to give $\gamma_0 = 0.555$. It is also noticed that some of the values of γ go negative as the Universe evolves. This is illustrated, but not remarked upon, in Appleby and Weller's paper [113]. The effect of letting γ go negative is to allow Ω_m^γ and, hence, δ'_m/δ_m to be larger than they would otherwise be. Thus, whatever value δ_m starts with at some earlier stage, it has a larger value today than it otherwise would have. This is illustrated in Figure 3.25 for three models: standard Einstein gravity, Erf Model 1, for which γ goes negative, and Erf Model 2, for which $\gamma > 0$.

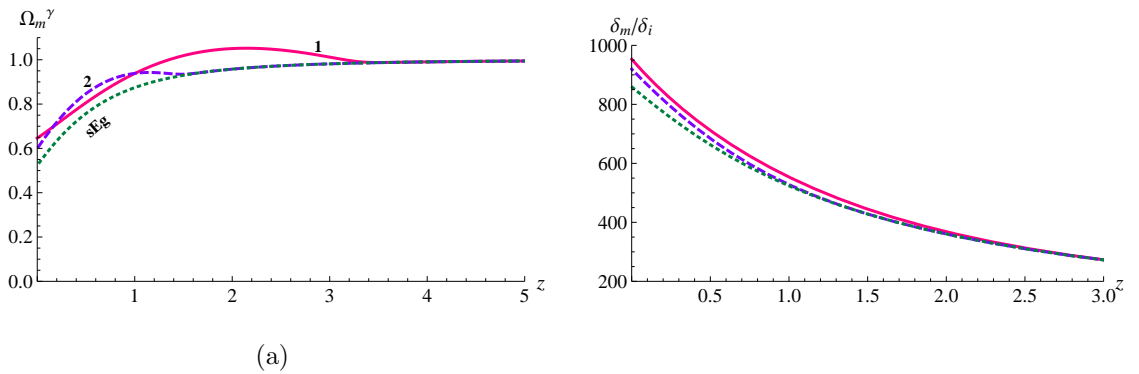


Figure 3.25: Comparing the effect of γ going negative as opposed to its always being positive. Illustrated are standard Einstein gravity (**sEg**, dotted green), Erf Model 1 (**1**, continuous pink) and Erf Model 2 (**2**, dashed mauve). The evolution of γ for these models is shown in Figure 3.9. Pane (a), above, shows how Ω_m^γ varies with z while (b) shows late detail of the evolution of the ratio δ_m/δ_i , where δ_i is the value of δ_m at $z = 1095$, the point at which evolution of γ was started. For $z \gtrsim 3$, in these cases the values of δ_m/δ_i are indistinguishable. At $z = 0$, the respective values of δ_m/δ_i are 859 for standard Einstein gravity, 919 for Erf Model 2 and 953 for Erf Model 1.

The graphs were obtained by numerically solving (3.15) for γ and then integrating (3.14) for δ_m . The initial value of z was taken to be 1095, at which $\gamma = 6/11$ and $\delta_m = \delta_i$. Assuming Erf Model 1 to be an extreme case, we see that $F(R)$ models give a deviation, today, for γ of up to around 10% from the standard Einstein gravity case but that cases in which γ does not go negative achieve almost as much.

The next step could be to try to construct an $F(R)$ model which could give realistic values within their range of uncertainty to all the cosmological parameters currently measured.

Chapter 4

The $w_{\text{eff}} < -1$ Theorem for $F(R)$ Models

4.1 Introduction

Excluding Λ CDM, all practical $F(R) = R + f(R)$ models have the property that $f(R) \rightarrow -2\Lambda$, as $R \rightarrow \infty$ and they all have graphs similar to Figure 3.1 in the matter and radiation eras. Further, $f_R(R) < 0$, $f_{RR}(R) > 0$ such that $f_R(R) \rightarrow 0$ and $f_{RR}(R) \rightarrow 0$, as $R \rightarrow \infty$. All instances of graphs of w_{eff} for these $F(R)$ models show that it is slightly less than -1 at high z becoming more negative with time until it reaches a local minimum [47, 68, 97, 101, 115]. In this chapter, we prove that in the radiation and matter eras, $w_{\text{eff}} < -1$ and decreases.

4.2 The theorem

Theorem: For $F(R)$ models which tend to Λ CDM as $R \rightarrow \infty$, which is $a \rightarrow 0$, w_{eff} decreases from -1 as a increases from 0 through the radiation and matter eras.

Proof: To prove this we use $w_{\text{eff}} = -1 - \rho'_{\text{eff}}/(3\rho_{\text{eff}})$, which is (1.84), and show that $\rho'_{\text{eff}}(N) > 0$ in the radiation and early matter eras. A difficulty arises in that, at early times, $f(R)$ lies extremely close to -2Λ , while being above it, for a very long time; see Figure 3.1(a). $\rho'_{\text{eff}}(N)$ will be numerically very small indeed for much of the history of the Universe up to the present time. Figure 4.1, which compares $8\pi G\rho_{\text{eff}}/H_0^2$ with corresponding w_{eff} , shows one example.

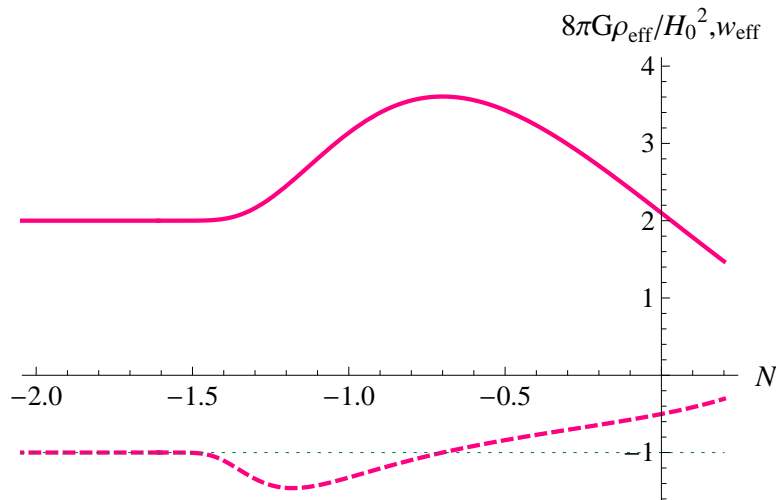


Figure 4.1: A combined graph showing how $8\pi G\rho_{\text{eff}}/H_0^2$ (continuous) and corresponding w_{eff} (dashed) vary with N . Data are from Erf Model 1 of subsection 3.2.1.

As yet, making no assumptions, let our variable be $N = \log a$, as usual, and introduce a new parameter, $\chi = 8\pi G\rho_{\text{eff}}/3$. Thus

$$H^2 = \frac{8\pi G\rho_r}{3} + \frac{8\pi G\rho_m}{3} + \frac{8\pi G\rho_{\text{eff}}}{3} \quad (4.1)$$

$$= \alpha e^{-4N} + \beta e^{-3N} + \chi, \quad (4.2)$$

$$\Rightarrow w_{\text{eff}} = -1 - \frac{\chi'}{3\chi}, \quad (4.3)$$

where α and β are constants. χ will tend to $\Lambda/3$ as $R \rightarrow \infty$. From this we find

$$2HH' = -3H^2 + 3\chi + \chi' - \alpha e^{-4N}. \quad (4.4)$$

$$R = 3H^2 + 9\chi + 3\chi' - 8\pi G\rho_r. \quad (4.5)$$

From the field equation (1.75),

$$3H\partial_0 F_R(R) + \left(3H^2 - \frac{R}{2}\right) F_R(R) + \frac{1}{2}F(R) = 3H^2 - 3\chi \quad (4.6)$$

$$\Rightarrow 3H\partial_0 f_R(R) + \left(3H^2 - \frac{R}{2}\right) f_R(R) + \frac{1}{2}f(R) = -3\chi. \quad (4.7)$$

From the trace, (1.76),

$$3\Box F_R(R) + R F_R(R) - 2F(R) = 8\pi G(-\rho + 3P) \quad (4.8)$$

$$\Rightarrow -3\partial_0^2 f_R(R) - 9H\partial_0 f_R(R) - R + R f_R(R) - 2f(R) = -3H^2 + 3\chi + 8\pi G\rho_r \quad (4.9)$$

$$\Rightarrow -3\partial_0^2 f_R(R) - 9H\partial_0 f_R(R) + R f_R(R) - 2f(R) = 12\chi + 3\chi'. \quad (4.10)$$

Adding $4 \times (4.7)$ to (4.10) and then dividing by 3 gives

$$-\partial_0^2 f_R(R) + H\partial_0 f_R(R) + \left(4H^2 - \frac{R}{3}\right) f_R(R) = \chi'. \quad (4.11)$$

In the regions we are concerned with, χ' and $f_R(R)$ are first order small quantities. In expressing the values of the terms on the left hand side of (4.11) to form (4.21), we make use the following zero-th order approximations, $2HH' = -(4 - \theta)H^2$, $R = 3\theta H^2$ and $R' = -3R$. The parameter θ has been introduced to indicate where in the radiation and matter eras we are operating. In the matter era, $\theta = 1$ while, in the radiation era, $\theta = 0$, except we must be careful not to let $R = 0$ where so doing would be incorrect. θ takes values between 0 and 1.

We can express $f(R)$ as a convergent power series in a but because it is so flat in the radiation era and most of, if not all of, the matter era, we can express $f(R)$ as

$$f(R) = -2\Lambda + a^n \sum_{i=0}^{\infty} \mu_i a^i, \quad (4.12)$$

where the μ_i are constants, $\mu_0 > 0$, $a^n \sum_{i=0}^{\infty} \mu_i a^i > 0$ and n will be very large. In view of the flatness of $f(R)$ and that $0 < a \ll 1$, at early times, we need only

consider the leading term, so let

$$f(R) = -2\Lambda + \mu_0 a^n, \quad (4.13)$$

$$= -2\Lambda + \mu_0 e^{nN}, \quad (4.14)$$

using $N = \log a$. We now express $f_R(R)$ in terms of N and evaluate $\partial_0 f_R(R)$ and $\partial_0^2 f_R(R)$.

$$f_R(R) = \frac{f'(R)}{R} \quad (4.15)$$

$$= -\frac{n\mu_0}{3R} e^{nN}. \quad (4.16)$$

$$\partial_0 f_R(R) = -\frac{Hn\mu_0}{3} \left(\frac{e^{nN}}{R} \right)' \quad (4.17)$$

$$= -\frac{n(n+3)\mu_0 H}{3R} e^{nN}. \quad (4.18)$$

$$H\partial_0 f_R(R) = -\frac{n(n+3)\mu_0 H^2}{3R} e^{nN}. \quad (4.19)$$

$$\partial_0^2 f_R(R) = -\frac{n(n+3)(2n+2+\theta)\mu_0 H^2}{6R} e^{nN}. \quad (4.20)$$

Putting these into (4.11) gives

$$\chi' = \frac{n[2n^2 + (6+\theta)n - 8 + 5\theta]\mu_0 H^2}{6R} e^{nN} \quad (4.21)$$

$$\simeq \frac{n^3\mu_0 H^2}{3R} e^{nN} > 0. \quad (4.22)$$

Initially, when $a = 0$ and $N \rightarrow -\infty$, χ' will be zero because, although H^2/R is proportional to e^{-N} in the radiation era, χ' is proportional to $e^{(n-1)N}$ which tends to zero as $N \rightarrow -\infty$. So starting from $f(R) = -2\Lambda$, where $w_{\text{eff}} = -1$, $e^{(n-1)N}$ increases. That is, χ' increases with N while, to very good approximation, χ remains constant. χ'/χ increases so that w_{eff} decreases into the phantom region. It continues to do so until the proposed expression for $f(R)$, (4.13), fails to be a good approximation.

Chapter 5

Evolution of Perturbations

5.1 Introduction

In this chapter we consider matter and metric perturbations of the line element in an FRW Universe. In the Newtonian gauge these can be encoded via

$$ds^2 = -(1 + 2\Psi) dt^2 + a^2 (1 - 2\Phi) \delta_{ij} dx^i dx^j, \quad (5.1)$$

where Φ and Ψ are small, dimensionless perturbations to the FRW metric. We attempt to produce algebraic solutions to the evolution equations (A1) and (A2) and the linear Einstein equations (A3) and (A4) of Pogosian and Silvestri [79]. They are:

$$\delta' + \frac{k}{aH} V - 3(1+w)\Phi' + 3\left(\frac{\delta P}{\delta\rho} - w\right)\delta = 0, \quad (5.2)$$

$$V' + (1-3w)V - \frac{k}{aH}\left(\frac{\delta P}{\delta\rho} - \frac{\Pi}{\delta}\right)\delta - \frac{k}{aH}(1+w)\Psi = 0. \quad (5.3)$$

$$(1 + f_R) \left(6\Psi + 6\Phi' + 2\frac{k^2}{a^2 H^2} \Phi \right) = -\frac{3E_i}{H^2} \delta_i + 3f_{RR} \delta R' - f'_R (6\Psi + 3\Phi'), \\ - \left[3f_{RR} \left(1 + \frac{H'}{H} \right) - \frac{k^2}{a^2 H^2} f_{RR} - 3f'_{RR} \right] \delta R. \quad (5.4)$$

$$(1 + f_R)(k\Psi + k\Phi') = \frac{3a}{2H}E_i V_i + \frac{1}{2}k(f_{RR}\delta R)' - \frac{1}{2}kf_{RR}\delta R - \frac{1}{2}kf'_R\Psi. \quad (5.5)$$

These equations are in Fourier space with $\delta \equiv \delta\rho/\rho$, the density contrast, $V \equiv (1 + w)v$, where v is the scalar component of the velocity, and $E \equiv H^2/H_0^2$. E_i and δ_i are the various energy components of E and δ , respectively, so that as far as matter perturbations are concerned, $E_i\delta_i = E_m\delta_m = 8\pi G\rho_m\delta_m/(3H_0^2)$. δP is the pressure perturbation which, for matter, is zero and $\rho\Pi \equiv (\hat{k}^j\hat{k}_i - \delta^j_i/3)\pi^i_j$ is the anisotropic stress which is zero because π^i_j is the traceless component of the energy-momentum tensor [79]. In particular, $\Pi_m = 0$.

(5.4) is a corrected version of (A3) with three typographical errors removed. As a check they were compared to the equivalent equations in Ma and Bertschinger [116]. ' means differentiation with respect to $N = \log a$. We solve these equations, as applied to matter perturbations only, for a given co-moving k .

Some work, in this area, had already been done on this by Starobinsky [78], by Appelby et al. [101] and by Elizalde et al. [117], but they only considered what happens at early times in the matter era and the approach was different from ours. No initial conditions were applied. Tsujikawa [112] adopted different approach and found expressions for the perturbed potentials as powers of t . Our challenge was to produce a solution which remained viable up to the present time.

In trying to produce an algebraic solution to these equations, a series approach in terms of a single variable was adopted. This variable was chosen to remain as small as possible throughout the history of the Universe. The four equations above, were reduced, with the aid of the field equation and an expression for δR , to two coupled, second order, homogeneous, linear differential equations in Φ and Ψ . Approximate algebraic expressions in terms of this variable were then found for Φ and Ψ which contained both oscillating and non-oscillating components.

In order to illustrate the oscillations, graphically, it was necessary to define as

$x(N)$ a “difference” in Φ and Ψ , as defined in (5.54) different from $\Phi - \Psi$. To complement this, the sum, $y(N)$, was also constructed, (5.55). Initial conditions were applied to Φ and Ψ . Using the same initial conditions, the two differential equations were integrated, numerically, and the functions corresponding to the algebraic solutions for $x(N)$ and $y(N)$ produced and compared for differing models and for different values of k .

It was found that, while the algebraic and numeric solutions were in general agreement when $k \gtrsim 0.1 \text{h Mpc}^{-1}$, smaller values of k produced less agreement in the later stages of the Universe’s history. Also noticed in the solution for $x(N)$ was a “jump” which is due to the non-oscillating component of $x(N)$.

5.2 Matter perturbation equations in k -space for the Jordan Frame

The equations we solve are those of Pogosian and Silvestri [79]. Subscripts “m” refer to the matter component and the anisotropic stress is taken to be zero.

The anisotropy equation with no anisotropic contribution from matter, equation (30) of [79], is

$$F_R(\Phi - \Psi) = F_{RR}\delta R. \quad (5.6)$$

while the evolution equations for matter density perturbations and matter fluid velocity are

$$\delta'_m + \frac{k}{aH}V_m = 3\Phi', \quad (5.7)$$

$$V'_m + V_m = \frac{k}{aH}\Psi. \quad (5.8)$$

These are equations (A1) and (A2) of [79] with $w = 0$ and $\delta P/\delta\rho$ set to zero since P , the pressure of matter, is zero at all times. Π is also set to zero since we take π^i_j of equations (26) of [79] to be zero.

The 00 and 0, i components of the Einstein equations, perturbed to first order, give, with some manipulation,

$$F_R \left[\frac{k^2}{a^2} (\Phi + \Psi) - \left(6H^2 - \frac{R}{2} \right) (\Phi - \Psi) \right] + 3H^2 R' F_{RR} (\Phi' + \Psi) = -8\pi G \rho_m \left[\delta_m + \frac{3aH}{k} V_m \right] \quad (5.9)$$

$$F_R (\Phi' + \Psi' + \Phi + \Psi) - R' F_{RR} (\Phi - 2\Psi) = \frac{8\pi G \rho_m a}{Hk} V_m. \quad (5.10)$$

(5.9) is derived from (A3) and (A4) by eliminating $(F_{RR} \delta R)'$, (5.10) is (A4), (5.7) is (A1) and (5.8) is (A2). $\rho'_m = -3\rho_m$.

The perturbed Ricci scalar in k -space is [112, 118]

$$\delta R = -\frac{4k^2}{a^2} \Phi + \frac{2k^2}{a^2} \Psi - 6H^2 (\Phi'' + \Psi') - (12H^2 + R) \Phi' - 2R\Psi. \quad (5.11)$$

It should be borne in mind that, when converting a derivative with respect to time to one with respect to $N = \log a$, $d/dt = H d/dN$, so that, for example, $\ddot{\Phi} = HH'\Phi' + H^2\Phi''$.

If we can ignore radiation then the 00 component and the trace of the field equation give

$$6H^2 R'^2 F_{RRR} = -3F + (R + 6H^2) F_R - (R R' + 6H^2 R'') F_{RR}. \quad (5.12)$$

This will be needed when differentiating (5.10) and using (5.8) to eliminate V_m .

Introducing two new variables

$$\xi = \frac{3H^2 F_{RR}}{F_R}, \quad (5.13)$$

$$\lambda = \frac{k}{aH}, \quad (5.14)$$

and eliminating δR from (5.6) and (5.11) gives

$$\begin{aligned} \Phi'' + \left(2 + \frac{R}{6H^2} \right) \Phi' + \left(\frac{1}{2\xi} + \frac{2\lambda^2}{3} \right) \Phi \\ + \Psi' - \left(\frac{1}{2\xi} + \frac{\lambda^2}{3} - \frac{R}{3H^2} \right) \Psi = 0, \end{aligned} \quad (5.15)$$

and, from (5.8), (5.10) and (5.12),

$$\begin{aligned} & \Phi'' + \left(2 + \frac{R}{6H^2}\right) \Phi' + \frac{F}{2H^2 F_R} \Phi \\ & + \Psi'' + \left(2 + \frac{R}{6H^2} + \frac{R'\xi}{H^2}\right) \Psi' + \left(\frac{R}{H^2} - \frac{3F}{2H^2 F_R}\right) \Psi = 0. \end{aligned} \quad (5.16)$$

Now using $R = 12H^2 + 6HH'$ and $F = R + f$ these two equations become

$$\begin{aligned} & \Phi'' + \left(4 + \frac{H'}{H}\right) \Phi' + \left(\frac{1}{2\xi} + \frac{2\lambda^2}{3}\right) \Phi \\ & + \Psi' - \left(\frac{1}{2\xi} + \frac{\lambda^2}{3} - 1 - \frac{H'}{2H}\right) \Psi = 0, \end{aligned} \quad (5.17)$$

$$\begin{aligned} & \Phi'' + \left(4 + \frac{H'}{H}\right) \Phi' + \left(6 + \frac{3H'}{H} + \frac{f}{2H^2(1+f_R)}\right) \Phi \\ & + \Psi'' + \left(4 + \frac{H'}{H} + \frac{R'\xi}{H^2}\right) \Psi' - \left(6 + \frac{3H'}{H} + \frac{3f}{2H^2(1+f_R)}\right) \Psi = 0. \end{aligned} \quad (5.18)$$

In solving (5.17) and (5.18), it is assumed that $F(R)$ is Λ CDM at an early value of a in the matter era [79]. Numerical solution of these equations is relatively straightforward. Before attempting to solve them algebraically, we look at the Λ CDM case.

5.2.1 The Λ CDM model

In Λ CDM, $F(R) = R - 2\Lambda$ and $\xi = 0$. Equation (5.6) gives $\Phi = \Psi$ and (5.16) becomes

$$\Phi'' + \frac{5R - 12\Lambda}{2(R - 3\Lambda)} \Phi' + \frac{3\Lambda}{R - 3\Lambda} \Phi = 0. \quad (5.19)$$

Following Pogosian et al. in [79], the initial conditions are $\Phi = -1$ and $\Phi' = 0$. Numerical solution of this is shown in Figure 5.1, where we see that, today, Φ has risen to around -0.78 . Algebraic solution of (5.19) could be attempted. By substituting for R in terms of N , using $R = 3H_0^2 \Omega_{m,0} e^{-3N} + 4\Lambda$, gives $\Phi = A + B e^{-5N/2}$ as an approximating solution at early times, and $\Phi = C e^{-N}$ at late times as $R \rightarrow 4\Lambda$. For a better solution than this, a series approach would need to be taken using a variable such as $p = \Lambda / (R - 3\Lambda)$.

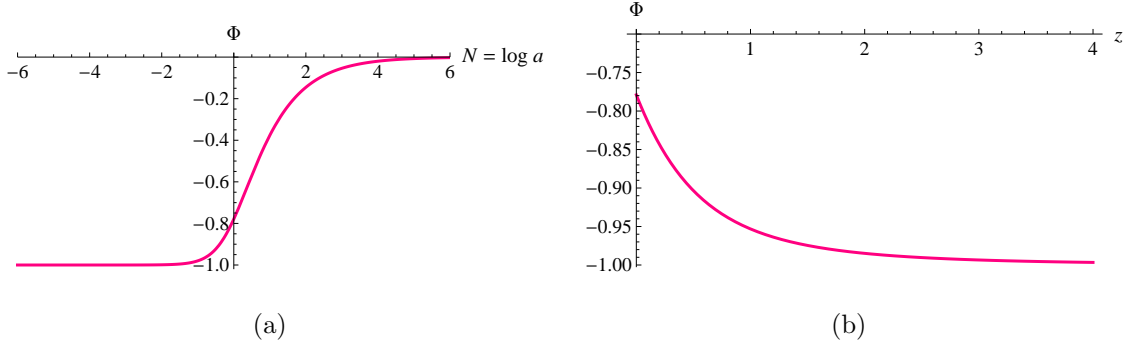


Figure 5.1: Λ CDM: Numerical solution of (5.19) shown against (a) $N = \log a$ and also (b) z . The value of Λ has been chosen to give $\Omega_{m,0} = 0.3$, namely, $\Lambda = 2.1 H_0^2$.

5.3 Approximating algebraic solutions

From now on, the dependence of variables on N will be shown. Subtracting (5.17) and (5.18) gives

$$\begin{aligned}
 & \left[\frac{1}{2\xi(N)} + \frac{2\lambda(N)^2}{3} - 6 - \frac{3H'(N)}{H} - \epsilon(N) \right] \Phi(N) \\
 = & \Psi''(N) + \left[3 + \frac{H'(N)}{H(N)} + \frac{R'(N)\xi(N)}{H(N)^2} \right] \Psi'(N) \\
 & + \left[\frac{1}{2\xi(N)} + \frac{\lambda(N)^2}{3} - 10 - \frac{5H'(N)}{H(N)} \right] \Psi(N) - 3\epsilon(N)\Psi(N) \quad (5.20)
 \end{aligned}$$

and equation (5.18) can be re-expressed as

$$\begin{aligned}
 & \Phi''(N) + \Psi''(N) + \left[4 + \frac{H'(N)}{H(N)} \right] [\Phi'(N) + \Psi'(N)] \\
 = & -\frac{R'(N)\xi(N)}{H(N)^2} \Psi'(N) \\
 & - \left[6 + \frac{3H'(N)}{H(N)} \right] [\Phi(N) - \Psi(N)] - \epsilon(N) [\Phi(N) - 3\Psi(N)]. \quad (5.21)
 \end{aligned}$$

Three parameters have been introduced in order to reduce the apparent complexity of these equations. They are $\xi(N)$, $\epsilon(N)$ and $\lambda(N)$ defined as follows:

$$\xi(N) = \frac{3H(N)^2 F_{RR}[R(N)]}{F_R[R(N)]}, \quad (5.22)$$

$$\epsilon(N) = \frac{f[R(N)]}{2H(N)^2 (1 + f_R[R(N)])}, \quad (5.23)$$

$$\lambda(N) = \frac{k}{aH(N)} = \frac{k e^{-N}}{H(N)}. \quad (5.24)$$

In order to introduce a degree of symmetry into equation (5.20) we replace $\xi(N)$ with $\zeta(N)$ defined by

$$\frac{1}{\zeta(N)} = \frac{1}{\xi(N)} + \lambda^2(N). \quad (5.25)$$

This changes (5.20) into

$$\begin{aligned} & \Psi''(N) + \left[3 + \frac{H'(N)}{H(N)} + \frac{R'(N)\xi(N)}{H(N)^2} \right] \Psi'(N) \\ & + \left[\frac{1}{2} \left(\frac{1}{\zeta(N)} - \frac{\lambda(N)^2}{3} \right) - 10 - \frac{5H'(N)}{H(N)} - 3\epsilon(N) \right] \Psi(N) \\ & - \left[\frac{1}{2} \left(\frac{1}{\zeta(N)} + \frac{\lambda(N)^2}{3} \right) - 6 - \frac{3H'(N)}{H} - \epsilon(N) \right] \Phi(N) = 0, \end{aligned} \quad (5.26)$$

while (5.21) is re-written as

$$\begin{aligned} & \Phi''(N) + \Psi''(N) + \left[4 + \frac{H'(N)}{H(N)} \right] [\Phi'(N) + \Psi'(N)] \\ & + \left[6 + \frac{3H'(N)}{H(N)} \right] [\Phi(N) - \Psi(N)] + \epsilon(N) [\Phi(N) - 3\Psi(N)] \\ & = -\frac{R'(N)\xi(N)}{H(N)^2} \Psi'(N). \end{aligned} \quad (5.27)$$

Equations (5.26) and (5.27) are the two differential equations we shall attempt to solve algebraically. We also notice that they are homogeneous and that at early times $\epsilon(N) \sim 0$, $\lambda(N) \sim 0$ and $\zeta(N) \sim 0$, which suggests, by inspection of equation (5.26), the possibility of high frequency oscillations in $\Psi(N)$ and, therefore, also in $\Phi(N)$. If there are oscillations, their frequency could be of order $1/\sqrt{\zeta(N)}$. There will also be solutions for $\Phi(N)$ and $\Psi(N)$ which do not oscillate.

Because (5.26) and (5.27) are homogeneous, oscillating solutions will be independent of non-oscillating solutions. Thus we can set $\Phi(N)$ and $\Psi(N)$ each to be the sum of an oscillating component and a non-oscillating component. We shall express $\Phi(N)$ and $\Psi(N)$ as follows:

$$\Phi(N) = \Phi_{\text{osc}}(N) + \left(\frac{1}{\zeta(N)} - \frac{\lambda(N)^2}{3} \right) \zeta(N)\Phi_0(N) + \zeta(N)\Phi_2(N), \quad (5.28)$$

$$\Psi(N) = \Psi_{\text{osc}}(N) + \left(\frac{1}{\zeta(N)} + \frac{\lambda(N)^2}{3} \right) \zeta(N)\Psi_0(N) + \zeta(N)\Psi_2(N). \quad (5.29)$$

$\Phi_{\text{osc}}(N)$ and $\Psi_{\text{osc}}(N)$ are the oscillating components while $\Phi_0(N)$ and $\Phi_2(N)$ are non-oscillating components of $\Phi(N)$ and similarly for $\Psi(N)$. The $\Phi_0(N)$ and $\Psi_0(N)$ terms are zero-th order in $\zeta(N)$, at early times. Using (5.25), the $\Phi_0(N)$ term migrates to $2/3 \times \Phi_0(N)$ at late times while the $\Psi_0(N)$ term migrates to $4/3 \times \Psi_0(N)$. The reason for expressing these terms in this way will become clear in subsection 5.3.2. The $\Phi_2(N)$ and $\Psi_2(N)$ terms are first order in $\zeta(N)$.

5.3.1 Oscillatory solution

Wishing to keep the expressions for $\Phi_{\text{osc}}(N)$ as simple as possible, we write

$$\Psi_{\text{osc}}(N) = \Psi_1(N) \sin \omega(N), \quad (5.30)$$

where $\Psi_1(N)$ is a function of N to be determined. Inspection of (5.26) shows that $\Phi(N)$ is a linear function of $\Psi''(N)$, $\Psi'(N)$ and $\Psi(N)$, which means that $\Phi(N)$ could contain both sine and cosine terms. It also means that the frequency of $\Phi(N)$ will be the same as $\Psi(N)$. We therefore write

$$\Phi_{\text{osc}}(N) = \Phi_1(N) \sin \omega(N) + \Phi_3(N) \cos \omega(N). \quad (5.31)$$

The expressions for $\Phi_{\text{osc}}(N)$ and $\Psi_{\text{osc}}(N)$ contain four unknown functions, viz, $\Phi_1(N)$, $\Psi_1(N)$, $\Phi_3(N)$ and $\omega(N)$. Taking the sine and cosine components of

equations (5.26) and (5.27) gives four independent equations. Unfortunately, because of the unknown frequency, and its integral with respect to N , $\omega(N)$, they are not linear and are, therefore, intractable. Therefore we must adopt a series approach and find expressions for the unknowns in terms of some variable which remains small throughout the history of the Universe.

Possibilities for this variable at early times are $\zeta(N)$, $\xi(N)$ and $1/\lambda(N)^2$ but how small do they remain? At early times in the matter era, $\lambda(N)^2 \propto a$ so it increases with time but we are dealing with subhorizon scales for which $k/aH(N) = \lambda(N) \gg 1$ which is why $1/\lambda(N)^2$ might be a contender. $k = 0$, however, means that $1/\lambda(N)$ does not even exist. Figure 5.2 shows an example using Model 1 of the Erf Model of Chapter 2 with $k = 0.1h \text{ Mpc}^{-1}$. The graphs of $\zeta(N)$, $\xi(N)$ and $1/\lambda(N)$ are plotted.

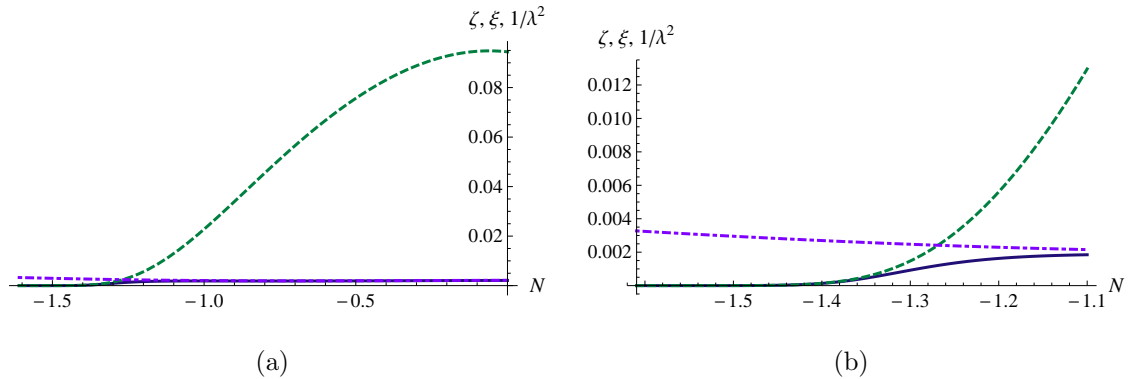


Figure 5.2: Graphs of $\zeta(N)$ (continuous, blue), $\xi(N)$ (dashed, green) and $1/\lambda(N)^2$ (dot-dashed, mauve) against N . (b) shows early detail.

We see that $\zeta(N)$ is tangential to $\xi(N)$ at early times, as can be seen also from (5.22) - (5.24), but at much later times it becomes closer to $1/\lambda(N)^2$. As the parameters of an $f(R)$ model are changed, or as we change the model itself, the numerical values of these three variables will change but not their relation with respect to one another. Thus the variable which remains smallest is $\zeta(N)$. At early times it is vanishingly small. This is on account of the requirement for $F(R)$ to pass the Solar System test (see subsection 1.4.8). In the Solar System,

$\zeta_s \approx \xi_s \approx R_s F_{RR}(R_s) < 10^{-23}$. At early times, any series expansion in $\zeta(N)$ will require very few terms in $\zeta(N)$ to be accurate, whereas, at later times, judging from Figure 5.2, it is possible that more terms would be required, with $k \rightarrow 0$ posing a problem. For any particular model, however, $\zeta(N)$ will be smallest, at late times, when k is largest.

Therefore, $\zeta(N)$ will be chosen as the variable with which to express $\Phi_1(N)$, $\Psi_1(N)$ and $\Phi_3(N)$. Accuracy will reduce, as N increases, unless the number of terms in $\zeta(N)$ increases. Accuracy also reduces as k becomes smaller.

The sine component of (5.26) gives

$$\omega'(N)^2 = \frac{1}{2\zeta(N)} - \frac{\lambda(N)^2}{6} - \left(\frac{1}{2\zeta(N)} + \frac{\lambda(N)^2}{6} \right) \frac{\Phi_1(N)}{\Psi_1(N)}. \quad (5.32)$$

All the terms on the right hand side of (5.32) are numerically much greater than unity. In finding (5.32), terms of order 1 or smaller have been ignored. These are $\Phi_1(N)/\Psi_1(N)$, $H'(N)/H(N)$, $\Psi_1'(N)/\Psi_1(N)$ and $\Psi_1''(N)/\Psi_1(N)$. Similarly, the sine component of (5.26)+(5.27) gives

$$\omega'(N)^2 = \frac{1}{2\zeta(N)} + \frac{\lambda(N)^2}{6} - \left(\frac{1}{2\zeta(N)} - \frac{\lambda(N)^2}{6} \right) \frac{\Psi_1(N)}{\Phi_1(N)}, \quad (5.33)$$

plus other terms of order 1 and also terms of uncertain order, at this stage, viz,

$$\left(4 + \frac{H'(N)}{H(N)} + \frac{\omega''(N)}{\omega(N)} \right) \frac{\Phi_3(N)\omega'(N)}{\Phi_1(N)} + 2 \frac{\omega'(N)\Phi_3'(N)}{\Phi_1(N)}. \quad (5.34)$$

The cosine component of (5.26) gives

$$\begin{aligned} & \frac{3}{2} + \frac{H'(N)}{2H(N)} + \frac{\xi(N)R'(N)}{2H(N)^2} + \frac{\Psi_1'(N)}{\Psi_1(N)} + \frac{\omega''(N)}{2\omega'(N)} \\ &= \frac{1}{4} \left(\frac{1}{\zeta(N)} + \frac{\lambda(N)^2}{3} \right) \frac{\Phi_3(N)}{\Psi_1(N)\omega'(N)}, \end{aligned} \quad (5.35)$$

in which the other terms:

$$\left(3 + \frac{\epsilon(N)}{2} + 3 \frac{H'(N)}{H(N)} \right) \frac{\Phi_3(N)}{\Psi_1(N)\omega'(N)} \quad (5.36)$$

have been discarded as being of smaller value.

Since $1/\omega'(N) \sim \sqrt{\zeta(N)}$, we can see from (5.35) that $\Phi_3(N)/\Psi_1(N)$ is of order $\zeta(N)\omega'(N) \sim \sqrt{\zeta(N)}$ so that the terms in (5.34) are of order $\zeta(N)\omega'(N)^2 \sim 1$ and need not appear in (5.33).

Equating (5.32) and (5.33), gives $\Phi_1(N) = -\Psi_1(N)$ or $(1/\zeta(N) + \lambda^2(N)/3)\Phi_1(N) = (1/\zeta(N) - \lambda^2(N)/3)\Psi_1(N)$. The second of these gives $\omega'(N) = 0$, which we reject, while the former gives

$$\omega'(N) = \frac{1}{\sqrt{\zeta(N)}}. \quad (5.37)$$

We already have the cosine component of (5.26) as (5.35). The cosine component of (5.27) gives,

$$\begin{aligned} \frac{3}{2} + \frac{H'(N)}{2H(N)} + \frac{\Psi_1'(N)}{\Psi_1(N)} + \frac{\omega''(N)}{2\omega'(N)} &= \frac{1}{4} \left(\frac{1}{\zeta(N)} + \frac{\lambda(N)^2}{3} - 2\omega'(N)^2 \right) \frac{\Phi_3(N)}{\Psi_1(N)\omega'(N)} \\ &= \frac{1}{4} \left(-\frac{1}{\zeta(N)} + \frac{\lambda(N)^2}{3} \right) \frac{\Phi_3(N)}{\Psi_1(N)\omega'(N)}. \end{aligned} \quad (5.38)$$

The term $\xi(N)R'(N)/(2H(N)^2)$ of equation (5.35) varies from $\mathcal{O}(\zeta(N))$ at early times to $\mathcal{O}(10^{-1})$, today, say, so should not be discarded.

From (5.35) and (5.38), it is deduced that

$$\Phi_3(N) = \sqrt{\zeta(N)}\Psi_1(N) \frac{\xi(N)R'(N)}{H(N)^2}, \quad (5.39)$$

$$\Psi_1(N) = \Psi_1(N_i) e^{-3(N-N_i)/2} \sqrt{\frac{H(N_i)}{H(N)}} \left(\frac{\zeta(N)}{\zeta(N_i)} \right)^{1/4} e^{-\nu(N)}, \quad (5.40)$$

$$\text{where } \nu(N) = \int_{N_i}^N \left(1 - \frac{\lambda(n)^2 \zeta(n)}{3} \right) \frac{\xi(n)R'(n)}{4H(n)^2} dn. \quad (5.41)$$

N_i is some initial value for N . For much of the history of the Universe, $e^{-\nu(N)}$ is close to 1 and increases very slowly. For example, for Erf Model 1, with $k = 0.1h \text{ Mpc}^{-1}$, it rises from around unity at $z = 1$ to achieve a value of 1.14, today. When $k = 0$, today's value rises with this model to around 1.22.

Thus, there are oscillations from some early time in the matter era, to date, with frequency approximated by equation (5.37). Oscillations at early time have

been studied by Song et al. in [119] and Starobinsky in [78]. Starobinsky looked at the oscillating nature of R , at high curvatures only, and concluded that it possessed an oscillating component with a frequency equivalent to $1/\sqrt{\xi(N)}$ but the amplitude of these oscillations grew into the past. The same effect has been studied in [120] and is discussed further in Chapter 6.

5.3.2 Non-oscillatory solution

The non-oscillatory terms of $\Phi(N)$ and $\Psi(N)$ are expressed in terms of two non-oscillatory functions, respectively, of N as

$$\Phi_n(N) = \left(\frac{1}{\zeta(N)} - \frac{\lambda(N)^2}{3} \right) \zeta(N)\Phi_0(N) + \zeta(N)\Phi_2(N), \quad (5.42)$$

$$\Psi_n(N) = \left(\frac{1}{\zeta(N)} + \frac{\lambda(N)^2}{3} \right) \zeta(N)\Psi_0(N) + \zeta(N)\Psi_2(N). \quad (5.43)$$

The reason for the rather complicated looking coefficients of $\Phi_0(N)$ and $\Psi_0(N)$ is to simplify the relation between $\Phi_0(N)$ and $\Psi_0(N)$, as will be seen.

Applying these expressions to (5.26) and (5.27) and adopting a series approach, gives $\Phi_0(N) = \Psi_0(N)$ satisfying

$$\begin{aligned} & \Psi_0''(N) + \left(4 + \frac{H'(N)}{H(N)} \right) \Psi_0'(N) \\ & - \left[\lambda(N)^2 \zeta(N) \left(2 + \frac{H'(N)}{H(N)} \right) + \epsilon(N) \left(1 + \frac{2\lambda(N)^2 \zeta(N)}{3} \right) \right] \Psi_0(N) = 0, \end{aligned} \quad (5.44)$$

which is algebraically soluble when $|\lambda(N)^2 \zeta(N)| \ll 1$ and $|\epsilon(N)| \ll 1$. Under Λ CDM, (5.44) is the same as equation (5.19).

From (5.26), an expression for $\left(1 + \frac{\lambda(N)^2}{3} \zeta(N) \right) \Phi_2(N) - \left(1 - \frac{\lambda(N)^2}{3} \zeta(N) \right) \Psi_2(N)$ (see equation (5.52)) is found in terms of $\Psi_0(N)$ and derivatives. Note that this approximates to $\Phi_2(N) - \Psi_2(N)$ at early times but could be markedly different at late times.

There is another expression, a complicated second order differential equation for $\Phi_2(N)$ and $\Psi_2(N)$, which is obtained from (5.27). It is not symmetric in $\Phi_2(N)$ and $\Psi_2(N)$ and, even with the use the expression above in terms of $\Phi_2(N)$ and $\Psi_2(N)$, it could only be solved numerically. If we wanted to solve these equations for $\Phi_2(N)$ and $\Psi_2(N)$, separately, we run into the problem that we can no longer assume $\zeta(N_i) = 0$ because, in the expressions for $\Phi(N)$ and $\Psi(N)$, equations (5.28) and (5.29), $\Phi_2(N)$ and $\Psi_2(N)$ appear as multiples of $\zeta(N)$. It therefore seems better, instead of showing $x(N) = \Phi(N) - \Psi(N)$, as [79] does, to show $x(N) = (1 + \frac{\lambda(N)^2}{3}\zeta(N))\Phi(N) - (1 - \frac{\lambda(N)^2}{3}\zeta(N))\Psi(N)$; see (5.54). This approximates to $\Phi(N) - \Psi(N)$ at early times and means that contributions from $\Phi_2(N)$ and $\Psi_2(N)$ can be shown in the algebraic expression for $x(N)$.

5.3.3 The combined algebraic solution

Putting the independent solutions from subsections 5.3.1 and 5.3.2 together gives a suggested algebraic solution to equations (5.26) and (5.27), up to $O(\zeta(N))$, as

$$\begin{aligned} \Phi(N) &= -\Psi_1(N) \sin \omega(N) + \Phi_3(N) \cos \omega(N), \\ &+ \left(\frac{1}{\zeta(N)} - \frac{\lambda(N)^2}{3} \right) \zeta(N) \Psi_0(N) + \zeta(N) \Phi_2(N), \end{aligned} \quad (5.45)$$

$$\begin{aligned} \Psi(N) &= \Psi_1(N) \sin \omega(N), \\ &+ \left(\frac{1}{\zeta(N)} + \frac{\lambda(N)^2}{3} \right) \zeta(N) \Psi_0(N) + \zeta(N) \Psi_2(N), \end{aligned} \quad (5.46)$$

$$\omega(N) = \int_{N_i}^N \frac{1}{\sqrt{\zeta(n)}} dn + \omega(N_i), \quad (5.47)$$

$$\Phi_3(N) = \sqrt{\zeta(N)} \Psi_1(N) \frac{\xi(N)R'(N)}{H(N)^2}, \quad (5.48)$$

$$\nu(N) = \int_{N_i}^N \left(1 - \frac{\lambda(n)^2 \zeta(n)}{3} \right) \frac{\xi(n)R'(n)}{4H(n)^2} dn, \quad (5.49)$$

$$\Psi_1(N) = \Psi_1(N_i) e^{-3(N-N_i)/2} \sqrt{\frac{H(N_i)}{H(N)}} \left(\frac{\zeta(N)}{\zeta(N_i)} \right)^{1/4} e^{-\nu(N)}, \quad (5.50)$$

in which N_i is a constant. $\Psi_0(N)$ solves

$$\begin{aligned} & \Psi_0''(N) + \left(4 + \frac{H'(N)}{H(N)}\right) \Psi_0'(N) \\ & - \left[\lambda(N)^2 \zeta(N) \left(2 + \frac{H'(N)}{H(N)}\right) + \epsilon(N) \left(1 + \frac{2\lambda(N)^2 \zeta(N)}{3}\right)\right] \Psi_0(N) = 0. \end{aligned} \quad (5.51)$$

The expression for $\left(1 + \frac{\lambda(N)^2 \zeta(N)}{3}\right) \Phi_2(N) - \left(1 - \frac{\lambda(N)^2 \zeta(N)}{3}\right) \Psi_2(N)$, denoting $\lambda(N)^2 \zeta(N)/3$ by $\text{lz}(N)$, is

$$\begin{aligned} & 2[1 + \text{lz}(N)] \Psi_0''(N) + \left[2(1 + \text{lz}(N)) \left(3 + \frac{H'(N)}{H(N)}\right) + 4\text{lz}'(N)\right] \Psi_0'(N) \\ & - \left[4(1 + 4\text{lz}(N)) \left(2 + \frac{H'(N)}{H(N)}\right) + 4\epsilon(N)(1 + 2\text{lz}(N))\right] \Psi_0(N) \\ & + \left[2\text{lz}'(N) \left(3 + \frac{H'(N)}{H(N)}\right) + 2\text{lz}''(N)\right] \Psi_0(N). \end{aligned} \quad (5.52)$$

Because this is the only tractable connection between $\Phi_2(N)$ and $\Psi_2(N)$ and to emphasise the oscillations by removing $\Psi_0(N)$, we consider the “difference” between $\Phi(N)$ and $\Psi(N)$, $x(N)$, as already mentioned, above, by defining it as

$$x(N) = \left(1 + \frac{\lambda(N)^2 \zeta(N)}{3}\right) \Phi(N) - \left(1 - \frac{\lambda(N)^2 \zeta(N)}{3}\right) \Psi(N) \quad (5.53)$$

At early times, $\lambda(N)^2 \zeta(N) \ll 1$, so, then, $x(N) \sim \Phi(N) - \Psi(N)$.

We define $y(N)$ to be the sum of $\Phi(N)$ and $\Psi(N)$. In it, we ignore any contribution from $\Phi_2(N)$ and $\Psi_2(N)$ because y is dominated by $\Psi_0(N)$, which approximates to -1 , and they are suppressed by the factor $\zeta(N)$.

In terms of their various components, $x(N)$ and $y(N)$ are given by

$$\begin{aligned} x(N) &= -2\Psi_1(N) \sin \omega(N) + \left(1 + \frac{\lambda(N)^2 \zeta(N)}{3}\right) \zeta(N) \Phi_2(N) \\ &\quad - \left(1 - \frac{\lambda(N)^2 \zeta(N)}{3}\right) \zeta(N) \Psi_2(N), \end{aligned} \quad (5.54)$$

$$y(N) = \Phi_3(N) \cos \omega(N) + 2\Psi_0(N). \quad (5.55)$$

We now go on to apply initial conditions to these at some value of N we call N_i .

5.3.4 Applying initial conditions to the algebraic approximation

We apply the initial conditions at $N = N_i$ at which time we assume there to be only slight deviation from Λ CDM, for which $\Phi_\Lambda(N) = \Psi_\Lambda(N)$ and $\Phi'_\Lambda = 0$. Here, $\zeta(N) \sim 0$ so that $x(N) \sim \Phi(N) - \Psi(N)$ and $\Phi_3(N) \sim 0$. $y(N) = \Phi(N) + \Psi(N) \sim 2\Psi_0(N)$. Near $N = N_i$, let $\Phi(N) = \Phi_\Lambda(N) + \delta\Phi$ and $\Psi(N) = \Phi_\Lambda(N) + \delta\Psi$. At $N = N_i$,

$$x(N_i) = \Phi(N_i) - \Psi(N_i) \quad (5.56)$$

$$= \delta\Phi_i - \delta\Psi_i. \quad (5.57)$$

To keep things simple, we'll choose the phase of the oscillations so that $x(N_i) = 0$ but let us choose N_i to be so early that we may consider, $\delta\Phi_i = \delta\Psi_i = 0$. Let $x'(N_i) = x'_i$. $y(N_i) = 2\Phi_\Lambda(N_i) = 2\Phi_0(N_i) \approx -2$ and $y'(N_i) = 0$.

$$x'_i = \delta\Phi'_i - \delta\Psi'_i, \quad (5.58)$$

$$y_i = 2\Phi_\Lambda(N_i) + \delta\Phi_i + \delta\Psi_i, \quad (5.59)$$

$$\Rightarrow 0 = 2\Phi'_\Lambda(N_i) + \delta\Phi'_i + \delta\Psi'_i. \quad (5.60)$$

Thus, $\delta\Phi'_i = -\Phi'_\Lambda(N_i) + x'_i/2$ and $\delta\Psi'_i = -\Phi'_\Lambda(N_i) - x'_i/2$ and the initial conditions are

$$\Phi(N_i) = \Phi_\Lambda(N_i), \quad (5.61)$$

$$\Psi(N_i) = \Phi_\Lambda(N_i), \quad (5.62)$$

$$\Phi'(N_i) = x'_i/2, \quad (5.63)$$

$$\Psi'(N_i) = -x'_i/2. \quad (5.64)$$

The values for $\Phi_\Lambda(N)$ and $\Psi_\Lambda(N)$ can be found at $N = N_i$ by solving the Λ CDM equations of subsection 5.2.1.

We choose the value of N_i to be the value at which we can reliably start the iterations which solve the original field equation, (1.75), for whichever model we

are using. For values of $N < N_i$, $F(R)$ is so close to Λ CDM that the difference is not discernible although the oscillations are suppressed into the past. They increase in frequency but their amplitude, given by $\Psi_1(N)$ in (5.50), dies away to zero.

Applying the initial conditions to the algebraic solution gives $\omega(N_i) = 0$, $\Psi_1(N_i) = -x'_i \sqrt{\zeta(N_i)}/2$, $\Phi_0(N_i) = \Phi_\Lambda(N_i)$ and $\Phi'_0(N_i) = 0$. The value of $\Phi_3(N_i)$ will be taken to be as defined by (5.48). This makes $\Psi_1(N)$, as specified in (5.50), become

$$\Psi_1(N) = -\frac{x'_i}{2} e^{-3(N-N_i)/2} \sqrt{\frac{H(N_i)}{H(N)}} \zeta(N_i)^{1/4} \zeta(N)^{1/4} e^{-\nu(N)}. \quad (5.65)$$

From (5.54), the amplitude of the oscillations in $x(N)$ is $2\Psi_1(N)$.

5.4 Algebraic and numerical solutions compared

In this section we take three values of k for Erf Model 1 (subsection 3.2.1) and compare the algebraic solutions of (5.54) and (5.55) to the equivalent solutions found by solving equations (5.26) and (5.27), numerically.

The values of k we choose, to demonstrate the accuracy of the algebraic solutions in relation to the numerical solutions, are $k = 0.1h \text{ Mpc}^{-1}$, $k = 0.01h \text{ Mpc}^{-1}$ and $k = 0$. For demonstration purposes in order to make the oscillations stand out, x'_i is initially taken to be 10 but is reduced to 1 in subsection 5.4.1 to see what effect that has. In all the graphs it should be remembered that they show a history and that today is represented by $N = 0$.

It should also be borne in mind that the amplitude today, for a given model, depends not only on the value of x'_i but also in the the value of N_i at which the initial conditions are applied. In practice, it is unrealistic to apply initial conditions at $z = 1000$ as is stated in [79] “when the deviations from GR are small”. At this

early value of z , however, the oscillation frequency will be extremely high then; computing facilities would not be able to cope. In this thesis, initial conditions are applied at a value of N_i so that the algebraic and numeric solutions can be compared fairly. However, it should be noted that the earlier initial conditions are applied, the smaller will be the amplitude of the oscillations, today. Putting $N = 0$ into the expression for the amplitude of oscillations of $x(N)$, derived from (5.65), gives for the amplitude, today, of oscillations

$$x'_i e^{3N_i/2} \sqrt{\frac{H(N_i)}{H_0}} \zeta(N_i)^{1/4} \zeta_0^{1/4} e^{-\nu_0} \quad (5.66)$$

$$= x'_i e^{3N_i/4} \zeta(N_i)^{1/4} (\Omega_{m,0} \zeta_0)^{1/4} e^{-\nu_0}, \quad (5.67)$$

and $e^{3N_i/4} \zeta(N_i)^{1/4}$ is smaller the earlier N_i is. This is because, at early times, $3H(N)^2 \approx R(N)$ and $F_R(R(N)) \approx 1$, and, using (5.25) and (5.22), $\zeta(N) \approx \xi(N) \approx R(N) f_{RR}(R(N)) \propto e^{-3N} f_{RR}(R(N))$ so that $e^{3N_i/4} \zeta(N_i)^{1/4} \propto [f_{RR}(R(N_i))]^{1/4}$. An earlier value of N_i gives a smaller value of $f_{RR}(R(N_i))$. We have discounted any changes in ν_0 , see (5.49), as $\nu(N)$ is close to zero for much of its history.

5.4.1 $k = 0.1h \text{ Mpc}^{-1}$

We present the full range solutions, first, the algebraic solution in Figure 5.3 and, secondly, the numerical solution in Figure 5.4. The corresponding solutions for $y(N)$ are given in Figure 5.5.

While Figures 5.3 and 5.4 look very similar there are some differences. The main difference is that, when trying to plot the algebraic solution for $x(N)$, it was impossible to compute $\int_{N_i}^N 1/\sqrt{\zeta(n)} dn$ for a sufficient number of values of N in the range $N_i \leq N \leq 0$, so an interpolating function had to be used. While this function agrees with $\int_{N_i}^N 1/\sqrt{\zeta(n)} dn$, initially, its derivative does not always do so which makes the frequencies, and therefore the phase, appear to disagree slightly as N increases. Fortunately these differences remain relatively small, as is discussed, below, and illustrated in Figure 5.6.

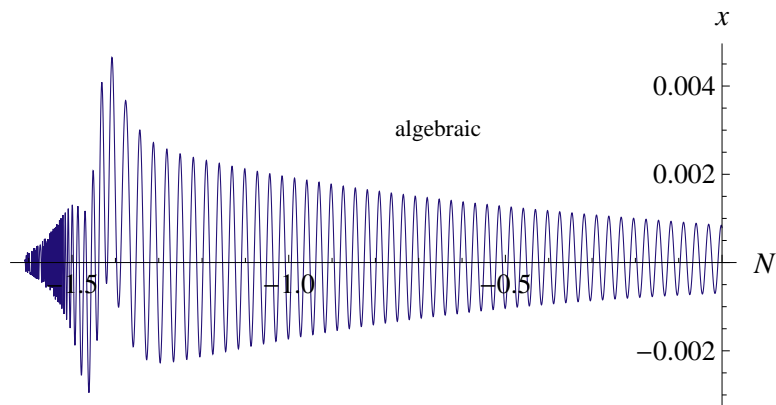


Figure 5.3: Algebraic solution, (5.54), for Erf Model Model 1 for $k = 0.1h \text{ Mpc}^{-1}$.

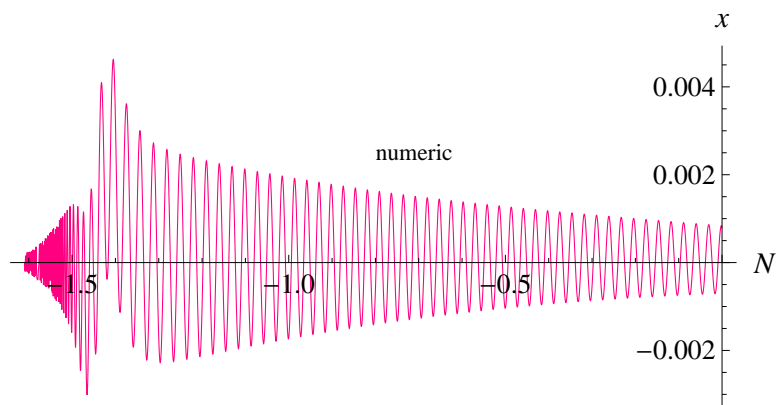


Figure 5.4: Numerical solution, as defined by (5.53), of equations (5.26) and (5.27) for Erf Model 1, for $k = 0.1h \text{ Mpc}^{-1}$.

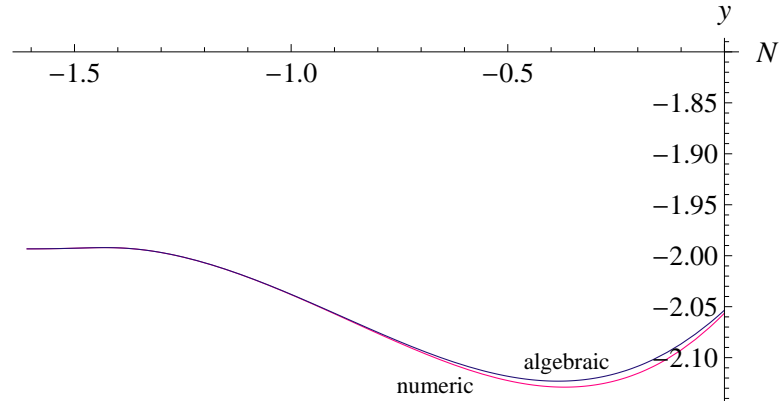


Figure 5.5: Algebraic and numeric solutions, $y(N) = \Phi(N) + \Psi(N)$, where $\Phi(N)$ and $\Psi(N)$ solve equations (5.26) and (5.27), for Erf Model 1, for $k = 0.1h \text{ Mpc}^{-1}$. There is close agreement between the two solutions for much of the history of the Universe but, at later times, some separation is evident.

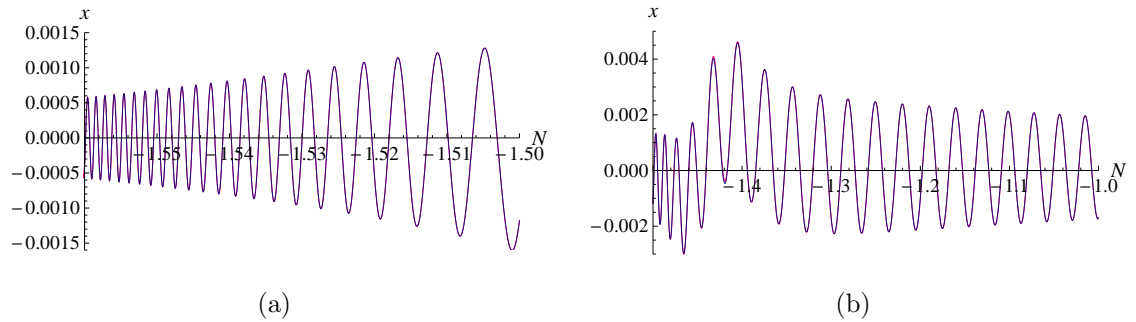


Figure 5.6: Comparison between algebraic and numeric solutions for $x(N)$ for Erf Model 1 when $k = 0.1h \text{ Mpc}^{-1}$ formed by overlaying them. That is, in (a) and (b), both algebraic and numeric solutions for $x(N)$ are plotted. (a) shows $-1.56 < N < 1.5$ while (b) shows $1.5 < N < 1.0$. On these scales, the respective frequencies seem to be very close, as do the envelopes.

Figure 5.6 shows that the envelopes of the algebraic and numeric solutions are very similar as are the frequencies. Note that these graphs do not go right down as far as N_i . If we can assume the frequency is represented by $1/\sqrt{\zeta(N)}$ and the phases agree at $N = N_i$, then the phase at all times is represented by

$$\omega(N) = \int_{N_i}^N \frac{1}{\sqrt{\zeta(n)}} dn. \quad (5.68)$$

It is unfortunate that, because of the very large value of $1/\sqrt{\zeta(N)}$ at early times, sine and cosine of $\omega(N)$ cannot be fairly computed for all values of N and that an approximation has to be used in order to plot the algebraic graphs. This introduces errors as shown in Figure 5.7(a) which shows the fractional difference between the the frequency represented by $1/\sqrt{\zeta(N)}$ and the approximating function; showing how closely they agree. Fractional differences when the frequency is high are to be expected. Fortunately, the disagreement is not large as can be seen from Figure 5.6. Since the disagreement in Figure 5.7(a) occurs at the same value of N as that in Figure 5.7(b) and noting the general agreement between the two pairs of curves in Figure 5.6, it seems reasonable to suppose that $1/\sqrt{\zeta(N)}$ does represent a good approximation to the oscillation frequency at any time.

Figure 5.8 shows how the frequency, as represented by $1/\sqrt{\zeta(N)}$, changes with N . Initially, it is very high but falls to a minimum (in this case at around $N = -1.35$) which corresponds to $z \approx 2.9$ whereafter it increases to a local maximum at $N \approx -0.7$ ($z \approx 1$).

The value $x'_i = 10$ was chosen to make the oscillations highly visible. Let us now see what the effect of reducing its value to unity is. See Figure 5.9. The amplitude of the oscillations will be reduced but should enable the underlying structure to be seen more clearly.

We see that the strange “jump” in the region $-1.5 < N < -1.4$ is still there. It is clear that it is due to non-oscillating term in (5.54), namely,

$$\zeta(N) \left[\left(1 + \frac{\lambda(N)^2}{3} \zeta(N) \right) \Phi_2(N) - \left(1 - \frac{\lambda(N)^2}{3} \zeta(N) \right) \Psi_2(N) \right] \quad (5.69)$$

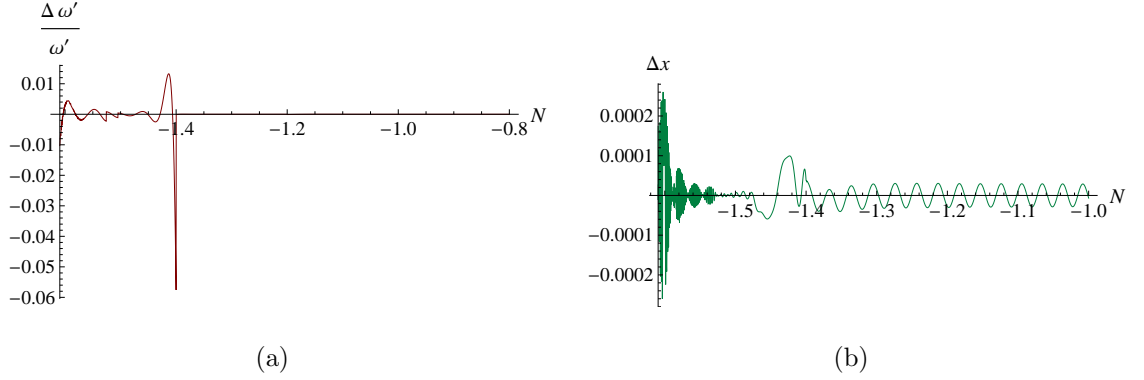


Figure 5.7: (a) The relative difference between frequency, in terms of the simplifying interpolating function used to plot the algebraic curves, and the frequency as represented by $1/\sqrt{\zeta(N)}$. (b) The difference between the algebraic solution, using an interpolating function for the phase of the sinusoidal components, and the numeric solution against N for Erf Model 1 when $k = 0.1h \text{ Mpc}^{-1}$. The spike in the relative frequency just before $N = -1.4$ has introduced a phase difference which makes Δx sinusoidal. Fortunately, the effect is small. $N_i = -1.609$.

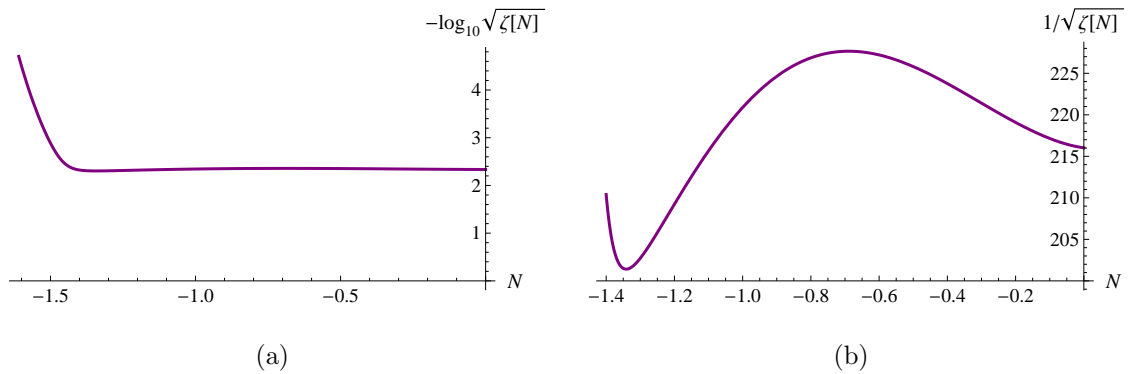


Figure 5.8: How the frequency of the oscillations changes with N for Erf Model 1 when $k = 0.1h \text{ Mpc}^{-1}$.

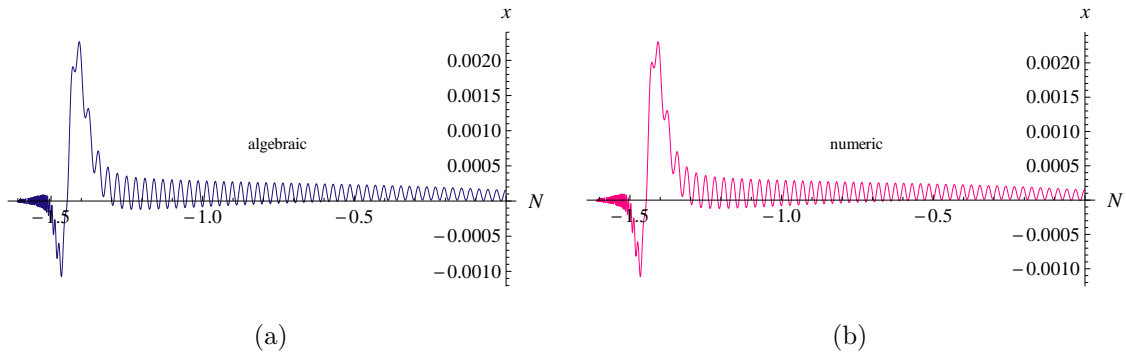


Figure 5.9: Model 1: The equivalent of Figures 5.3 and 5.4 with k still being $0.1h \text{ Mpc}^{-1}$ but x'_i changed from 10 to 1.

and shows up clearly in Figure 5.11(a). While the jump depends to some extent on the common factor, $\zeta(N)$, it also depends heavily on the multiple of $\zeta(N)$ in (5.69), as there is a change of sign involved. As is stated in subsection 5.3.2, this multiple depends on $\Psi_0(N)$. Looking at the evolution of $\Phi(N)$ and $\Psi(N)$ separately gives a jump at the right place in the difference between them, as shown in Figure 5.10. The difference in $\Phi(N)$ and $\Psi(N)$ is not maintained in

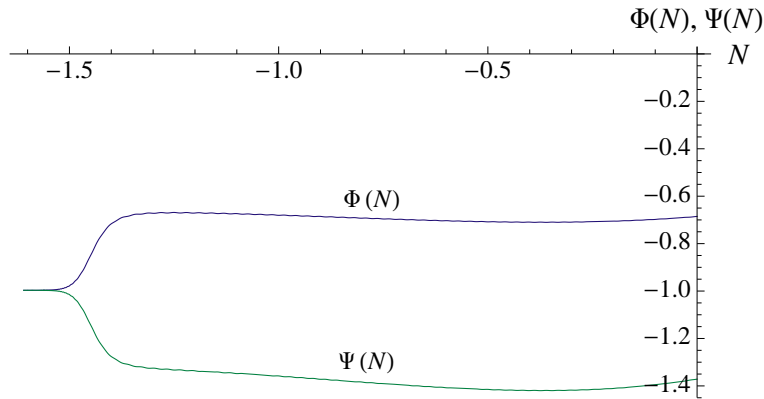


Figure 5.10: Model 1: The numeric solutions for $\Phi(N)$ and $\Psi(N)$ when $k = 0.1h \text{ Mpc}^{-1}$ and $x'_i = 10$. The scale of the graphs makes the oscillations barely visible.

$x(N)$ because, as can be seen from (5.53), while $x(N) \approx \Phi(N) - \Psi(N)$, initially, it becomes closer to $2(2\Phi(N) - \Psi(N))/3$ as $\zeta(N) \sim 1/\lambda(N)^2$, at later times.

The oscillating component of $x(N)$ is shown in Figure 5.11(b) with $x'_1 = 1$. It is proportional to x'_1 and depends on the value of k . The non-oscillating component is independent of x'_1 but does depend on k . Both components are model dependent.

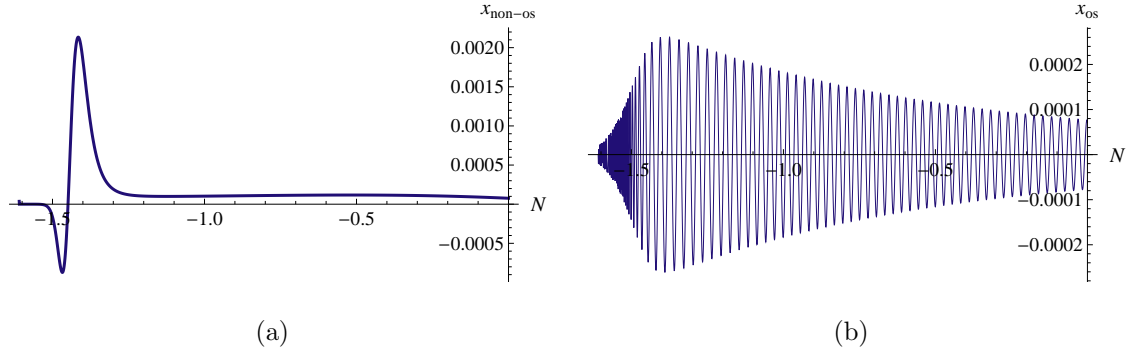


Figure 5.11: Model 1: For the algebraic solution, (a) shows the non-oscillating component of $x(N)$. (b) shows the oscillating component of $x(N)$ when $x'_1 = 1$. Both are for Erf Model 1 when $k = 0.1h \text{ Mpc}^{-1}$. The two components combine to give Figure 5.9(a).

5.4.2 $k = 0.01h \text{ Mpc}^{-1}$

With a smaller value of k , we see larger discrepancies between the algebraic and numeric solutions appear than when k was ten times larger. This is as expected and as discussed in subsection 5.3.1. Algebraic and numeric solution curves for $x(N)$ are shown in Figure 5.12 with detail in Figure 5.13. In these graphs we see how the effect of a much smaller value of k manifests itself by showing the algebraic solution at later times to be insufficient. The corresponding solutions for $y(N)$ are given in Figure 5.14.

How the frequencies vary, again as represented by $1/\sqrt{\zeta(N)}$ and to compare with Figure 5.8, is shown in Figure 5.15. Cursory measurement of the last four wavelengths of Figure 5.12 confirms, as N increases above $N = -1.2$, the frequency continues to fall, then rises a little and then falls, as shown in Figure 5.15, but that the mean frequency for $N > -1.4$ is overestimated by around 4%.

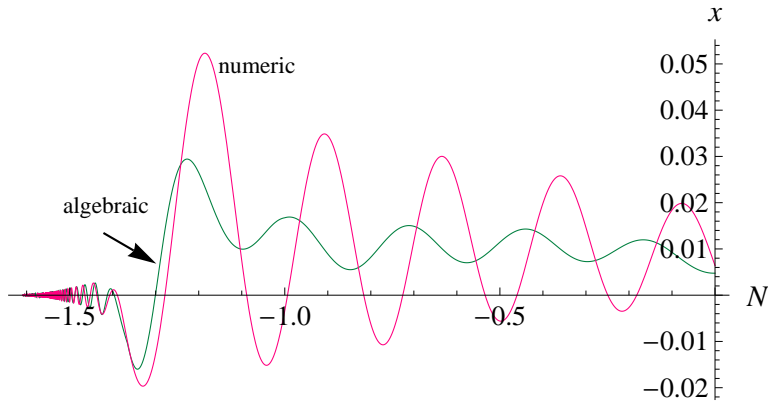


Figure 5.12: Algebraic and numerical solutions for $x(N)$ for Erf Model 1, when $k = 0.01h \text{ Mpc}^{-1}$ and $x'_i = 10$. Close agreement between the two solutions is now prior to $N = -1.4$. $1/\sqrt{\zeta(N)}$ remains a fair estimate of the oscillation frequency at later times.

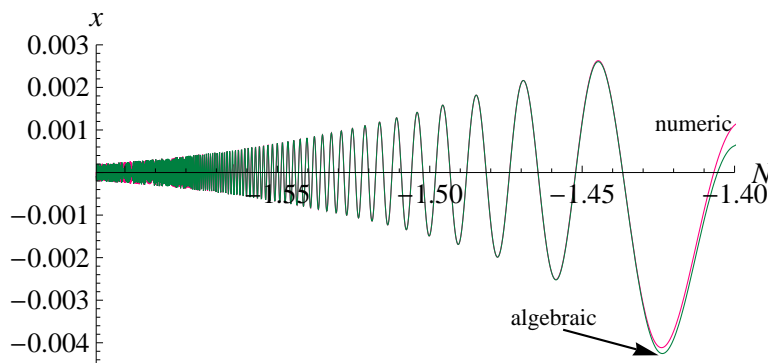


Figure 5.13: Detail of Figure 5.12 for $N < -1.4$, showing good agreement almost up to then and where the two curves diverge.

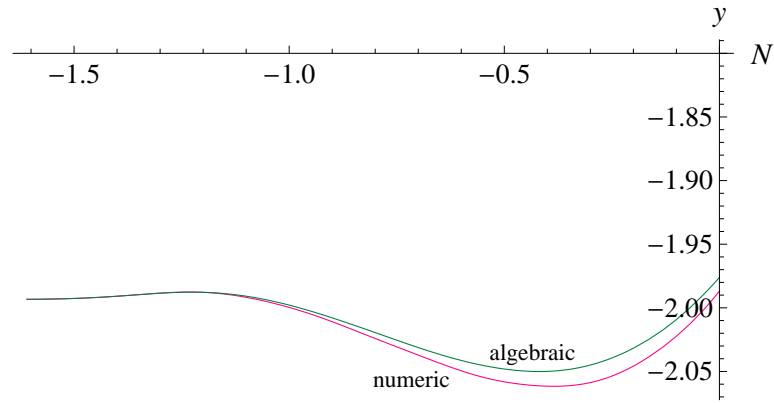


Figure 5.14: Algebraic and numeric solutions for $y(N) = \Phi(N) + \Psi(N)$, for Erf Model 1, when $k = 0.01h \text{ Mpc}^{-1}$. Compare Figure 5.5.

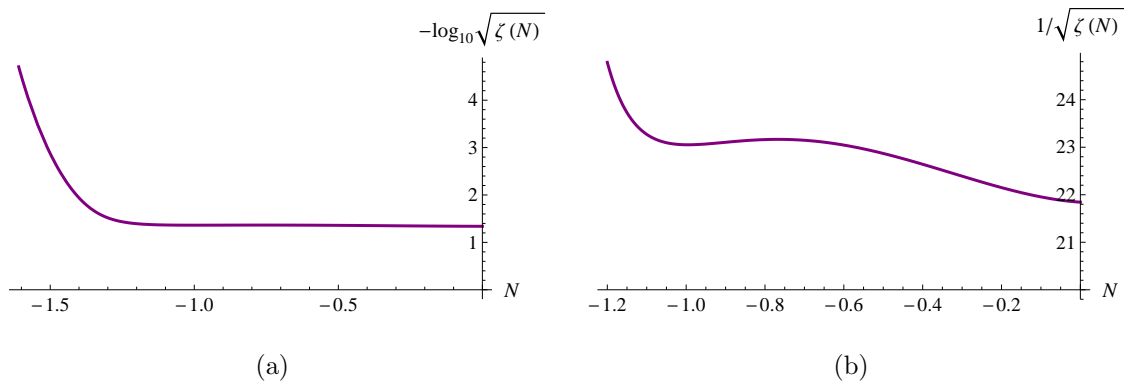


Figure 5.15: How the frequency of the oscillations changes with N for Erf Model 1 when $k = 0.01h \text{ Mpc}^{-1}$. It can be seen how the local minimum and maximum of Figure 5.8 are being eroded.

At later times, when $N > -1.2$, say, the frequency is around two orders of magnitude lower than when $k = 0.1h \text{ Mpc}^{-1}$ and $x'_i = 10$.

The graphs equivalent to those shown in Figure 5.11 are shown in Figure 5.16. $x'_i = 1$ so as to compare them.

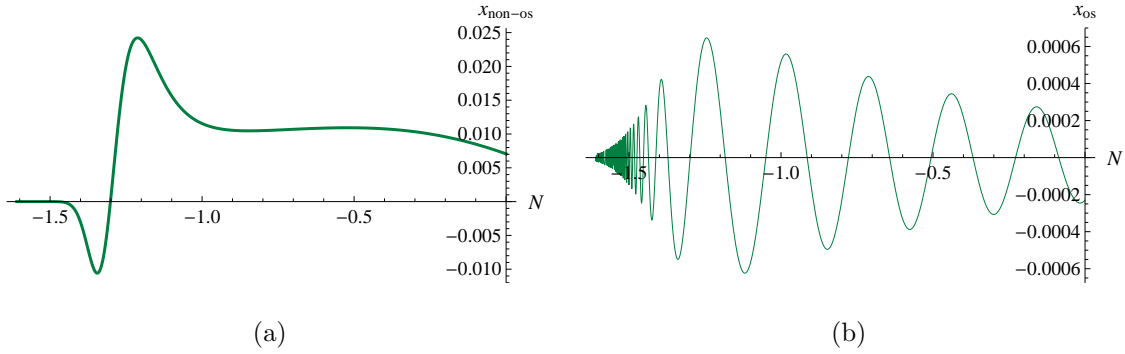


Figure 5.16: For the algebraic solution, (a) shows the non-oscillating component of $x(N)$. (b) shows the oscillating component of $x(N)$ when $x'_i = 1$. Both are for Erf Model 1 when $k = 0.01h \text{ Mpc}^{-1}$.

5.4.3 $k = 0$

The algebraic and numeric solution curves when $k = 0$ for Erf Model 1 are included, as Figures 5.17 and 5.18, just to see how the disagreement between the two types of solution continues. The corresponding solutions for $y(N)$ are given in Figure 5.19.

With $k = 0$, the frequency, as represented by $1/\sqrt{\zeta(N)}$, continuously falls as N increases. How it does so is shown in Figure 5.20.

The graphs equivalent to those shown in Figures 5.11 and 5.16 are shown in Figure 5.21. Again, $x'_i = 1$.

It is clear from all the graphs for $x(N)$ that, for values of N less than some value, say -1.5 , for the Erf Model 1, that the expression for $x(N)$ can be simplified for

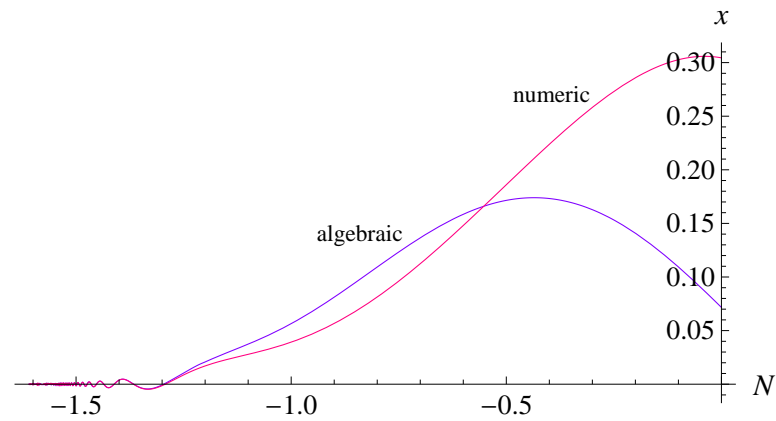


Figure 5.17: Algebraic and numerical solutions for $x(N)$ for Erf Model 1, when $k = 0$ and $x'_i = 10$. Again, For $N > -1.4$, say, the frequency of the oscillations of the algebraic solution does seem to be slightly larger than for the numeric one.

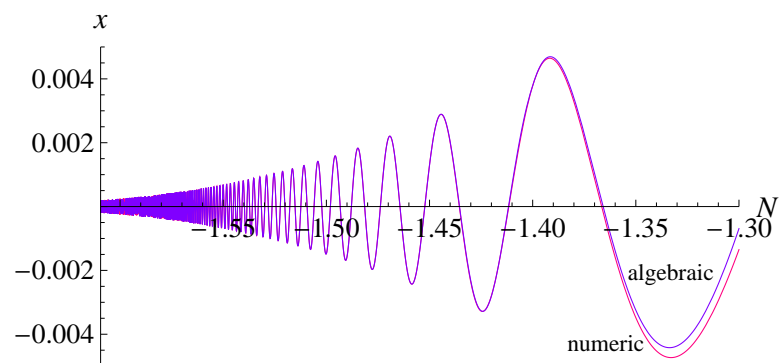


Figure 5.18: Detail of Figure 5.17 for $N < -1.3$.

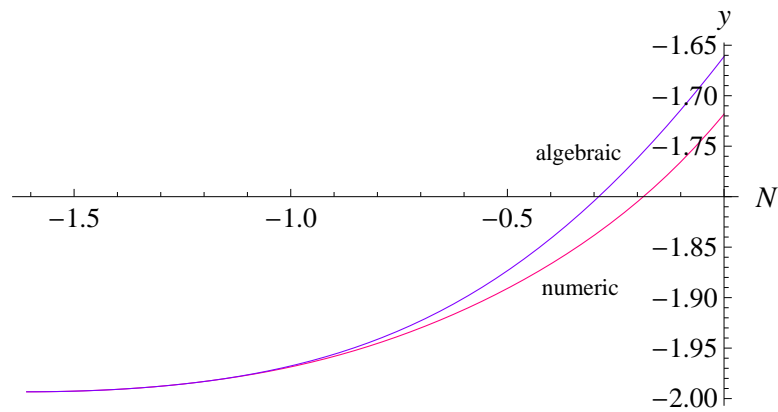


Figure 5.19: Algebraic and numeric solutions for $y(N) = \Phi(N) + \Psi(N)$, for Erf Model 1, when $k = 0$.

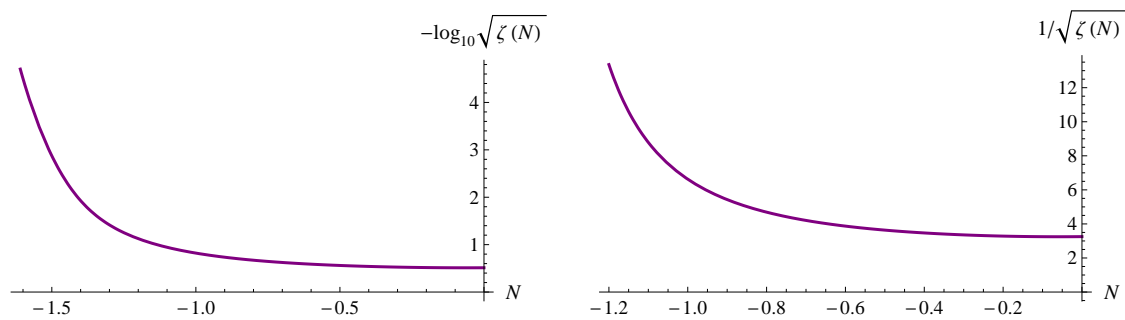


Figure 5.20: How the frequency of the oscillations, as represented by $1/\sqrt{\zeta(N)}$, changes with N for Erf Model 1 when $k = 0$. The erosion of the local minimum and maximum of Figure 5.8 is complete.

all values of k . At early times, the non-oscillating component of x is suppressed by the factor $\zeta(N)$ leaving $x(N)$ to be virtually sinusoidal, namely,

$$x(N) \approx -2\Psi_1(N) \sin \omega(N) \quad (5.70)$$

where $\Psi_1(N)$ is defined in (5.65).

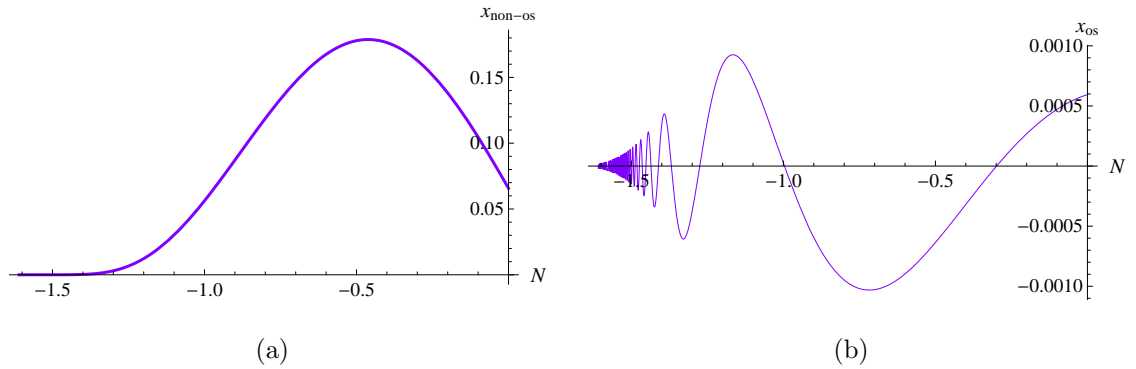


Figure 5.21: For the algebraic solution, (a) shows the non-oscillating component of $x(N)$. (b) shows the oscillating component of $x(N)$ when $x'_i = 1$. Both are for Erf Model 1 when $k = 0$.

5.4.4 Algebraic and numeric solutions for $x(N)$ compared for other models of chapter 3.

Before we leave this topic we should see how the results compare for the other models studied in this thesis. Thus we shall consider the comparison between the algebraic and numeric solutions for Models 2, 4 and 5 of Chapter 3. We shall assume $x'_i = 1$ and $k = 0.1h \text{ Mpc}^{-1}$ for all of them.

5.4.4.1 Model 2

This is from the Erf model with parameters $\Lambda_\infty = 2H_0^2$, $c = 1.5$ and $\log_{10} b = -0.914$. It is located in the de Sitter region of the contour plot, Figure 3.4.

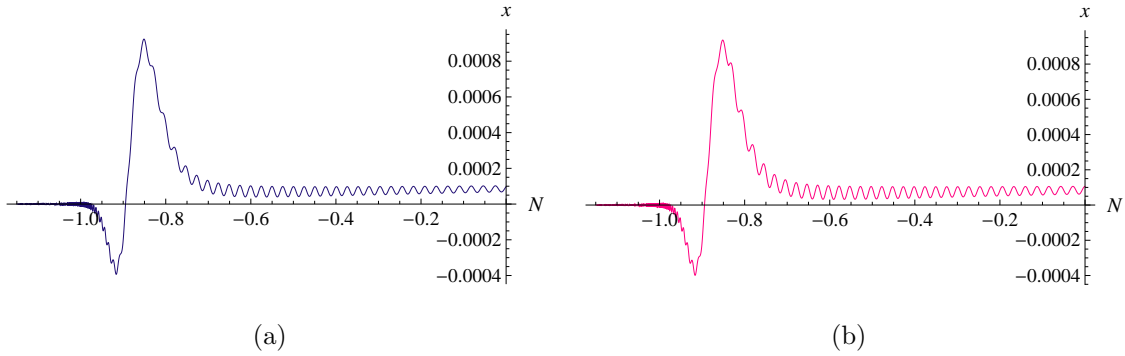


Figure 5.22: Algebraic (a) and Numeric solutions (b) for $x(N)$ for Model 2 when $k = 0.1h \text{ Mpc}^{-1}$ and $x'_s = 1$. Slight differences in the oscillation amplitude are apparent.

Considering how closely $f(R)$ (Figure 3.1) cleaves to $-2\Lambda_\infty$ until very recently, it is worth noting that the jump is still present. Some slight differences in oscillation amplitude, especially at around $N = -0.8$, are becoming visible.

5.4.4.2 Model 4

This is from the AB model with parameters $\Lambda_\infty = 1.92H_0^2$, $b = 1.2$. It is located in the de Sitter region of the contour plot, Figure 3.10.

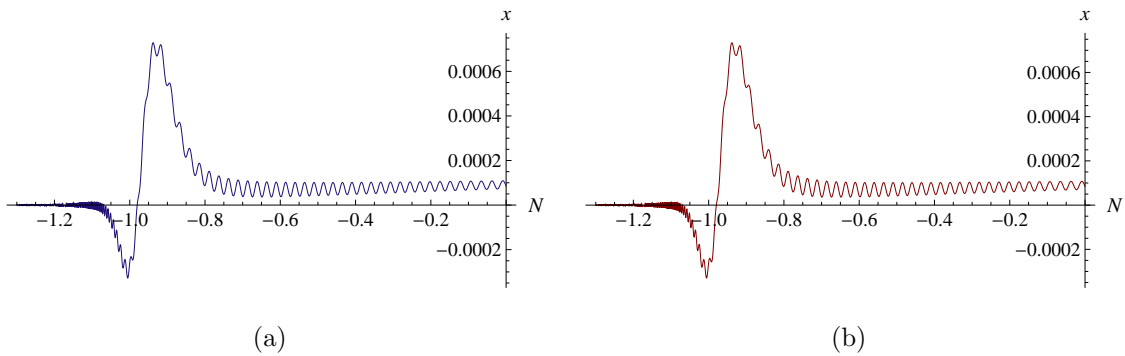


Figure 5.23: Algebraic (a) and Numeric solutions (b) for $x(N)$ for Model 4 when $k = 0.1h \text{ Mpc}^{-1}$ and $x'_s = 1$. There is no noticeable difference between the two. The corresponding graphs for y are also indistinguishable on these plotting scales.

5.4.4.3 Model 5

This is from the HSS model with parameters $n = 6$, $\Lambda_\infty = 1.2 H_0^2$, $\log_{10} c = -2.34$. It is located in the Minkowski region of the contour plot, Figure 3.17.

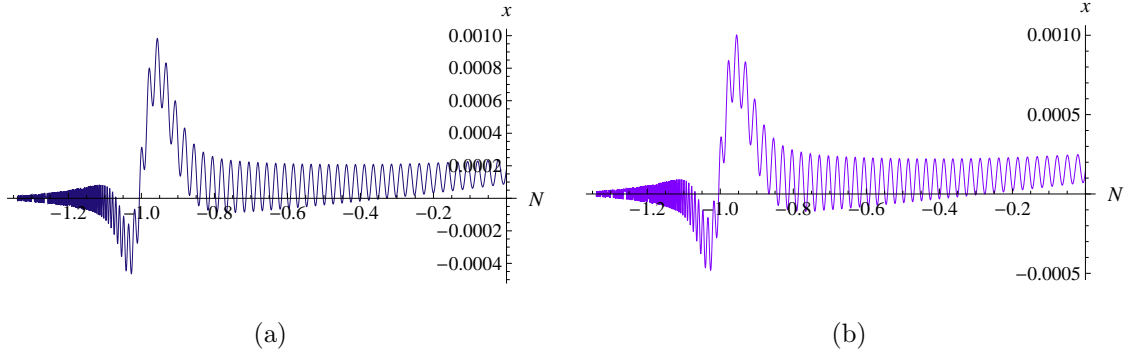


Figure 5.24: Algebraic (a) and Numeric solutions (b) for $x(N)$ for Model 5 when $k = 0.1h \text{ Mpc}^{-1}$ and $x'_s = 1$. There is reasonable agreement.

5.4.5 Comment

As is obvious from the graphs, above, there are differences between the algebraic and numeric solutions but these are small, to first order in $\zeta(N)$. The differences become more marked the smaller k is. Recall that $\zeta(N) = 1/[1/\xi(N) + \lambda(N)^2]$. If $\zeta(N)$ is not sufficiently small then more terms would be needed in the algebraic expression for $x(N)$ and $y(N)$ than are actually used. At early times, $\xi(N)$ is very small but rises with N , as we have seen. That leaves $\lambda(N)$ to be “large” when this happens. $\lambda(N) = k/(aH(N)) = k e^{-N}/H(N)$ so the larger the value of k the more easily this requirement is fulfilled.

It is noticeable from the graphs how reasonably accurate is $1/\sqrt{\zeta(N)}$ as an estimator of the true frequency of the oscillations, even at later times. It does seem to be less accurate, however, the smaller k is. It is also noticeable how the frequency at later times, say at $N = -1$, decreases as k decreases. At early times, the frequency depends mainly on the value of $\xi(N)$ which is a function

of the model only. In the case of $k = 0$, since $\zeta(N) = \xi(N)$, and since $\xi(N)$ increases with N , then the frequency of oscillations decreases with N , given that $1/\sqrt{\zeta(N)}$ remains a valid estimator of the oscillation frequency.

The jump in $x(N)$, evident when $k \neq 0$ for $N > -1.5$, is caused by the non-oscillating component of $x(N)$ and the effect seems to increase in amplitude and also spread out as k becomes smaller. Figure 5.25 shows the equivalent graphs to those of Figures 5.11, 5.16 and 5.21 but with $k = 0.005h \text{ Mpc}^{-1}$. One could also claim, for a particular model, that the jump is moving to smaller values of N .

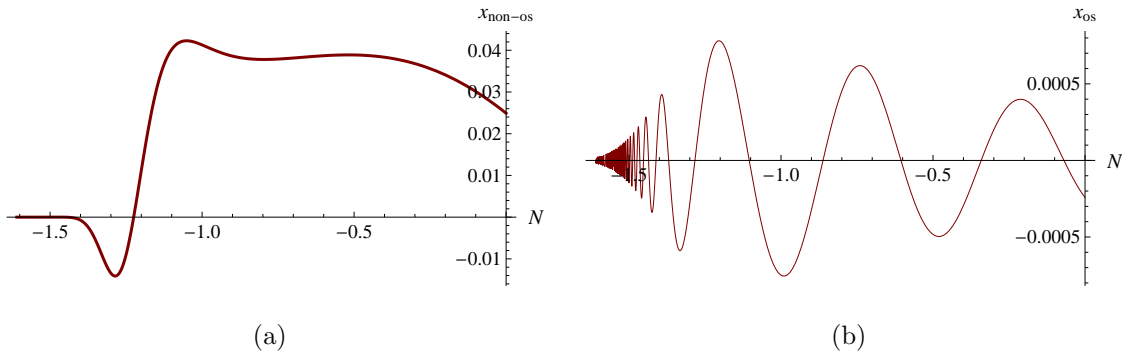


Figure 5.25: For the algebraic solution, (a) shows the non-oscillating component of $x(N)$. (b) shows the oscillating component of $x(N)$ when $x'_i = 1$. Both are for Erf Model 1 when $k = 0.005h \text{ Mpc}^{-1}$.

5.5 Conclusion

This was an attempt to gain some insight into the size and nature of the oscillations in the perturbed FRW metric. In all fairness one could say there has been partial success with very good accuracy when k is large and of the order of $0.1h \text{ Mpc}^{-1}$, or higher. Over a wide range, that is, throughout the matter era from equality right up to the present time in the vacuum era, the frequency of the oscillations is well represented by $1/\sqrt{\zeta(N)}$. This contrasts with Starobinsky in [78] and also Appleby in [101] who restricted themselves to the early matter

era, where $R \propto a^{-3}$, and considered the oscillations inherent in δR ; see (5.11) which were termed δR_{osc} . It was found that the frequency of these oscillations was, in effect¹, the same as $1/\sqrt{\xi(N)}$ which is what $1/\sqrt{\zeta(N)}$ reduces to at early times, as has been discussed. However, the amplitude of the oscillations decreases with time but becomes unbounded as $R \rightarrow \infty$. However, before that can happen, as R grows into the past, the conditions for the validity of the defining differential equation (equation (13) in [78]) are broken. It is clear, from that differential equation, that $F_{RR}(R) \rightarrow 0$ implies that $\delta R_{\text{osc}} \rightarrow 0$. At high curvatures, $F_{RR}(R) \rightarrow 0$ as R increases further, when $F(R)$ gravity becomes more and more indistinguishable from Λ CDM.

At early times, in the matter era, the amplitude of the oscillations, as represented in (5.45) and (5.46), is proportional to $e^{-3N/2}/\sqrt{H(N)}\xi(N)^{1/4}$, which itself is proportional to $R^{1/4}[R F_{RR}(R)]^{1/4}$ and decreases into the past. In other words, as N increases from N_i , the amplitude of the oscillations, as specified by $|\Psi_1(N)|$ in (5.65), increases and continues to do so until $\lambda(N)^2 \sim 1/\xi(N)$ when what happens next depends on the value of k . If $k = 0$, the amplitude continues to increase, as is shown in Figure 5.17. For larger k , the amplitude starts to decrease, as is illustrated in Figure 5.12 when $k = 0.01h \text{ Mpc}^{-1}$ and in Figure 5.4 when $k = 0.1h \text{ Mpc}^{-1}$. This a complicated effect and deserves more study. It depends on the tension between $e^{-3N/2}$, which decreases, between $e^{-\nu(N)}/\sqrt{H(N)}$, which increases, and between $\zeta(N)$, which rises, falls and rises again, as N increases.

A feature which has not been seen before is the ‘‘jump’’ in $x(N)$ which originates from the non-oscillatory solution. As k decreases, the cross-over value of N^2 increases and the numerical values of the local maximum and minimum on either side of it also increase. The jump is, however, the result of the way $x(N)$ is constructed and due to the sudden divergence between $\Phi(N)$ and $\Psi(N)$, as

¹They considered functions of time.

²The value of N where $x(N) = 0$ between the negative local minimum and positive local maximum of the non-oscillating component of $x(N)$.

explained in subsection 5.4.1. Had merely the difference, $\Phi(N) - \Psi(N)$, been plotted rather than the expression for $x(N)$ of (5.53) then this jump, now a step, would have been missed and the oscillations rendered invisible as Figure 5.26(a) shows.

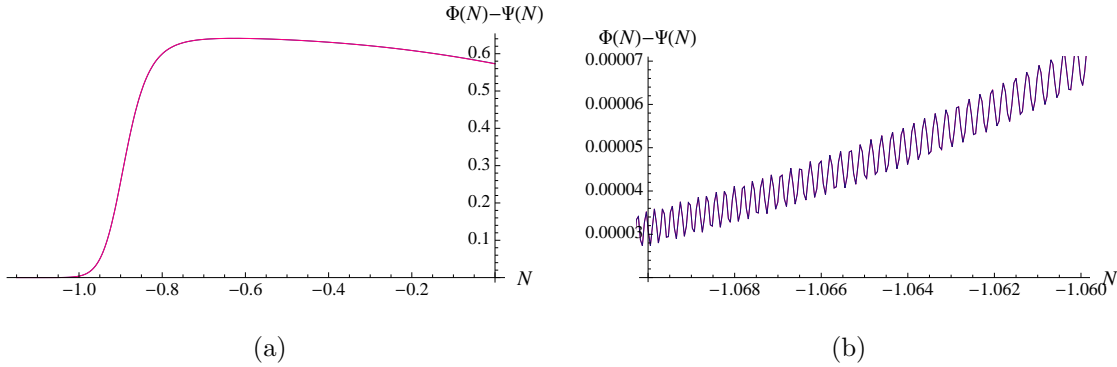


Figure 5.26: Erf Model 2: Both graphs show both the numeric and algebraic solutions, $\Phi(N) - \Psi(N)$, superimposed on one another, for different ranges of N . Differences between the algebraic and numeric graphs are indiscernible. In (a), which shows the full range of N , the oscillations are invisible but the restricted range of (b) shows them and also how the mean value of $\Phi(N) - \Psi(N)$ is increasing with N . The range of (b) is of necessity restricted; a larger range renders the oscillations to be much less visible because the algebraic and numeric graphs become steeper and, reducing the values of N shown, means that the frequency becomes too large to be manageable. $k = 0.1h \text{ Mpc}^{-1}$ and $x'_s = 1$.

How large the oscillations could be, today, with any model, is debatable. If the initial conditions are applied at around $z = 1000$, for which $N_i \approx -7$, and $\zeta(N)$ and the amplitude of the oscillations can be detected if they are of order α , today, then we must have $x'_i \zeta(N_i)^{1/4} \sim \alpha 10^{4.5} / \zeta(N_0)^{1/4} \sim 10^6 \alpha$, say, or larger, which may or may not be realistic. If not then the oscillations are invisible. In other words, the smaller $\zeta(N_i)$ is, the larger must be x'_i . At the very outside for all models, because of the Solar System constraint, $\zeta(N_i) \ll 10^{-23}$, see Chapter 3, section 3.2.1 (3.5), so it is quite likely that $\zeta(N_i)$ will be considerably smaller.

Thus a first attempt at quantifying the matter perturbations has been made for all times in the post-radiation era. A brief comparison between this and work done on perturbing the Ricci scalar by Starobinsky [78] and by Appleby, Battye and Starobinsky [101], now follows.

5.5.1 Oscillations in δR

The oscillations in Φ and Ψ are the same as those found by authors who studied perturbations of the Ricci scalar at high curvature. The result, as quoted in [101] is

$$\delta R = C a^{-3/2} [F_{RR}(R_{GR})]^{-3/4} \sin \left[\int \frac{1}{\sqrt{3F_{RR}(R_{GR})}} dt \right], \quad (5.71)$$

where C is a constant. This translates, using $R_{GR} = R = 3H^2$, $R \propto a^{-3}$, $\zeta N \approx \xi(N) \approx 3H^2 F_{RR}(R)$, so that R now represents the non-oscillating part of R , for simplicity, and $dN/dt = H$, into

$$\delta R = D \sqrt{R} [F_{RR}(R)]^{-3/4} \sin \left[\int \frac{1}{\sqrt{\zeta(N)}} dN \right], \quad (5.72)$$

where D is a constant. Using just the significant oscillatory components at high R for $\Phi(N)$ and $\Psi(N)$, namely,

$$\Psi(N) = A \frac{e^{-3N/2} \zeta(N)^{1/4}}{\sqrt{H(N)}} \sin \left[\int \frac{1}{\sqrt{\zeta(N)}} dN \right] \quad (5.73)$$

$$= -\Phi(N), \quad (5.74)$$

where A is a constant, and substituting these expressions for $\Phi(N)$ and $\Psi(N)$ into the expression for δR in equation (5.11), gives as the most significant term

$$\delta R = -2A \sqrt{R} [F_{RR}(R)]^{-3/4} \sin \left[\int \frac{1}{\sqrt{\zeta(N)}} dN \right]. \quad (5.75)$$

on the assumption that $(k/a)^2 \Psi(N)$ is not significant and that $0 < F_{RR}(R) \ll 1/(n^2 R)$ given that, at high R , $f_R(R)$ can be described by (4.16). There is agreement.

Chapter 6

Conclusions

6.1 Summary

This thesis is concerned with attempting to solve, often algebraically, some of the equations which result after modifying gravity by replacing the Ricci scalar, R , by $F(R)$ in the action represented by equation (1.47). There has been a good deal of success especially when one considers how complicated some of the equations are. The areas looked at were: finding all $F(R)$ for which the Universe has a standard Einstein Gravity expansion history; introducing a new model and exploring, for given $\Omega_{\text{eff},0}$, how extreme the present value of the effective equation of state parameter, $w_{\text{eff},0}$, for this model, the AB model and the HSS model could become; proving that the effective equation of state parameter for $F(R)$ models that tend to standard Einstein Gravity at high curvature must lie below the phantom divide and continue to decrease throughout the radiation era and some of the matter era; finding expressions for the oscillations of potentials Φ and Ψ in the Newtonian gauge induced by perturbing the FRW metric.

6.1.1 Models with standard Einstein Gravity expansion history

The expansion of the Universe is measured by the scale factor a for which $\dot{a} > 0$ as it expands. The Hubble parameter, $H = \dot{a}/a$, the fractional rate of expansion, is used to define the expansion history of the Universe. Standard Einstein gravity has an expansion history given by equation (2.2), in which Λ is the cosmological constant. The corresponding curvature at any value of a is given by equation (2.3). The complete solutions for $F(R)$ in the matter and vacuum eras are given, as infinite power series, by equation (2.13), when $R > 4\Lambda$, and also at late time, when $4\Lambda \leq R \leq 5\Lambda$ by (2.23); today is at $R_0 \approx 4.4\Lambda$. Application of the various constraints suffered by $F(R)$ models, of which the Solar System constraint is the severest, restricts the coefficients of these solutions to such an extent that they are barely discernible from the standard Einstein Gravity model, $F(R) = R - 2\Lambda$.

In section 2.3, a series solution was found for $F(R)$ in the radiation era but, because of the very large value of R/Λ , we need only concern ourselves with the solution $F(R) = R + A\Lambda\rho_0 (R/\Lambda)^{4/3}$. Constraints limit $A\rho_0$ such that $0 \leq A\rho_0 \ll 10^{-25}$.

Concern has been shown in, for example, [78, 101] about the singularity in the scalaron mass which occurs in cases where $F(R)$ tends to $R - 2\Lambda$ as $R \rightarrow \infty$; the scalaron mass tends to infinity and can be very large at relatively low values of R . An attempt has been designed to alleviate this problem by adding the term, $R^2/(6M^2)$, to $F(R)$, where M is some large mass scale. In [101], for example, it is stated that if the quadratic term is to drive inflation then $M \sim 10^{12} \text{ GeV} \simeq 10^{54} H_0$. This term is only significant at very high curvatures but limits the scalaron mass to being of the order of M when the term is significant. While not alleviating the problem, the solution $F(R) = R + A\Lambda\rho_0 (R/\Lambda)^{4/3}$ gives a scalaron mass of order of R at high curvature.

6.1.2 Extreme values generated by $F(R)$ models

In Chapter 3, a new model, based on the error function and which we have termed the *Erf model*, was used. The idea behind it was that we wished to generate values of $w_{\text{eff},0}$ which were further from the phantom divide than other models in use. We needed a model which stuck closely to standard Einstein Gravity as z decreased until comparatively recently, when z is of the order of a few and when w_{eff} would still be very close to -1 , and then swing away sharply to give relatively larger values of $|1 + w_{\text{eff},0}|$ than had been seen before. The close adherence to the phantom divide was necessitated by the stringent requirement of the Solar System constraint. The Erf model was compared to the AB and HSS models. In the past, restrictions on the parameters of a model caused by the possibility of there being a late time de Sitter attractor solution, R_{dS} , for which $R_{\text{dS}} = 12H_{\text{dS}}^2$, have produced relatively small values of $|1 + w_{\text{eff},0}|$. This was discussed for each model and showed how allowing late-time Minkowski solutions could greatly extend the range of $|1 + w_{\text{eff},0}|$. We argued that, should there be a problem beyond today, we could amend the particular $F(R)$, by re-defining it for the future, so that any problems caused by having a Minkowski solution are evaded. For example, the HSS model has a problem with $F_{RR}(R)$ becoming zero and going negative at some time in the future but it is generally saved by having de Sitter attractor solutions.

One constraint that was applied to all models was that we insisted that today's value of the effective dark energy density parameter, $\Omega_{\text{eff},0}$, was the same token value of 0.7. Because $w_{\text{eff},0}$ and R_0 are connected by the relation, $R_0 = 3H_0^2(1 - 3w_{\text{eff},0}\Omega_{\text{eff},0})$, extreme values of $w_{\text{eff},0}$ generate extreme and, therefore, unrealistic values of R_0 , that is, outside the range for R_0 given in section 3.2. However, we never allowed R_0 to go negative.

This aspect of $F(R)$ gravity, of finding extreme values of measurable parameters given certain constraints, is most interesting and points a way forward. See

section 6.2.

6.1.3 Theorem

It is noticeable that, for all examples of $F(R)$ models which have the property of tending to standard Einstein Gravity as $R \rightarrow \infty$, graphs show w_{eff} falling below the phantom divide, as z decreases, and they continue to do so until they return to cross the phantom divide in the recent past, now or, maybe, in the near future. This has been discussed in relation to specific models in [47, 49, 68, 97]. It is one property of $F(R)$ gravity which may distinguish it from other types of model and certainly from quintessence.

By assuming that $f(R)$, where $F(R) = R + f(R)$, can be approximated by $-2\Lambda + \mu_0 a^n$ where μ_0 is a positive constant and n is a very large number, we prove the first part of this, namely that as a increases from 0, w_{eff} decreases from -1 and continues to do so until the expression for $f(R)$ ceases to be valid. Because n is very large, which it has to be because of the Solar system constraint, this will happen at a value of R within the matter or vacuum eras. To show that w_{eff} then reaches a local minimum would require more knowledge of how $f(R)$ evolves with time.

6.1.4 Oscillations of the potentials of the perturbed FRW metric

In Chapter 5, the perturbed FRW metric can be written, to first order in the Newtonian gauge, as:

$$ds^2 = -(1 + 2\Psi) dt^2 + a^2 (1 - 2\Phi) \delta_{ij} dx^i dx^j. \quad (6.1)$$

A total of seven relevant equations were distilled into two to produce a pair of coupled, second-order, homogeneous, linear, differential equations for the potentials Φ and Ψ in terms of the variable $N = \log a$. These equations were solved both numerically and algebraically with the same initial conditions. Algebraically, both of the potentials were shown to consist of an oscillating component and a non-oscillating component.

It was clear that both oscillating components had the same frequency and an expression was found which appeared to be robust right from early times to the present. This is in contrast to previous work ([78, 101, 117]), in which were considered the oscillations of the perturbed Ricci scalar but only at early times. When the units were changed so that the frequencies could be compared it was found that our solutions agreed with them. The expression for the frequency of our solutions was proportional to the reciprocal of the scalaron mass, at early times, migrating to $k/(aH)$, at late times, around today, where k is the co-moving wavenumber. How the oscillation frequency changed over time for a particular model, Erf Model 1, was illustrated and how it depended on the value of k . Approximations to the envelope of each waveform were determined, as were the non-oscillating components up to order $\zeta(N)$, which is defined in equation (5.25). Then initial conditions were applied and the phase of the oscillations chosen so that the algebraic approximations could be given for $\Phi(N)$ and $\Psi(N)$ in terms of just one parameter, x'_i .

In order to make the oscillations visible when plotting graphs, the variable $x(N)$ was formed which removes the largest of the non-oscillating terms of $\Phi(N)$ and $\Psi(N)$ and which approximates to $\Phi(N) - \Psi(N)$ at high z but to $(4\Phi(N) - 2\Psi(N))/3$ at recent times. In order to display the non-oscillating components the sum $y(N) = \Phi(N) + \Psi(N)$ was formed which was dominated by the lowest order non-oscillating components. To illustrate how accurate the algebraic solutions were, the algebraic and numeric solutions for $x(N)$ and $y(N)$ were compared graphically.

This exercise was completed for four example models. There was always good agreement at early times. At later times, near today, there was good agreement when k was of the order of $k = 0.1h \text{ Mpc}^{-1}$ but the algebraic solutions were less accurate for smaller k with the greatest errors being when $k = 0$. The reason for this is that at late times $\zeta(N)$ is proportional to $1/k^2$ while, at early times, it is independent of k . The efficacy of the algebraic solution requires that $\zeta(N)$ is always small, which puts a model-dependent condition on k . This explains why, for a given value of k , different models gave slightly different disagreements between the algebraic and corresponding numeric solutions.

One feature of the graphs of $x(N)$ against N which was unexpected was the appearance of a “jump” in $x(N)$ at a value of N where the expression for $\zeta(N)$ changes from being dominated from one expression, $\xi(N)$, to being dominated by another, $1/\lambda(N)^2$.

The oscillations in $\Phi(N)$ and $\Psi(N)$ have been shown to be the same, at high curvature, as those studied as perturbations in the Ricci scalar in [78, 101].

There remains the problem that the amplitude of the oscillations for $\Phi(N)$ and $\Psi(N)$ increase, initially, into the future (see Figure 5.11), whereas for δR the amplitude of the oscillations increases into the past. The oscillations for $\Phi(N)$ and $\Psi(N)$ really start before the formation of the CMB so that they start at some value of $z \gg 10^3$. The same should be true for δR ; that they only recede into the past as far as this point which would give the oscillations a maximum amplitude which is finite. In Einstein Gravity $\delta R = 0$, so there could be no oscillations in δR until this point when they suddenly “appear” with maximum amplitude to decay over time. This gives credence to the suggestion, in [26], that all $F(R)$ functions should be modified by the addition of the $R^2/(6M^2)$ term mentioned in subsection 6.1.1, above, which would at least limit the maximum amplitude and frequency at high values of z .

6.2 Outlook

1. The time has come for researchers to test $F(R)$ models against parameters determined from observations. Current results from Planck, assuming a Λ CDM background and a flat FRW Universe, in effect constrain $w_{\text{eff},0}$, $w'_{\text{eff},0}$, H_0 , $\Omega_{\text{eff},0}$, $\Omega_{\text{m},0}$ and $\Omega_{\text{r},0}$, the last being coupled to the previous via the value of z at equality. It would be interesting to see how the tight variations in these cosmological parameters constrain the parameters of all the successful models proposed and what these models would then predict. What are their similarities and how do they differ?
2. Is it possible to prove, for all viable $F(R)$ models that w_{eff} reaches a local minimum below the phantom divide sometime in the recent past?
3. An attempt could be made to find more complete algebraic solutions which would represent better what happens today. Are oscillations in potentials, Φ and Ψ , detectable and, if so, of what order might they be?

Bibliography

- [1] J. C. Mather, *Cosmic background explorer (COBE) mission*, in *Infrared Spaceborne Remote Sensing* (M. S. Scholl, ed.), vol. 2019 of *Society of Photo-Optical Instrumentation Engineers (SPIE) Conference Series*, pp. 146–157, Oct., 1993.
- [2] N. W. Boggess, J. C. Mather, R. Weiss, C. L. Bennett, E. S. Cheng, E. Dwek, S. Gulbis, M. G. Hauser, M. A. Janssen, T. Kelsall, S. S. Meyer, S. H. Moseley, T. L. Murdock, R. A. Shafer, R. F. Silverberg, G. F. Smoot, D. T. Wilkinson, and E. L. Wright, *The COBE mission - Its design and performance two years after launch*, **397** (Oct., 1992) 420–429.
- [3] **Planck Collaboration** Collaboration, P. Ade *et. al.*, *Planck 2013 results. I. Overview of products and scientific results*, [arXiv:1303.5062](https://arxiv.org/abs/1303.5062).
- [4] **WMAP Collaboration** Collaboration, C. Bennett *et. al.*, *First year Wilkinson Microwave Anisotropy Probe (WMAP) observations: Preliminary maps and basic results*, *Astrophys.J.Suppl.* **148** (2003) 1, [[astro-ph/0302207](https://arxiv.org/abs/astro-ph/0302207)].
- [5] **WMAP Collaboration** Collaboration, D. Spergel *et. al.*, *First year Wilkinson Microwave Anisotropy Probe (WMAP) observations: Determination of cosmological parameters*, *Astrophys.J.Suppl.* **148** (2003) 175–194, [[astro-ph/0302209](https://arxiv.org/abs/astro-ph/0302209)].
- [6] **WMAP Collaboration** Collaboration, G. Hinshaw *et. al.*, *Nine-Year*

- Wilkinson Microwave Anisotropy Probe (WMAP) Observations: Cosmological Parameter Results*, [arXiv:1212.5226](#).
- [7] **WMAP Collaboration** Collaboration, C. Bennett *et. al.*, *Nine-Year Wilkinson Microwave Anisotropy Probe (WMAP) Observations: Final Maps and Results*, [arXiv:1212.5225](#).
- [8] A. Einstein, *The Foundation of the General Theory of Relativity*, *Annalen Phys.* **49** (1916) 769–822.
- [9] H. Lorentz, *The Principle of Relativity*. Dover Publications, Inc, 1923.
- [10] L. Infeld, *Equations of Motion in General Relativity Theory and the Action Principle*, *Rev.Mod.Phys.* **29** (1957) 398–411.
- [11] S. M. Carroll, *Spacetime and geometry: An introduction to general relativity*. Adison Wesley, 2004.
- [12] A. H. Guth, *The Inflationary Universe: A Possible Solution to the Horizon and Flatness Problems*, *Phys.Rev.* **D23** (1981) 347–356.
- [13] A. D. Linde, *Particle physics and inflationary cosmology*, *Contemp.Concepts Phys.* **5** (1990) 1–362, [[hep-th/0503203](#)].
- [14] D. Coule, *Canonical measure and the flatness of a FRW universe*, *Class.Quant.Grav.* **12** (1995) 455–470, [[gr-qc/9408026](#)].
- [15] G. Lemaître, *Expansion of the universe, A homogeneous universe of constant mass and increasing radius accounting for the radial velocity of extra-galactic nebulae*, *1931MNRAS..91..483L* (1931).
- [16] G. Tammann, *The Ups and Downs of the Hubble Constant*, *Rev.Mod.Astron.* **19** (2006) 1, [[astro-ph/0512584](#)].
- [17] **Planck Collaboration** Collaboration, P. Ade *et. al.*, *Planck 2013 results. XVI. Cosmological parameters*, [arXiv:1303.5076](#).

-
- [18] R. Feynman, F. Morinigo, W. Wagner, and B. Hatfield, *Feynman lectures on gravitation*, .
- [19] E. W. Kolb and M. S. Turner, *The Early Universe*, *Front.Phys.* **69** (1990) 1–547.
- [20] A. A. Starobinsky, *Future and origin of our universe: Modern view*, *Grav.Cosmol.* **6** (2000) 157–163, [[astro-ph/9912054](#)].
- [21] A. A. Penzias and R. W. Wilson, *A Measurement of excess antenna temperature at 4080-Mc/s*, *Astrophys.J.* **142** (1965) 419–421.
- [22] R. Dicke, P. Peebles, P. Roll, and D. Wilkinson, *Cosmic Black-Body Radiation*, *Astrophys.J.* **142** (1965) 414–419.
- [23] C. L. Bennett, N. W. Boggess, E. S. Cheng, M. G. Hauser, T. Kelsall, J. C. Mather, S. H. Moseley, Jr., T. L. Murdock, R. A. Shafer, and R. F. Silverberg, *Scientific results from COBE*, *Advances in Space Research* **13** (Dec., 1993) 409–.
- [24] R. Sachs and A. Wolfe, *Perturbations of a cosmological model and angular variations of the microwave background*, *Astrophys.J.* **147** (1967) 73–90.
- [25] T. Giannantonio, R. Scranton, R. G. Crittenden, R. C. Nichol, S. P. Boughn, *et. al.*, *Combined analysis of the integrated Sachs-Wolfe effect and cosmological implications*, *Phys.Rev.* **D77** (2008) 123520, [[arXiv:0801.4380](#)].
- [26] L. Amendola, M. Kunz, and D. Sapone, *Measuring the dark side (with weak lensing)*, *JCAP* **0804** (2008) 013, [[arXiv:0704.2421](#)].
- [27] **Supernova Cosmology Project** Collaboration, S. Perlmutter *et. al.*, *Discovery of a supernova explosion at half the age of the Universe and its cosmological implications*, *Nature* **391** (1998) 51–54, [[astro-ph/9712212](#)].

-
- [28] M. S. Turner, *Why cosmologists believe the universe is accelerating*, astro-ph/9904049.
- [29] W. Chakraborty, *Accelerating Expansion of the Universe*, arXiv:1105.1087.
- [30] A. De Felice, D. F. Mota, and S. Tsujikawa, *Matter instabilities in general Gauss-Bonnet gravity*, *Phys.Rev.* **D81** (2010) 023532, [arXiv:0911.1811].
- [31] S. Nojiri and S. D. Odintsov, *Unified cosmic history in modified gravity: from $F(R)$ theory to Lorentz non-invariant models*, *Phys.Rept.* **505** (2011) 59–144, [arXiv:1011.0544].
- [32] T. P. Sotiriou and V. Faraoni, *$f(R)$ Theories Of Gravity*, *Rev.Mod.Phys.* **82** (2010) 451–497, [arXiv:0805.1726].
- [33] A. De Felice and S. Tsujikawa, *$f(R)$ theories*, *Living Rev.Rel.* **13** (2010) 3, [arXiv:1002.4928].
- [34] T. Clifton, P. G. Ferreira, A. Padilla, and C. Skordis, *Modified Gravity and Cosmology*, *Phys.Rept.* **513** (2012) 1–189, [arXiv:1106.2476].
- [35] A. Guarnizo, L. Castaneda, and J. M. Tejeiro, *Boundary Term in Metric $f(R)$ Gravity: Field Equations in the Metric Formalism*, *Gen.Rel.Grav.* **42** (2010) 2713–2728, [arXiv:1002.0617].
- [36] E. Poisson, *A relativist's toolkit : the mathematics of black-hole mechanics*. 2004.
- [37] E. J. Copeland, M. Sami, and S. Tsujikawa, *Dynamics of dark energy*, *Int.J.Mod.Phys.* **D15** (2006) 1753–1936, [hep-th/0603057].
- [38] R. Adler, B. Casey, and O. Jacob, *Vacuum catastrophe: An Elementary exposition of the cosmological constant problem*, *Am.J.Phys.* **63** (1995) 620–626.

- [39] J. Martin, *Everything You Always Wanted To Know About The Cosmological Constant Problem (But Were Afraid To Ask)*, *Comptes Rendus Physique* **13** (2012) 566–665, [arXiv:1205.3365].
- [40] A. Goobar, S. Perlmutter, G. Aldering, G. Goldhaber, R. Knop, *et. al.*, *The acceleration of the universe: Measurements of cosmological parameters from type Ia supernovae*, *Phys.Scripta* **T85** (2000) 47–58.
- [41] S. Weinberg, *Anthropic Bound on the Cosmological Constant*, *Phys.Rev.Lett.* **59** (1987) 2607.
- [42] S. Weinberg, *The Cosmological Constant Problem*, *Rev.Mod.Phys.* **61** (1989) 1–23.
- [43] T. Padmanabhan and H. Padmanabhan, *CosMIn: The Solution to the Cosmological Constant Problem*, arXiv:1302.3226.
- [44] A. Einstein, *Do gravitational fields play an essential part in the structure of the elementary particles of matter?*, *Sitzungsber.Preuss.Akad. Wiss.Berlin (Math.Phys.)* **1919** (1919) 433.
- [45] A. Dolgov, M. Einhorn, and V. I. Zakharov, *The Vacuum of de Sitter space*, *Acta Phys.Polon.* **B26** (1995) 65–90, [gr-qc/9405026].
- [46] G. Cognola, E. Elizalde, S. Odintsov, P. Tretyakov, and S. Zerbini, *Initial and final de Sitter universes from modified $f(R)$ gravity*, *Phys.Rev.* **D79** (2009) 044001, [arXiv:0810.4989].
- [47] H. Motohashi, A. A. Starobinsky, and J. Yokoyama, *Future Oscillations around Phantom Divide in $f(R)$ Gravity*, *JCAP* **1106** (2011) 006, [arXiv:1101.0744].
- [48] W. Hu, *Crossing the phantom divide: Dark energy internal degrees of freedom*, *Phys.Rev.* **D71** (2005) 047301, [astro-ph/0410680].

- [49] L. Amendola and S. Tsujikawa, *Phantom crossing, equation-of-state singularities, and local gravity constraints in $f(R)$ models*, *Phys.Lett.* **B660** (2008) 125–132, [arXiv:0705.0396].
- [50] K. Bamba, C.-Q. Geng, S. Nojiri, and S. D. Odintsov, *Crossing of Phantom Divide in $F(R)$ Gravity*, *Mod.Phys.Lett.* **A25** (2010) 900–908, [arXiv:1003.0769].
- [51] J. Frieman, M. Turner, and D. Huterer, *Dark Energy and the Accelerating Universe*, *Ann.Rev.Astron.Astrophys.* **46** (2008) 385–432, [arXiv:0803.0982].
- [52] L. Amendola and S. Tsujikawa, *Dark Energy: Theory and Observations*. 2010.
- [53] L. Amendola, D. Polarski, and S. Tsujikawa, *Are $f(R)$ dark energy models cosmologically viable ?*, *Phys.Rev.Lett.* **98** (2007) 131302, [astro-ph/0603703].
- [54] **Supernova Search Team** Collaboration, A. G. Riess *et. al.*, *Observational evidence from supernovae for an accelerating universe and a cosmological constant*, *Astron.J.* **116** (1998) 1009–1038, [astro-ph/9805201].
- [55] **Supernova Cosmology Project** Collaboration, S. Perlmutter *et. al.*, *Measurements of Omega and Lambda from 42 high redshift supernovae*, *Astrophys.J.* **517** (1999) 565–586, [astro-ph/9812133].
- [56] G. Huey, L.-M. Wang, R. Dave, R. Caldwell, and P. J. Steinhardt, *Resolving the cosmological missing energy problem*, *Phys.Rev.* **D59** (1999) 063005, [astro-ph/9804285].
- [57] D. Polarski and A. Ranquet, *On the equation of state of dark energy*, *Phys.Lett.* **B627** (2005) 1–8, [astro-ph/0507290].

- [58] V. Sahni and A. A. Starobinsky, *The Case for a positive cosmological Lambda term*, *Int.J.Mod.Phys.* **D9** (2000) 373–444, [[astro-ph/9904398](#)].
- [59] S. M. Carroll, W. H. Press, and E. L. Turner, *The Cosmological constant*, *Ann.Rev.Astron.Astrophys.* **30** (1992) 499–542.
- [60] P. Peebles and B. Ratra, *The Cosmological constant and dark energy*, *Rev.Mod.Phys.* **75** (2003) 559–606, [[astro-ph/0207347](#)].
- [61] V. Sahni and A. Starobinsky, *Reconstructing Dark Energy*, *Int.J.Mod.Phys.* **D15** (2006) 2105–2132, [[astro-ph/0610026](#)].
- [62] T. Padmanabhan, *Cosmological constant: The Weight of the vacuum*, *Phys.Rept.* **380** (2003) 235–320, [[hep-th/0212290](#)].
- [63] S. Tsujikawa, *Modified gravity models of dark energy*, *Lect.Notes Phys.* **800** (2010) 99–145, [[arXiv:1101.0191](#)].
- [64] E. Di Pietro and J. Demaret, *A constant equation of state for quintessence?*, *Int.J.Mod.Phys.* **D10** (2001) 231–237, [[gr-qc/9908071](#)].
- [65] R. Caldwell, *An introduction to quintessence*, *Braz.J.Phys.* **30** (2000) 215–229.
- [66] I. Zlatev, L.-M. Wang, and P. J. Steinhardt, *Quintessence, cosmic coincidence, and the cosmological constant*, *Phys.Rev.Lett.* **82** (1999) 896–899, [[astro-ph/9807002](#)].
- [67] D. Polarski, *Dark energy*, *AIP Conf.Proc.* **1514** (2012) 111–117.
- [68] K. Bamba, C.-Q. Geng, and C.-C. Lee, *Phantom crossing in viable $f(R)$ theories*, *Int.J.Mod.Phys.* **D20** (2011) 1339–1345, [[arXiv:1108.2557](#)].
- [69] M. Kunz and D. Sapone, *Crossing the Phantom Divide*, *Phys.Rev.* **D74** (2006) 123503, [[astro-ph/0609040](#)].

- [70] A. A. Starobinsky, *A New Type of Isotropic Cosmological Models Without Singularity*, *Phys.Lett.* **B91** (1980) 99–102.
- [71] P.J.E.Peebles, *Large Scale Structure of the Universe*. Princeton University Press, 1980.
- [72] L.-M. Wang and P. J. Steinhardt, *Cluster abundance constraints on quintessence models*, *Astrophys.J.* **508** (1998) 483–490, [astro-ph/9804015].
- [73] D. Rapetti, S. W. Allen, A. Mantz, and H. Ebeling, *The Observed Growth of Massive Galaxy Clusters III: Testing General Relativity on Cosmological Scales*, *Mon.Not.Roy.Astron.Soc.* **406** (2010) 1796–1804, [arXiv:0911.1787].
- [74] E. V. Linder, *Cosmic growth history and expansion history*, *Phys.Rev.* **D72** (2005) 043529, [astro-ph/0507263].
- [75] A. J. Lopez-Revelles, *Growth of matter perturbations for realistic $F(R)$ models*, *Phys.Rev.* **D87** (2013) 024021, [arXiv:1301.2120].
- [76] S. A. Appleby and R. A. Battye, *Do consistent $F(R)$ models mimic General Relativity plus Λ ?*, *Phys.Lett.* **B654** (2007) 7–12, [arXiv:0705.3199].
- [77] L. Amendola, R. Gannouji, D. Polarski, and S. Tsujikawa, *Conditions for the cosmological viability of $f(R)$ dark energy models*, *Phys.Rev.* **D75** (2007) 083504, [gr-qc/0612180].
- [78] A. A. Starobinsky, *Disappearing cosmological constant in $f(R)$ gravity*, *JETP Lett.* **86** (2007) 157–163, [arXiv:0706.2041].
- [79] L. Pogosian and A. Silvestri, *The pattern of growth in viable $f(R)$ cosmologies*, *Phys.Rev.* **D77** (2008) 023503, [arXiv:0709.0296].

- [80] A. Nunez and S. Solganik, *The Content of $f(R)$ gravity*, hep-th/0403159.
- [81] A. Krause and S.-P. Ng, *Ghost cosmology: exact solutions, transitions between standard cosmologies and ghost dark energy/matter evolution*, *Int.J.Mod.Phys.* **A21** (2006) 1091–1122, [hep-th/0409241].
- [82] B. Himmetoglu, C. R. Contaldi, and M. Peloso, *Ghost instabilities of cosmological models with vector fields nonminimally coupled to the curvature*, *Phys.Rev.* **D80** (2009) 123530, [arXiv:0909.3524].
- [83] N. Deruelle, M. Sasaki, Y. Sendouda, and A. Youssef, *Inflation with a Weyl term, or ghosts at work*, *JCAP* **1103** (2011) 040, [arXiv:1012.5202].
- [84] A. Dolgov and M. Kawasaki, *Can modified gravity explain accelerated cosmic expansion?*, *Phys.Lett.* **B573** (2003) 1–4, [astro-ph/0307285].
- [85] G. J. Olmo, *Post-Newtonian constraints on $f(R)$ cosmologies in metric and Palatini formalism*, *Phys.Rev.* **D72** (2005) 083505, [gr-qc/0505135].
- [86] V. Faraoni, *Solar System experiments do not yet veto modified gravity models*, *Phys.Rev.* **D74** (2006) 023529, [gr-qc/0607016].
- [87] S. Tsujikawa, *Observational signatures of $f(R)$ dark energy models that satisfy cosmological and local gravity constraints*, *Phys.Rev.* **D77** (2008) 023507, [arXiv:0709.1391].
- [88] M. Colless, *First results from the 2dF galaxy redshift survey*, astro-ph/9804079.
- [89] J. Loveday, *The Sloan Digital Sky Survey*, *Contemporary Physics* **43** (June, 2002) 437–449, [astro-ph/0207189].
- [90] **SDSS Collaboration** Collaboration, D. J. Eisenstein *et. al.*, *SDSS-III: Massive Spectroscopic Surveys of the Distant Universe, the Milky Way*

- Galaxy, and Extra-Solar Planetary Systems, Astron.J.* **142** (2011) 72, [arXiv:1101.1529].
- [91] K. S. Dawson *et. al.*, *The Baryon Oscillation Spectroscopic Survey of SDSS-III, Astron.J.* **145** (2013), no. 1 10, [arXiv:1208.0022].
- [92] S. Fay, S. Nesseris, and L. Perivolaropoulos, *Can $f(R)$ Modified Gravity Theories Mimic a Λ CDM Cosmology?*, *Phys.Rev.* **D76** (2007) 063504, [gr-qc/0703006].
- [93] P. K. Dunsby, E. Elizalde, R. Goswami, S. Odintsov, and D. S. Gomez, *On the Λ CDM Universe in $f(R)$ gravity*, *Phys.Rev.* **D82** (2010) 023519, [arXiv:1005.2205].
- [94] T. Chiba, T. L. Smith, and A. L. Erickcek, *Solar System constraints to general $f(R)$ gravity*, *Phys.Rev.* **D75** (2007) 124014, [astro-ph/0611867].
- [95] G. Arfken and H. Weber, *Mathematical Methods for Physicists*. Elsevier Academic Press, 2005.
- [96] S. M. Carroll, *Why is the universe accelerating?*, *eConf* **C0307282** (2003) TTH09, [astro-ph/0310342].
- [97] W. Hu and I. Sawicki, *Models of $f(R)$ Cosmic Acceleration that Evade Solar-System Tests*, *Phys.Rev.* **D76** (2007) 064004, [arXiv:0705.1158].
- [98] E. V. Linder, *Exponential Gravity*, *Phys.Rev.* **D80** (2009) 123528, [arXiv:0905.2962].
- [99] K. Bamba, C.-Q. Geng, and C.-C. Lee, *Cosmological evolution in exponential gravity*, *JCAP* **1008** (2010) 021, [arXiv:1005.4574].
- [100] M. Martinelli, A. Melchiorri, and L. Amendola, *Cosmological constraints on the Hu-Sawicki modified gravity scenario*, *Phys.Rev.* **D79** (2009) 123516, [arXiv:0906.2350].

- [101] S. A. Appleby, R. A. Battye, and A. A. Starobinsky, *Curing singularities in cosmological evolution of $F(R)$ gravity*, *JCAP* **1006** (2010) 005, [arXiv:0909.1737].
- [102] D. K. Hazra and A. Shafieloo, *Test of Consistency between Planck and WMAP*, arXiv:1308.2911.
- [103] M. Doran and G. Robbers, *Early dark energy cosmologies*, *JCAP* **0606** (2006) 026, [astro-ph/0601544].
- [104] M. Realdi, *The Universe of Willem de Sitter*, 2007.
- [105] A. de la Cruz-Dombriz and A. Dobado, *A $f(R)$ gravity without cosmological constant*, *Phys.Rev.* **D74** (2006) 087501, [gr-qc/0607118].
- [106] S. Tsujikawa, K. Uddin, and R. Tavakol, *Density perturbations in $f(R)$ gravity theories in metric and Palatini formalisms*, *Phys.Rev.* **D77** (2008) 043007, [arXiv:0712.0082].
- [107] A. V. Frolov, *A Singularity Problem with $f(R)$ Dark Energy*, *Phys.Rev.Lett.* **101** (2008) 061103, [arXiv:0803.2500].
- [108] V. Faraoni, *De Sitter attractors in generalized gravity*, *Phys.Rev.* **D70** (2004) 044037, [gr-qc/0407021].
- [109] H. Motohashi, A. A. Starobinsky, and J. Yokoyama, *Analytic solution for matter density perturbations in a class of viable cosmological $f(R)$ models*, *Int.J.Mod.Phys.* **D18** (2009) 1731–1740, [arXiv:0905.0730].
- [110] D. Polarski and R. Gannouji, *On the growth of linear perturbations*, *Phys.Lett.* **B660** (2008) 439–443, [arXiv:0710.1510].
- [111] E. V. Linder and R. N. Cahn, *Parameterized Beyond-Einstein Growth*, *Astropart.Phys.* **28** (2007) 481–488, [astro-ph/0701317].

- [112] S. Tsujikawa, *Matter density perturbations and effective gravitational constant in modified gravity models of dark energy*, *Phys.Rev.* **D76** (2007) 023514, [arXiv:0705.1032].
- [113] S. A. Appleby and J. Weller, *Parameterizing scalar-tensor theories for cosmological probes*, *JCAP* **1012** (2010) 006, [arXiv:1008.2693].
- [114] S. Tsujikawa, R. Gannouji, B. Moraes, and D. Polarski, *The dispersion of growth of matter perturbations in $f(R)$ gravity*, *Phys.Rev.* **D80** (2009) 084044, [arXiv:0908.2669].
- [115] H. Motohashi, A. A. Starobinsky, and J. Yokoyama, *$f(R)$ Gravity and its Cosmological Implications*, *Int.J.Mod.Phys.* **D20** (2011) 1347–1355, [arXiv:1101.0716].
- [116] C.-P. Ma and E. Bertschinger, *Cosmological perturbation theory in the synchronous and conformal Newtonian gauges*, *Astrophys.J.* **455** (1995) 7–25, [astro-ph/9506072].
- [117] E. Elizalde, S. Odintsov, L. Sebastiani, and S. Zerbini, *Oscillations of the $F(R)$ dark energy in the accelerating universe*, *Eur.Phys.J.* **C72** (2012) 1843, [arXiv:1108.6184].
- [118] R. Bean, D. Bernat, L. Pogosian, A. Silvestri, and M. Trodden, *Dynamics of Linear Perturbations in $f(R)$ Gravity*, *Phys.Rev.* **D75** (2007) 064020, [astro-ph/0611321].
- [119] Y.-S. Song, W. Hu, and I. Sawicki, *The Large Scale Structure of $f(R)$ Gravity*, *Phys.Rev.* **D75** (2007) 044004, [astro-ph/0610532].
- [120] S. Appleby and R. Battye, *Aspects of cosmological expansion in $F(R)$ gravity models*, *JCAP* **0805** (2008) 019, [arXiv:0803.1081].